Surface Acoustic Wave Resonators with Trenches and High Aspect Ratio Structures for Gas Sensing Applications

A thesis submitted

for the award of the degree of

DOCTOR OF PHILOSOPHY

by

VIVEK LUKOSE

DEPARTMENT OF ELECTRONICS AND ELECTRICAL ENGINEERING

INDIAN INSTITUTE OF TECHNOLOGY GUWAHATI

GUWAHATI-781039, ASSAM, INDIA

JULY 2019

Certificate

This is to certify that the thesis entitled "**Surface Acoustic Wave Resonators with Trenches and High Aspect Ratio Structures for Gas Sensing Applications**", submitted by Vivek Lukose (10610225), a research scholar in the Department of Electronics and Electrical Engineering, Indian Institute of Technology Guwahati, for the award of the degree of Doctor of Philosophy, is a record of an original research work carried out by him under my supervision and guidance. The thesis has fulfilled all requirements as per the regulations of the institute and in my opinion has reached the standard needed for submission. The results embodied in this thesis have not been submitted to any other University or Institute for the award of any degree or diploma.

Dated:

Guwahati

Prof. Harshal B. Nemade
Professor
Department of Electronics and Electrical Engineering
Indian Institute of Technology Guwahati
Guwahati - 781 039, Assam, India.

Declaration

This is to declare that the thesis entitled "**Surface Acoustic Wave Resonators with Trenches and High Aspect Ratio Structures for Gas Sensing Applications**", submitted by me to the Indian Institute of Technology Guwahati for the award of the degree of Doctor of Philosophy is a bonafide record of research work carried out by me under the supervision of Prof. Harshal B. Nemade. Hereby I declare that the contents of this thesis, in full or in parts, have not been submitted to any other University or Institute for the award of any degree or diploma.

Dated:

Guwahati

Vivek Lukose

Abstract

Surface acoustic wave (SAW) is a sound wave that travels on the surface of an elastic material with amplitude decaying exponentially along the depth of the material. A SAW device is conveniently made on a piezoelectric substrate using interdigital transducer(IDT), a pair of comb-shaped metallic electrodes, patterned on the surface of the substrate for the transduction of electric energy to acoustic energy and vice versa. SAW is highly sensitive to perturbation along the propagation path, and SAW devices can be designed as sensors sensitive to variations in the surrounding medium. The variations can be measured as the change in resonance frequency, phase or attenuation in the SAW device. SAW devices based on Rayleigh waves are often used for making highly sensitive gas sensors.

There is always a demand for high performance gas sensors for detecting and monitoring various inorganic gases, volatile organic chemicals, and chemical warfare agents. Conventionally in a SAW sensor, a film of sensing material selective to particular analyte is coated on the surface of SAW device. The researchers have reported improvement in sensing performance by either modifying the sensing material e.g. embedding nanoparticles, or modifying the structure of sensing material e.g. introducing porosity, all without changing the structure of the basic SAW device. Therefore the objective of the thesis is to improve the sensitivity of SAW sensors by introducing structural changes in the basic SAW device, complementing the current research.

The thesis mainly focuses on the investigation of the structural changes in conventional SAW one-port resonator for sensing application leading to higher sensitivity. Two structural changes are proposed, i) introducing trenches between the IDT fingers, ii) adding high aspect ratio structures.

The first major contribution of the thesis is the analysis of one-port SAW resonator with a trench made in the space between each IDT finger pair and its application in gas sensing by coating the sensing material inside the trench. Finite element (FE) analysis of the proposed device shows that the resonance frequency of the device decreases with increase in trench depth. The maximum change in frequency with respect to change in trench depth is observed at a particular trench depth of about 0.14λ for YZ $LiNbO_3$ piezo-substrate. The simulations using the proposed structure with trench depth of 0.14λ are carried out for the detection of DMMP and H_2 gases using BSP3 polymer and Pd metal sensing film placed at the bottom of the trench. An increase in resonance frequency is observed in proposed devices, while the conventional devices have shown decrease in resonance frequency for the same

concentrations of gases. The detailed analysis of individual effect of change in density and thickness of sensing film due to absorption of gas in the proposed devices has revealed that the swelling of sensing film in the trench due to absorption of gas decreases the effective trench depth and leads to increase in resonance frequency. For sensing DMMP gas, a sensitivity of approximately 35 kHz/mg/m^3 is shown in proposed device and is about 14 times greater than that of conventional device.

The second major contribution of the thesis is the study of one-port SAW resonator with high aspect ratio (HAR) structures and its application in gas sensing by coating the sensing material in the space between the HAR structures. Two types of HAR structure are investigated, i) using thick nickel IDT fingers and ii) using SiO_2 HAR structure over each IDT finger. FE simulations of the proposed devices show that the resonance frequency of the device decreases with increase in height of HAR structures and the change in frequency is maximum at a particular height of about 0.1λ for nickel IDT and 0.19 λ for SiO_2 HAR structures. The simulations using the proposed structure with optimized height for the detection of DMMP and H_2 gas are carried out using SXFA and Pd sensing films placed in the space between HAR structures. In both the devices, an increase in resonance frequency is observed while conventional devices have shown decrease in resonance frequency for the same concentrations of gas. The detailed FE analysis into the underlying mechanism shows that the swelling of sensing films due to absorption of gases decreases the effective height of HAR structures in the proposed device and leads to increase in resonance frequency. For sensing DMMP gas, the sensitivity observed is approximately 5.64 kHz/mg/m^3 for thick nickel IDT structure and 6.15 kHz/mg/m^3 for SiO_2 HAR structure.

The third major contribution of the thesis is the fabrication of one-port SAW resonators with SiO_2 HAR structure followed by experimental validation of potential application in sensing gases. A batch of fabricated devices is used to detect H_2 gas with Pd sensing film deposited between SiO_2 HAR structures. Experimental results show an increase in resonance frequency with increase in concentration of H_2 gas as predicted in simulations. A sensitivity of 30 kHz/% corresponding to 3 Hz/ppm of H_2 gas is obtained from the experiment. Another batch of fabricated devices is used to detect TCE vapor with PIB sensing film coated between SiO_2 HAR structures. The experiments have shown increase in resonance frequency of the device in the presence of TCE vapor. Thus it is experimentally confirmed that in proposed devices the resonance frequency increases with absorption of gas, in contrast with conventional SAW devices which show decrease in frequency, and the mechanism behind the unusual behavior exhibited by proposed devices has been explained above which is supported by elaborate simulations.

Acknowledgment

I express my deepest and most sincere gratitude to my PhD advisor Prof. Harshal B. Nemade for his guidance, help and encouragement throughout my research work. I greatly admire his attitude towards research and creative thinking. His insightful feedbacks have helped me greatly in improving myself scientifically and personally.

I am thankful to the members of my doctoral committee, Prof. Ratnajit Bhattacharjee, Prof. Roy paily and Prof. K. S. R. Krishna Murthy for their support, encouragement, and suggestions rendered during my research work. My special thanks to the technical staff of the Department of Electrical and Electronics Engineering for their support in various tasks.

I am highly thankful to Indian Nanoelectronics User Program (INUP), and Centre for Nano Science and Engineering (CeNSE), IISc., Bangalore, for providing the fabrication facility to carry out my experimental work. I would like to thank Dr. Sanjiv Srivastav, INUP coordinator for his tremendous help during my stay at IISc, Bangalore.

I offer my gratitude to Mr. Thomas T. Daniel for his sincere effort and precious time to execute my project. My special thanks to Dr. Ramakrishnan, Dr. Ashish, Mandar, Dr. Sai Krishna Santosh, Dr. Basudeba, Dr. Shyam, Dr. Jitendra, Sushanta , Namami and Ujjwol for their help, support, and all the useful technical discussions.

I would like to thank Dr. A Rajesh, Dr. Tony Jacob, and other faculty members of the Department of Electronics and Electrical Engineering, IIT Guwahati, for their care and support. I would also like to acknowledge the help and support given by Dr. Benny George K, Dr. Ganesh Natarajan, Dr. Suresh Kartha and Dr. Vibin Ramakrishanan.

I am thankful to my friends Vasudevan , Aswathy , Hrishikesan , Vijith Kumar, Anoop, Sajith, Dileep, Amurtha, Suvin, Rouf, Piyoosh , Arun Mathew, Vishnu, Dr. Jiss, Dr. Sandeep , Dr. Haris, Lijiya, Dr. Govind and to all the research scholars of Control and Instrumentation laboratory for their help and support. I am extremely thankful to Mrs. Leena Nemade for the care and support given to me during my stay at IITG. I would like to thank my friends from the entire Malayalee community at IITG and the church members for their love and support.

My acknowledgment would be incomplete without mentioning the contributions of 56 club towards successful completion of my Ph.D. journey. I would like to thank my entire 56 group, playing 56 with you all has been one of the most enriching experiences of my life.

Last but not the least, my deepest gratitude and thanks to my family, my parents T. P. Lukose, Shina Lukose, my sister Vineetha and my brother Eldho for their unconditional love, support, and encouragement throughout my studies. Alice, word fall short to describe your sacrifices. Your love and support is what kept me going during the most difficult phases of this thesis.

Vivek Lukose

List of figures

List of tables

List of abbreviations

BAW	Bulk Acoustic Wave
BSP3	Fluorinated bisphenol-containing polymer
COM	Coupling-of-Mode
DI	Deionized
DMMP	Dimethyl methylphosphonate
DOF	Degrees of Freedom
FBAR	Thin Film Bulk Acoustic Resonator
FE	Finite Element
FEM	Finite Element Method
FPW	Flexural Plate Wave
GUI	Graphical User Interface
HAR	High Aspect Ratio
IDT	Interdigital Transducer
INUP	Indian Nano Users Program
IPA	Isopropyl Alcohol
ITO	Indium Tin Oxide
LB	Langmuir-Blodgett
LOD	LOD Limit of Detection
LW	Love Wave
MEMS	Micro Electro Mechanical System
MFC	Mass Flow Controller
PBD	Pyrrolobenzodiazepine
PDMS	Polydimethylsiloxane
PECH	Polyepichlorhydrine
PECVD	Palsma Enhanced Chemical Vapor Deposition
PEI	Polyethyleneimine
PIB	Polyisobyutelene
QCM	Quartz Crystal Microbalance
RF	Radio Frequency
RFID	Radio Frequency Identification
R-SAW	Rayleigh Surface Acoustic Wave
SAW	Surface Acoustic Wave
SH	Shear Horizontal

SH-APM	Shear Horizontal Acoustic Plate Mode
SH-SAW	Shear Horizontal Surface Acoustic Wave
SLPM	Standard Liter Per Minute
STW	Surface Transverse Wave
SXFA	Fluoroalcholpoly siloxane
TEA	Triethanolamine
TSM	Thickness Shear Mode

Contents

List of symbols

T	Time period
p	IDT finger pitch
t	Time
v	SAW phase velocity
v_0	Free surface SAW phase velocity in substrate
λ	SAW wavelength
f_r	Synchronous or resonance frequency
D_{ij}	Electric displacement
k	Wave number
N_p	Number of IDT finger pairs
N_r	Number of reflector strips
r_s	Reflection coefficient of one strip
A_i	Amplitude of waves
ω	Angular frequency
a_0	Amplitude of step response
G_0	Admittance of SAW transmission lines
C_s	Capacitance per IDT finger pair
L	Length of transducer
Δf	bandwidth at half of the peak-conductance
P_R	Mean power density of transported by the wave
θ	Periodic section transit angle
R_0	Mechanical impedance
C_s	Electrode capacitance per electrode (static)
j	Imaginary unit
ϕ	Turns ratio of an acoustic-to-electric circuit transformer
C_T	Total capacitance of IDT
$G_a(f)$	Radiation conductance
$B_a(f)$	Susceptance
α	Transduction coefficient
ε	Permittivity
C_f	Interdigital capacitance in one transduction period

κ	Reflection parameter
P_{11} and P_{22}	Reflections coefficients of IDT in P-Matrix
P_{12} and P_{21}	Transmission coefficients of IDT in P-Matrix
P_{13} and P_{23}	Excitation coefficients of IDT in P-Matrix
P_{31} and P_{32}	Current generated by the wave arriving at acoustic ports of IDT
P_{33}	Admittance of IDT in P-matrix
S	Strain
T	Stress
V_{in}	Input electric potential to IDT
V	Scalar electric potential
$\mathbf{u}$	SAW particle displacement
u'_i	Particle velocity of SAW along i direction
$T_{ij(mech)}$	Stress due to mechanical strain
$T_{ij(elec)}$	Stress due to electric field
ε_{ij}	Permittivity tensor of dielectric medium
c^E_{ijkl}	Stiffness tensor for constant electric field
S_{ij}	Strain components
ε^s_{ij}	Permittivity tensor for constant stress
E_j	Electric field vector
ρ	Material density
k_1 and k_2	Material constants of the substrate
h	Height of sensing film
$\mathbf{E}$	Electric field
$\Delta\gamma/k_0$	perturbation in the complex wave propagation factor per wavenumber
$\Delta\alpha/k_0$	change in attenuation per wave number
c	SAW-film coupling parameter
ρ_p	Polymer film density with absorption of gas
G and K	Shear and bulk modulus
c_v	Concentration of gas
ρ_0	Density of polymer film without absorption of gas
ρ_v	Density of targeted gas

k	Partition coefficient
k_o	Unperturbed wave number
u_l,	Displacements at left side of boundaries
v_l	Potentials at left side of boundaries
u_r	Displacements at right side of boundaries
v_r	Potentials at right side of boundaries
Γ_{Right}	Denotes right side boundary of the SAW resonator geometry
d	Depth of trench
f_0	Free surface resonance frequency
Q_r	Quality factor at resonance frequency
Δf	Bandwidth at half of the peak-conductance
h_p	Polymer film thickness with absorption of gas
h_{SiO2}	SiO_2 HAR height
α_p	Transaction coefficient per period of fingers
γ	Attenuation per period of IDT fingers
v_f	Free surface SAW phase velocity
v_m	Metallized surface SAW phase velocity
ρ_0	Density of polymer film
S_{11}	Scattering parameter (return loss)
K^2	Electromechanical coupling coefficient
x_i	Co-ordinate axis (i = 1, 2, 3)
Z_o	Acoustic impedance
V_{in}	Input voltage to IDT
V_o	Output voltage from IDT

1

Introduction

The Surface acoustic wave (SAW) devices are one of the major parts in the microelectromechanical system (MEMS) industry. SAW devices have been used in commercial application since the 1970's [1]. Due to their versatility and efficiency in controlling and processing electrical signals and their compactness and low cost, SAW devices are popular in electronic industries [2]. The concept of Rayleigh SAW, was described by Lord Rayleigh in 1885 and he analyzed surface waves in solids [3]. The SAW devices on piezoelectric substrate were first developed by White and Voltmer in 1965 and the devices involved generating and receiving of a surface wave on piezoelectric medium using interdigital transducers (IDTs) [4].

In 1970's the SAW devices were primarily used in pulse compression filters for radar systems [1]. In 1980's and 1990's SAW devices found useful in convolvers, bandpass filters, resonators, oscillators and matched filters [5]. Due to their low insertion loss, small size and high operating frequency, SAW devices have applications in instrumentation, signal processing and communication that include satellite receiver, remote control with keyless entry system, radio frequency identification (RFID) television set, mobile phones and actuators [6].

In 1990's, there has been a tremendous growth in research in SAW devices for sensing applications. The SAW devices have been used in wide range of physical, chemical and biochemical sensors for sensing gas, temperature, pressure, torque, force, displacement, vibration, acceleration etc. In last two decades, the advances in SAW sensors have been made to allow sensing in harsh environment applications, where the sensor has to withstand severe conditions related to radiations, electromagnetic fields, temperature, pressure and toxicity. There is always a need for SAW sensors with improved sensitivity, selectivity, repeatability, limit of detection (LOD) and stability. It can be achieved by using proper materials and improving device design and fabrication techniques. This thesis mainly focuses on improving sensitivity of SAW devices for sensing applications by introducing structural changes in conventional SAW devices. The thesis includes design of the new structures, simulation of the

new structures, optimization of the structure based on analysis of simulation results, simulation of proposed devices for gas sensing, comparison of sensor response with conventional SAW devices, and fabrication and testing of proposed SAW device for sensing gases.

1.1 Introduction to acoustic wave devices

Acoustic wave devices have been employed in wide range of applications such as filters, resonators, sensors, and actuators. Acoustic wave devices are mainly based on the propagation of sound waves through an elastic medium. Acoustic waves can be generated by using pulsed laser, ultraviolet beam, magnetic field and electric field [7, 8]. Electric field applied on a piezoelectric material is widely used for the generation of waves [9]. Depending upon the propagation mode, acoustic wave devices are mainly classified into two: Bulk acoustic wave (BAW) devices and SAW devices. In BAW devices, the acoustic wave propagates into the volume of the substrate, and in SAW devices the acoustic wave propagates along the surface of the substrate. An acoustic wave is generated by any impulse disruption of an elastic material. In an elastic material, all the atoms are bound together by strong chemical bonds and exhibit the resistive force, which is linearly related to an applied deformation. When an external force is applied, particles (atoms) are displaced of from their original positions and the resistive force acts to restore the particles to their equilibrium positions causing the generation of acoustic wave in the elastic medium [10]. For a sinusoidal excitation with single frequency, three patterns of particle motion, viz. linear, elliptical and circular polarizations are possible [10].

Acoustic waves can also be classified according to particle displacement relative to either the propagation direction of the wave (longitudinal or transverse) or the devices surface (vertical or horizontal) [11]. In longitudinal or compressional wave the displacement of the particles is parallel to the wave propagation direction as shown in figure 1.1 (a), while in shear or transverse wave the particle displacement is perpendicular to the wave propagation direction as shown in figure 1.1(b). The particle displacement of a vertical wave is normal to the surface of the devices while the particle displacement of horizontal wave is parallel to the surface.

The devices, which generate the vertical waves, are not suitable for liquid sensing applications. When the liquid is in contact with such devices, the wave will radiate into the liquid and form a compressional wave, which causes severe attenuation. Thus, for working in liquid applications, it is necessary to minimize the acoustic radiation into the medium and therefore shear horizontal wave are mostly used.

In general, the acoustic wave devices use piezoelectric material as substrate for the generation of acoustic waves. The types of acoustic wave generated in piezoelectric material mainly depends on substrate material properties, crystal cut and structure of the electrode used in transducers [11, 12]. Most commonly used types of acoustic wave for sensing applications are Thickness Shear Mode (TSM) acoustic wave used in QCM devices, BAW used in Thin Film Bulk Acoustic Resonator

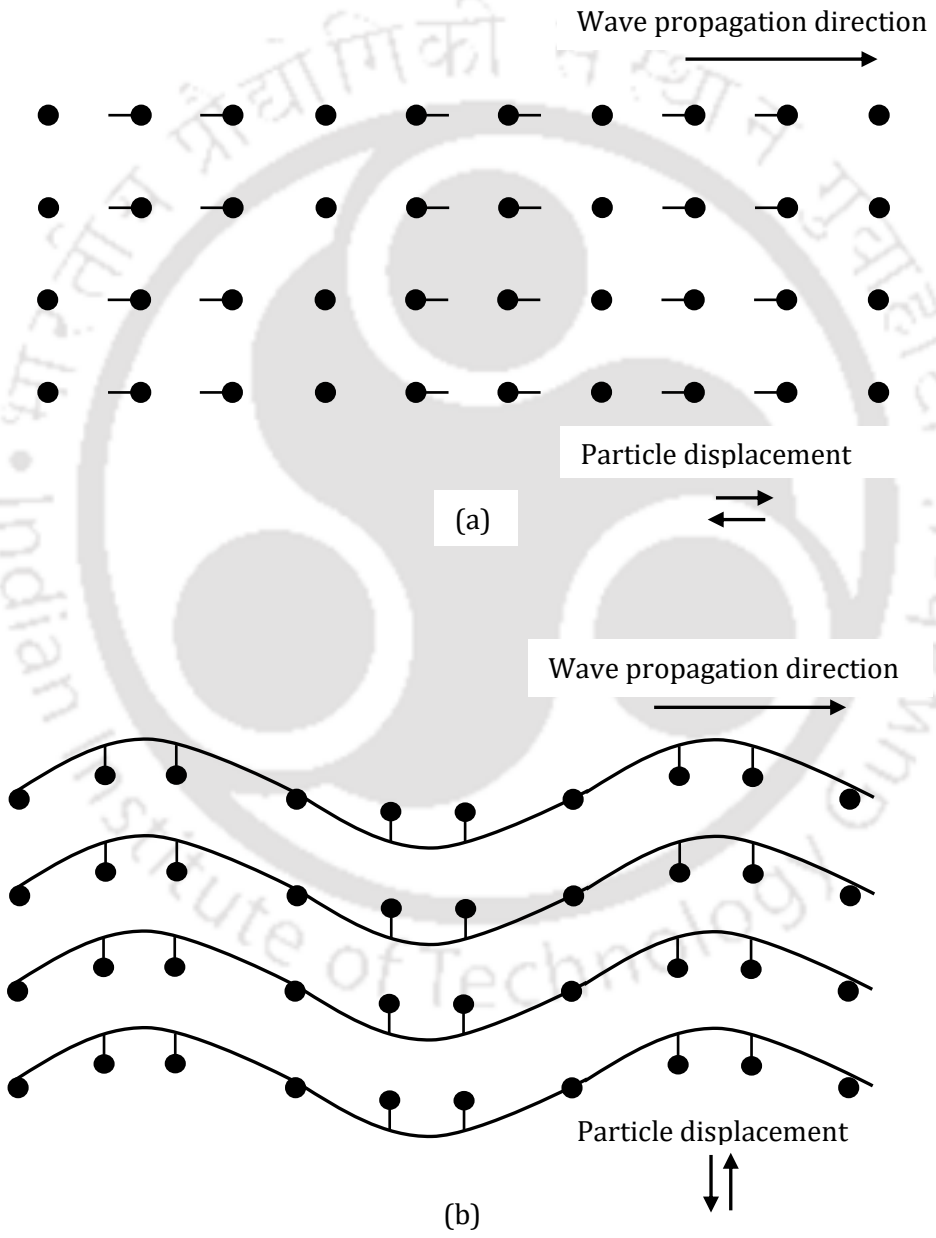

Figure 1.1 Schematic of acoustic wave propagation for (a) longitudinal or compressional wave, (b) shear or transverse wave.

(FBAR), Rayleigh wave (R-SAW), Shear Horizontal Wave (SH-SAW), Love Wave (LW), Surface Transverse Wave (STW), Shear Horizontal Acoustic Plate Mode (SH-APM) wave and Flexural Plate Wave (FPW) [13]. The QCM and FBAR devices are classified as BAW devices and the others are classified as SAW devices. The limitation of BAW devices is that the sensitivity of the devices depends upon the thickness of piezoelectric substrate. The higher the frequency of operation, thinner is the crystal and more difficult to work with [14].

SAW is an acoustic wave, which concentrates most of the energy at the surface of solid. Rayleigh wave is a type of SAW and is a two-dimensional wave confined to the surface of solid down to depth of about one wavelength. In Rayleigh wave, the particles have both surface normal and surface parallel components with respect to the direction of wave propagation. A schematic of Rayleigh wave with particle displacement and propagation is shown in figure 1.2. For a wave propagating from left to right, the movement of particles at the top surface is

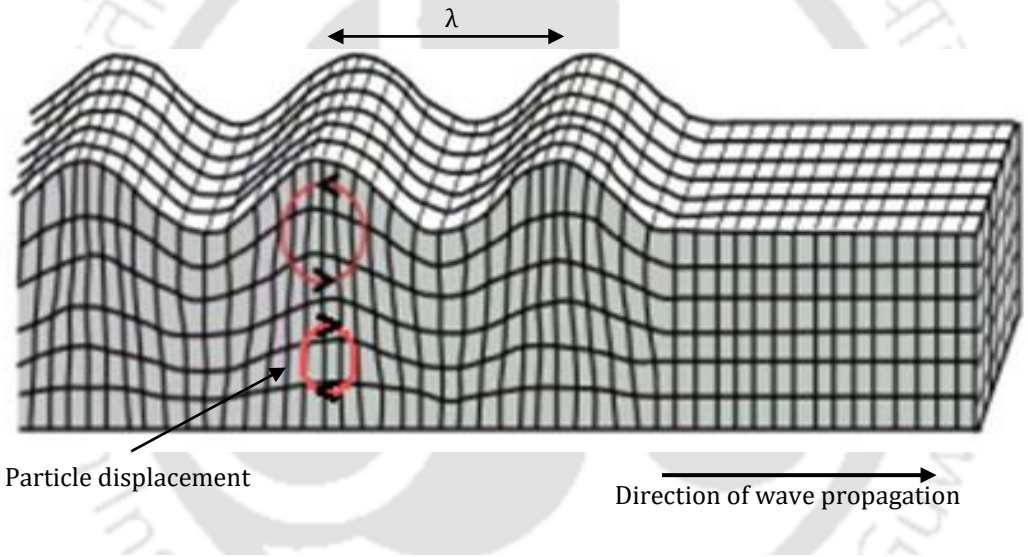

Figure 1.2 Schematic of Rayleigh wave propagation in perturbed medium, adapted from *www.acoustic.org.*

elliptical in anticlockwise direction that reverses along the depth of a wavelength of the medium.

Since the wave propagation characteristics are highly sensitive to perturbation along the propagation path, SAW devices can be designed as sensors exhibiting high sensitivity towards small variations in the surrounding medium. The change in characteristics of the acoustic wave propagation path results in modification of the wave velocity and amplitude, and can be measured as change in frequency, phase and attenuation in the device.

1.2 Generation of SAW in piezoelectric medium

The ability of a piezoelectric material to convert electrical energy to acoustic energy and vice versa allows the generation and detection of acoustic waves. The principle of piezoelectricity is explained in chapter 2. For the generation of SAW in piezoelectric medium an electric field is applied to piezoelectric substrate by using interdigitated transducers (IDTs). An IDT is thin metal film pattern of interlocking fingers deposited onto the surface of the piezoelectric substrate as shown in figure 1.3(a). The thin metal film pattern is made by using photolithography. By applying an electric filed across the fingers of the IDT, stresses are generated at the surface of the piezoelectric substrate. The stress developed due to compression and expansion of the substrate causes the acoustic wave to be launched and

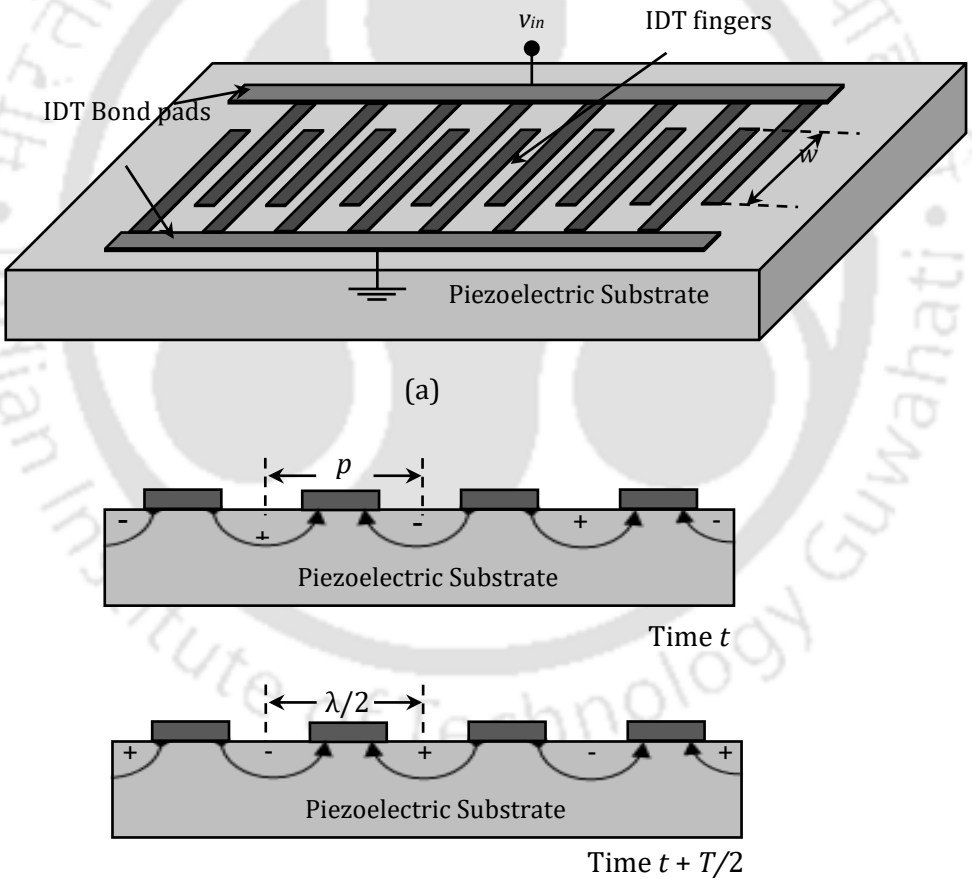

Figure 1.3 (a) Schematic of interdigital transducer (IDT) with bond pads on a piezo-substrate. (b) Polarities of applied potentials on IDT fingers at time t and at time $t + T/2$.

propagating away from IDT in both directions [15].

When an alternating electric potential is applied to the IDT, deformation is produced in the piezoelectric material at its fingers. If the distance between the fingers (pitch) p equals half the acoustic wavelength which depends upon the frequency of excitation, all the waves produced by fingers constructively interfere with each and produce SAW that propagates outwards from the fingers.

The figure 1.3(b) illustrates the constructive generation of SAW on piezoelectric substrate. When an applied potential is sinusoidal with period T, the wave generated by a pair of IDT fingers travels a distance of half wavelength ($\lambda/2$) in the time interval of half period ($T/2$) with speed of SAW phase velocity. At time ($t + T/2$) the generated wave reaches the neighbor IDT finger pair where it adds constructively with the wave generated during the next half of the input sinusoid [15].

The stress waves generated by each finger pair add constructively with the stress waves generated by other finger pairs in the subsequent cycles of input excitation resulting in resonance. The resonance frequency or synchronous frequency f_R is related to the pitch p of the IDT and SAW phase velocity v as

$$f_R = {}^{v}/_{\lambda} \tag{1.1}$$

$$\lambda = 2p \tag{1.2}$$

where, λ is the acoustic wavelength. The bandwidth of the SAW device is determined by the number of finger pairs in a uniform IDT.

1.3 Basic configurations of SAW devices

The SAW devices consist of IDTs deposited on the surface of piezoelectric substrates such as lithium niobate, lithium tantalite, langasite and quartz. Depending upon the number of IDTs used there are two types of configurations in SAW devices: Delay line and Resonator. In SAW delay line, two IDTs separated by a few wavelengths are fabricated on the substrate. The resonator is again classified into two, one-port resonator and two-port resonators. In one-port resonator, one IDT is used and in two-port resonator, two IDTs separated by small distance are used. The figure 1.4 shows the basic configurations used in SAW devices.

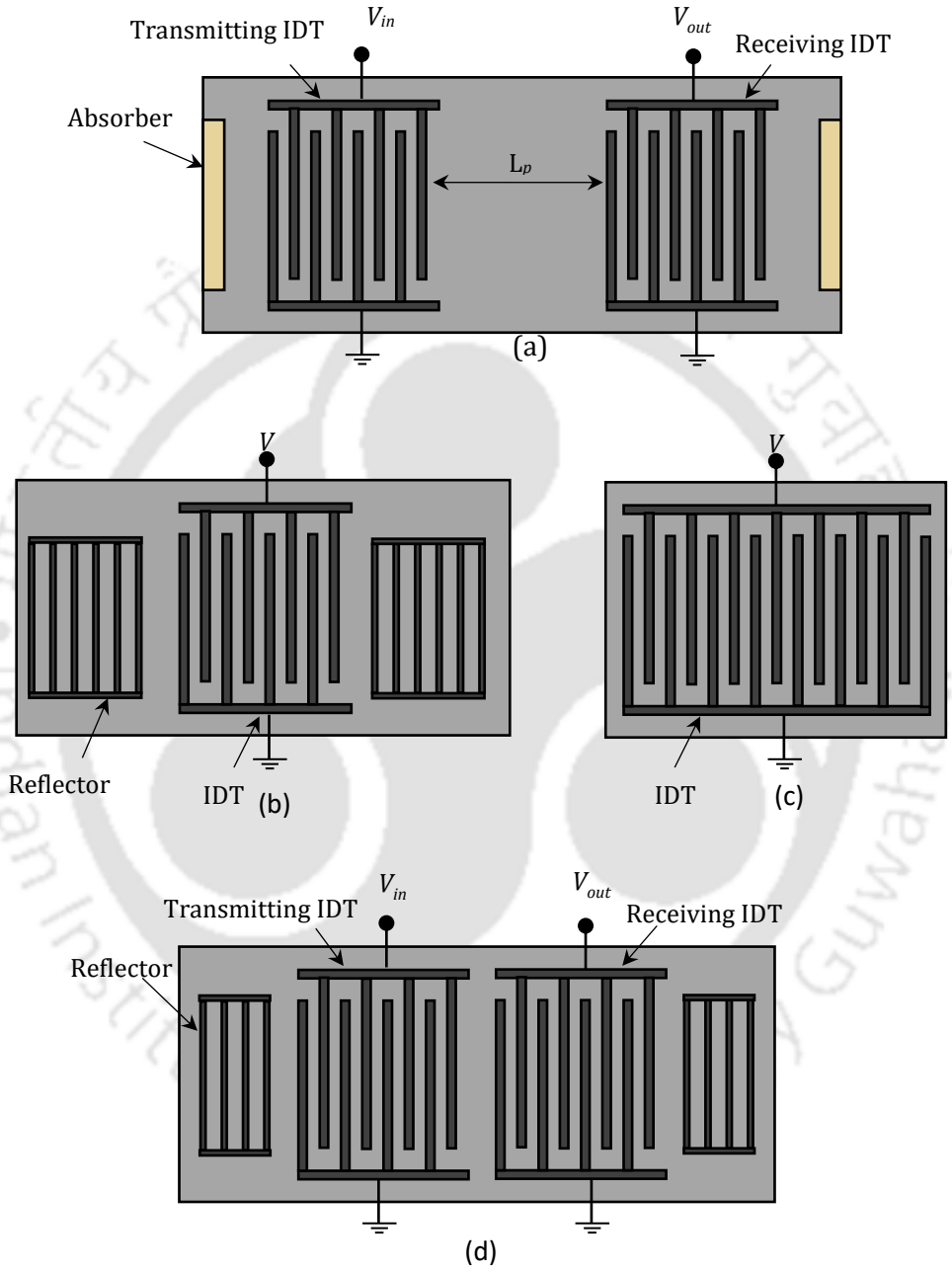

Figure 1.4 Schematic diagrams of different configurations used in SAW devices, (a) SAW delay line device, (b) One-port SAW resonator with reflectors, (c) One-port SAW resonator with long IDT, (d) Two-port SAW resonator with reflectors.

1.3.1 SAW delay line

In SAW delay line configuration, transmitter and receiver IDTs are used. The figure 1.4(a) shows the SAW delay line configuration. The absorber is used at the ends of the device so that wave is absorbed and not reflected back to the IDTs. When an electrical excitation is given to the transmitter IDT, SAW is generated and it travels towards the receiver IDT where it is converted back to electrical signal. The delay time (τ) i.e. time taken by the wave to reach the receiver IDT can be calculated using the relation $\tau = L_p/v_0$ where L_p is distance between the transmitter IDT and receiver IDT and v_0 is the SAW velocity. The important design parameters of the SAW delay line are the periodicity of transducers, number of finger pairs the IDT, IDT center to center distance and acoustic aperture. The frequency response of SAW delay line devices depends upon finger width, spacing between the fingers and acoustic aperture *w*.

1.3.2 SAW resonators

The SAW resonator is similar to the crystal resonator except that only one of the surfaces resonates. The SAW resonator consists of IDT and reflectors. In SAW resonator, the wave propagates within a resonant cavity which is confined to the region between the reflector gratings placed on either side of the IDT, such that wave is reflected back to generating IDT. The reflectors are made of metal strip either shorted or open. Grooves are also used as reflectors. To get the reflections from the individual finger in phase and coherent, the periodicity of the reflector electrode should be equal to half the wavelength [12]. For the surface wave to be completely reflected from the grating, $N|r_s|>1$ where N is the number of reflector fingers and r_s is the reflection coefficient of a finger. Typically, $|r_s|$ is about 2% and the value of N is about 200 or more [12].

SAW resonators are of two types, one-port SAW resonator and two- port SAW resonator. In one-port SAW resonator, bidirectional IDT is fabricated between the two sets of reflectors. The figure 1.4(b) shows a one-port SAW resonator configuration with reflectors. A two-port SAW resonator is similar to one-port SAW resonator except that there are transmitter IDT and receiver IDT separated by a small distance between the reflector gratings. The figure 1.4(d) shows the two-port SAW resonator configuration. The SAW resonator can also be made without reflectors using large number of fingers in IDT, where multiple reflections within the IDT leads to standing wave and resonance at particular frequency. The figure 1.4(c) shows a one-port SAW resonator

configuration without reflectors. In this thesis, one-port SAW resonator configuration without reflector gratings is used as device for sensing gases.

1.4 Operation of SAW devices in sensor applications

When the SAW propagates on the surface of an elastic material, any changes to the characteristic of the propagation path perturb the velocity and amplitude of the wave. Change in velocity can be monitored by measuring the frequency or phase characteristics of the device and can be then correlated to the corresponding physical or chemical quantity being measured. The SAW devices are sensitive to mechanical perturbations, temperature changes and electrical perturbations [16]. The operation of a SAW based sensor consists of three major processes (i) excitation of SAW in piezoelectric medium (ii) modulation of the wave characteristics in the propagation path and (iii) detection of the wave. The excitation and detection of SAW can be achieved by using IDTs whereas the modulation occurs due to the interaction of the wave with physical and chemical parameters. The change in propagation characteristics of the wave can be detected experimentally by measuring frequency, insertion loss or phase of the corresponding output signal.

The SAW devices based on various types of acoustic wave such as Rayleigh wave, Stoneley wave, Shear horizontal (SH), Love wave, Lamb wave and Leakey wave have been used for sensing applications. In Rayleigh wave the particles in the medium are displaced in longitudinal and shear vertical direction, in SH-SAW particle are displaced in horizontal direction. Love wave is horizontally polarized wave observed in layered structure and

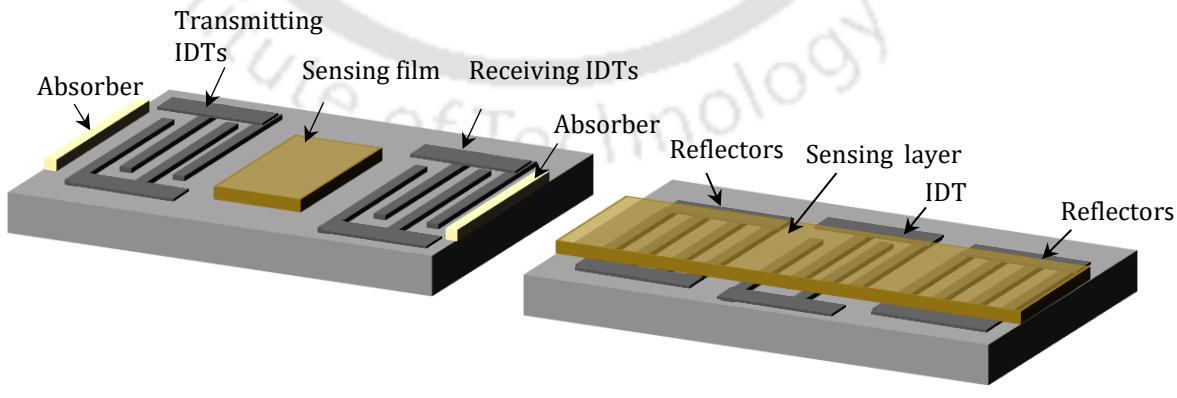

Figure 1.5 Schematic diagrams of conventional sensors based on (a) SAW delay line and (b) One-port SAW resonator

Stoneley wave is vertically polarized wave observed in solid-solid interface. For gas sensing applications, Rayleigh wave is found to be highly sensitive and a large number review papers have been published on Rayleigh wave based gas sensors [17, 18, 19, 20, 21, 22, 23, 24, 25]. The thesis is mainly aimed at improving the sensitivity of conventional Rayleigh wave based SAW sensors by incorporating structural changes, e.g. trenches and high aspect ratio structures in the SAW devices.

Figure 1.5 (a) shows a conventional delay line based SAW sensor. The transmitting and receiving IDTs with a gap are deposited on piezoelectric substrate. The film of sensing material is coated in the region between the IDTs. Based on the length of the region between the IDTs and SAW velocity there will be a delay in time between the input and output signals. The interaction of sensing film with a selective chemical or gas causes change in the properties and dimension of the film and changes the velocity, amplitude and phase of SAW [12]. The change in delay time is measured and is related to concentration of the chemical or gas. Figure 1.5 (b) shows a conventional one-port SAW resonator based sensor. The layer of sensing material is deposited over the entire acoustic path. The interaction of selective chemical or gas with sensing layer causes change in resonance frequency of the sensor and is measured. Compared to delay line, resonators offer smaller insertion attenuation and impedance matching in resonators is less stringent. In addition, small phase change in passband in resonators makes the oscillator design simpler [26]. Therefore, the thesis focuses on one-port SAW resonators and improving sensitivity of sensors based on one-port SAW resonators. The work involves simulations and experimental testing of SAW resonators for sensing application.

1.5 Literature based on SAW Sensors

Several works of literature on SAW sensors (devices with sensing layers) to detect various gases and chemical vapor are available. These sensors work on the principle of perturbation in SAW path due to changes induced by the variation in properties of the sensing layer when it is exposed to the target analyte. SAW sensors based on massloading have been extensively used for the detection of gases such as hydrogen (H_2), ammonia (NH_3), carbon tetrachloride (CCl_4) vapor, carbon monoxide (CO), uranine vapor, alexa vapor, sulfur dioxide(SO_2), nitrogen dioxide (NO_2) and hydrogen sulfide (H_2S). In 1981 Bryant et al. developed a set of SAW sensors to detect SO_2 gas and compared their detection sensitivities with that of a BAW sensor. They observed that SAW sensor was more sensitive (at least an order of magnitude) than corresponding sensor based on BAW [27]. Table 1 shows the list of some SAW sensors from literature for the detection of various gases or chemical vapor.

Table 1.1 List of selected published work in SAW devices for sensing various gases and chemical vapors

No	Transducer	Sensing Medium	Analyte	Sensitivity(S) and LOD	Reference and Year
1	Delay line, YZ $LiNbO_3$	Palladium(Pd)	H_2	LOD=50ppm	Amico et al. [28], 1982
2	Delay line, YZ $LiNbO_3$, 60 MHz	Triethanolamine (TEA), Tungsten trioxide (WO_3)	SO_2, H_2S	LOD=70ppb S=100 Hz/ppm	Bryant et al. [29], 1983
3	Resonator, 109 MHz, ZnO-on-Si	ZnO	Organic vapors		Martin and Schweizer [30], 1984
4	Delay line, YZ $LiNbO_3$	Lead Phthalocyanne (PbPc)	NO_2		A J Ricco et al. [31], 1985
5	Delay line, ST Quartz	Platinum (Pt)	NH_3		Amico et al. [32], 1987
6	Delay line, YZ $LiNbO_3$	Tungsten trioxide (WO_3)	H_2S	LOD < 10ppb	Veletino et al. [33], 1987
7	Delay line, ZnO/SiO_2/Si	Copper phtalocyanine (CuPC)	NO_2	S =200 Hz/ppm	Nieuwenhuizen et al. [34], 1989
8	Delay line, 41 MHz, $LiNbO_3$	Tungsten trioxide (WO_3)	H_2S		Falconer et al. [35], 1990
9	Resonator and delay line, ST-Quartz	Langmuir-Blodgett (LB) film of poly(vinyl tetradecanal)	Organic vapors	S=32.3 Hz/(ng/cm^2)	J. W. Grate and M. Klusty [36] 1991
10	Delay line, YZ $LiNbO_3$	Polyisobyutelene (PIB)	CCl4 vapors	LOD=300ppm	Pfeifer et al. [37], 1994
11	Delay line, 54 MHz, $LiTaO_3$	CdS	SO_2	LOD=200ppb	Lee et al. [38],1998
12	Delay line, 42 MHz, YX $LiNbO_3$	Langmuir-Blodgett (LB) coated polypyrrol	NH_3		Penza et al. [39], 1998

13	Two-port resonator, 250 MHz, ST Quartz	N,N-bis_(p-methoxybenzyidene) -α-α'-bi-p-toluidine (BMBT),Polyethyleneimine (PEI),Versamid 900	CO_2 and Humidity	S=5.7 kHz/% change in humidity	Korsah et al. [40], 1998
14	Delay line, 363MHz, Y-Z $LiNbO_3$	SnO_2, Polyepichlorhydrine (PECH)	CH_4,NO_2, Toluene		Beck et al. [41], 1999
15	Delay line, 131MHz, AT cut Quartz	Triethanalamine (TEA)-boricacid composite	SO_2	S=200 Hz/ppm	Qin et al. [42], 2000
16	Two-port resonator, 250MHz, ST Quartz	Antibodies	Uranine vapors, Alexa vapor		Stubbs et al. [43], 2002
17	Delay line, 700MHz, AIN	Imprinted polymers, polyurethane	Benezene, Toulene, p_Xyelene, ethane, butane and propoane		Bender et al. [44], 2003
16	Delay line, 100MHz, 128° Y-X $LiNbO_3$	L-glutamic hydrochloride	NH_3	S=0.476 ppm/ppm	Shen et al. [45], 2004
18	One-port and two-port resonator, 433.92MHz, ST-quartz	Bisphenol	DMMP	LOD=0.1 ppm	Nimal et al. [46], 2006
19	Delay line, 39.6–264 MHz, ST-X Quartz	PIB, PECH, PDMS, PBD, PIP	Nerve agent simulant (DMMP)		Joo et al. [47], 2007
20	Delay line, 286MHz, 128° X-Y $LiNbO_3$	Single walled carbon Nano tube	CO_2		Sivaramakrishan et al. [48], 2008
21	One-port resonator, 434 MHz, Quartz	polymethyl[3-(2-hydroxy)phenyl] siloxane (PMPS),	DMMP	S=3 kHz/ppm	Du et al. [49], 2008

22	Delay line, 100 MHz, ST-X Quartz	SXFA, OV25, PECH	DCP, DMMP		Alizadeh and Zeynali [50],2008
23	Resonator and delay line, Quartz, $LiNbO_3$ and ZnO/glass	Drop-dried polymers	TNT,DNT, Sarine and DMMP		Nimal et al. [51], 2009
24	Delay line, 102MHz, 36° YX $LiTaO_3$	Graphene nano sheets	H_2 and CO		Arsat et al. [52], 2009
25	Dual track SAW device, 101.76MHz, 128° XY $LiNbO_3$	WO_3	NO_2		Wen et al. [53], 2010
26	Delay line, 200 MHz, ST-X Quartz	PIB, PDMS, PECH, PEI	VOCs, DMMP, DNT, TNT		Jha and Yadava [54],2010
27	Delay line, 42MHz, 128° YX $LiNbO_3$	Multiwall carbon nanotube	SF6	7.4 kHz/ ppm	Wen et al. [55], 2011
28	Delay line, 440MHz, 41° YX $LiNbO_3$	Teflon AF2400, Indium tin oxide (ITO)	CO_2, NO_2	S=2.12◦/ppm for CO2 and 51.5◦/ppm for NO2	Lim et al. [56], 2011
29	Delay-line, 157 MHz, ST-X quartz	PECH, PIB, PEM, carbowax	DMMP, DCE, VOCs		Matatagui et al. [57], 2011
30	Two-port resonator, 433MHz, ST-X Quartz	Zinc oxide (ZnO)	VOC		Tasaltin et al. [58], 2012
31	Delay line, YX $LiNbO_3$	InO_x	H_2		Wang et al. [59], 2012
32	One-port resonator, 433.9 MHz, ST-X Quartz	ZnO, TeO_2, SnO_2, and TiO_2	Chemical Warfare Agents (DMMP)		Raj et al. [60], 2013
33	Delay line, 118.5MHz, 64° YX $LiNbO_3$	Singlewalled carbon nanotube decorated with Cu nano particle	H_2S	LOD=5 ppm	Asad and Sheikhi [61], 2014

34	Resonator, 200 MHz, ST Quartz	ZnO/SiO_2	NH_3		Tang et al. [62], 2014
35	Resonator, 262 MHz, ST Quartz	Graphene	NO_2	S=25 Hz/ppm	Thomas et al. [63], 2014
36	One-port SAW resonator, 433.9 MHz, ST-X Quartz	ZnO, TeO_2, SnO_2, and TiO_2	DMMP and methanol	LOD=100 ppb (DMMP)	Singh et al. [64], 2014
37	Delay line, 70 MHz, Quartz	Nanoporous Pd and ZnO layer	H_2	S=0.31 (pd), S=0.01 (ZnO) LOD=50 ppm (pd), LOD=316 ppm(ZnO)	Viespe [65],2014
38	One-port resonator, 433.9 MHz, ST-X Quartz	ZnO	Nerve agent simulant		Raj et al. [66], 2015
39	Delay line, 434MHz, YZ $LiNbO_3$	Fluoroalcholpoly siloxane (SXFA)	DMMP	S=20.1°/(mg/m^3), LOD<0.5 mg/m^3	Xu et al. [67], 2015
40	Delay line, 300 MHz, ST-X Quartz	Fluorinated bisphenol-containing polymer (BSP3)	DMMP	LOD=0.004 mg/m^3 S= 3.09 kHz/mg/m^3	Wang et al. [68]. 2015
41	Two-port Resonator, 299.4 MHz, ST-X Quartz	Cryptophane-A	CH_4	S= 204 Hz/%, LOD=0.05%	Wang et al. [69], 2016
42	One-port Resonator, 433.9 MHz, ST-X Quartz	SXFA	Methanol, benzene, diesel, DMMP		Singh et al. [70], 2016

43	Delay line, 99.8MHz, 128° YX $LiNbO_3$	Bi-layer structure SnO_2 with Pd nanoparticle layer	H_2	S=57.9 Hz/ppm (115.9 kHz towards 2000ppm of H_2 @175°c)	Yang et al. [71], 2017
44	Resonator, 99.5MHz, ST-Quartz	ZnO thin film	NO_2		Rana et al. [72], 2017
45	Delay line, 69.5MHz, Quartz	Pd/ZnO bi-layer	H_2	S =0.51 Hz/ppm, LOD=59 ppm	Viespe and Miu [73], 2017
46	Delay line, 126.54 MHz, AIN-Si structure	Nanocomposite Pd-graphene	H_2	S=5Hz/ppm (25 kHz for 0.5% of H_2)	Ha et al. [74], 2017
47	Resonator, 392MHz, AIN/Si layered structure	Graphene oxide thin film	Humidity sensor	S=182.51kHz /%RH (at 95%RH)	Le et al. [75], 2018
48	Resonator, 69MHz, ST -quartz	PZT thin film	NO_2	S= 9.6 Hz/ppm	Rana et al. [76], 2018
49	Resonator, 69MHz, ST -Quartz	Fe_3O_4 nanoparticles embedded in a polyethylenimine polymer	Ethanol	LOD=65ppm	Viespe and Miu [77], 2018
50	Two-port resonator, 69.5MHz, ST-X Quartz	Nanoporous bilayer Pd/WO_3 films	H_2	S=0.13 Hz/ppm, LOD=4540 ppm	Miu et al. [78], 2018

1.6 State-of-the-art and motivation

SAW devices with polymer sensing material have gained great importance for sensing and detection of gases owing to their excellent selectivity, high sensitivity, fast response time, linearity, reversibility and stability [77]. From the literature survey given in previous section, it is observed that the initial work on the sensors based on SAW devices is mainly focused on sensing variety of gases by employing appropriate sensing materials, polymers being introduced subsequently.

Recent developments in SAW based sensors are targeted towards improving sensitivity by incorporating nano-scale materials. To improve the sensitivity and LOD of the device, researchers have modified the sensing material by employing bi-layer nanofilms, nanostructures, nanoporous films and nanoparticles into polymers. Viespe [65] developed and investigated nanoporous films of Pd and ZnO in SAW delay line sensors for sensing hydrogen at room temperature. For a concentration between 0.2 – 0.8 % hydrogen/synthetic airs, the response time was 15 – 44 s and 6 – 27 s and LOD was 50 ppm and 315 ppm for Pd and ZnO, respectively. Wang et al. [59] developed a hydrogen sensor using SAW delay line covered by sensing layer of InO_x with nanograins obtained using RF diode sputtering and reported improved response of 11.83 kHz frequency shift at 400 ppm hydrogen gas at room temperature. Tang et al. [62] fabricated and characterized an ammonia gas sensor based on SAW resonator having ZnO nanofilm deposited on a nanofilm of silicon dioxide (SiO_2) obtained from sol-gel process giving porous ZnO top layer. The sensor exhibited a frequency shift of 2 kHz towards 30 ppm of ammonia gas with good repeatability and stability. Viespe and Miu [77] developed a SAW resonator sensor for volatile organic compounds using sensing layer of nanocomposite of Fe_3O_4 nanoparticles embedded in a polyethylenimine polymer, and reported up to five times improvement in LOD after embedding nanoparticles in the polymer.

From the literature survey on SAW based gas sensors given above, it is noted that all the sensors use conventional SAW devices and the improvement in sensing performance is achieved by modifying either the sensing material or the structure of sensing material. However, these studies include no changes in the basic structure of the SAW device, and use SAW devices, either delay line or resonator, having conventional construction shown in figure 1.4. Therefore it motivated us to investigate on introducing structural changes in the basic SAW device and its effect on the performance of the modified SAW device for application in gas sensing.

1.7 Problem definition

As discussed in the previous section, the research work in this thesis is aimed at introducing structural changes in the conventional SAW devices and study the performance of the modified SAW devices when employed in gas sensing. Two main structural changes in SAW devices are investigated. In the first structure trenches are made in the space between the IDT fingers and the sensing material is placed inside the trench. The second structure employs high aspect ratio (HAR) structures on the active surface and the sensing material is placed in the space between HAR structures. Finite element simulations on the proposed SAW devices are performed to analyze and optimize the design parameters and check the performance of

the proposed devices for use in gas sensing. To validate the simulation results, one-port SAW resonators having SiO_2 HAR structures built on IDT fingers with sensing film coated in the space between HAR structures are fabricated and experiments are performed to test their applicability for sensing gases.

The main objectives of the thesis are as follows.

- To perform FE simulations to analyze one-port SAW resonator with trenches made in the space between IDT fingers, optimize design parameters and demonstrate the proposed structure for gas sensing application by placing sensing material at the bottom of the trench.
- To analyze, using FE simulations, one-port SAW resonator with thick IDT fingers as HAR structures, optimize IDT thickness and demonstrate the application of the device for gas sensing by depositing sensing material in the space between thick IDT fingers.
- To perform FE simulations to analyze one-port SAW resonator with SiO_2 HAR structure made over each IDT finger, optimize SiO_2 height and demonstrate the application of the device in sensing gases by placing sensing material in the space between IDT fingers.
- To fabricate proposed one-port SAW resonators having SiO_2 HAR structures with sensing film placed in the space between HAR structures and validate experientially the use of proposed device for sensing gases.

1.8 Scope of the thesis

The scope of the thesis is limited to the investigation of proposed SAW devices having structural changes introduced in conventional devices for application in gas sensing. It includes simulations of the proposed devices to determine optimal design parameters and to demonstrate their application for sensing gases, and fabrication and experimental validation of the proposed devices for application in gas sensing. The objective of the research work is not to develop a particular gas sensor but to contribute new structures of SAW devices based on which variety of sensors can be developed.

1.9 Organization of thesis

In chapter 2, we introduce basics of piezoelectricity and the SAW devices, and discuss various modeling techniques such as equivalent circuit method, coupling of modes (COM) model, P-matrix approach and impulse response method and finite element method (FEM). 2D FE simulation of one-port SAW resonator using Y cut Z propagating lithium niobate (YZ $LiNbO_3$) substrate generating Rayleigh wave is carried out by optimizing the mesh and applying

appropriate boundary conditions. The free surface velocity, metalized surface velocity, electromechanical coupling coefficient, admittance, and Q factor for YZ $LiNbO_3$ substrate are calculated. The sensing mechanism used in SAW gas sensor is explained.

Chapter 3 presents the simulation of a one-port SAW resonator with trenches made in the space between the IDT fingers and its application in gas sensing. The FE analysis of proposed SAW one-port SAW resonator is discussed. The effect of trench depth on the resonance frequency of the device is studied. The effect of sensing film thickness on sensor response is discussed. Results of FE simulations of proposed device structure for sensing dimethyl methylphosphonate (DMMP) and H_2 gases using BSP3 polymer and Pd metal as sensing materials are presented, and the reasons for increase in sensitivity compared to a conventional SAW gas sensor are discussed.

Chapter 4 presents the simulation of one-port SAW resonator with HAR structures and its application in gas sensing. Various aspects pertinent to the proposed SAW devices, viz. structure height, thickness of sensing film, IDT materials and individual effect of mass loading and thickness of sensing film on sensor response are studied. The FE simulation results of proposed SAW structure with SXFA and Pd sensing film placed in the space between HAR structures for sensing DMMP and H_2 gases are presented, and the reasons for increase in sensitivity compared to a conventional SAW gas sensor are discussed.

Chapter 5 describes design and fabrication of one-port SAW resonator having silicon dioxide (SiO_2) HAR structure for sensing gases. The fabrication process, experimental setup, measurement techniques and results on proposed SAW one-port resonator with SiO_2 HAR structure for sensing gases are discussed. An increase in resonance frequency of the proposed device with increase in concentration of gases is observed. Validation of experimental results with FE simulation of the proposed SAW one-port resonator structure is carried out.

Chapter 6 lists the conclusions of the research work and recommendations for future work.

2

Modelling and simulation of one-port SAW resonator

Modelling and simulation of devices along with fabrication facilitated the development of modern SAW devices. The modelling and fabrication of the IDT on the piezoelectric substrate are the key factors in making SAW devices and several methods of modelling such as delta function method, impulse response method, equivalent circuit method, coupling-of-mode (COM) method, and P-matrix method [11, 15] can be used to describe the function of IDT fabricated in a SAW device. The simulation using finite element method (FEM) is used to analyze the SAW device response. This chapter presents a brief description about the fundamental of piezoelectricity, various modelling techniques and FEM used for SAW devices. The chapter also presents the 2D finite element (FE) simulations of a conventional one-port SAW resonator using COMSOL Multiphysics and the results are discussed.

2.1 Basics of piezoelectricity

A solid is said to be an elastic when it deforms by an applied external force and returns to its original form when the force is removed. The forces like mechanical, electrical, magnetic and thermal forces can be employed for the generation of elastic waves in an elastic medium. The material in which stress varies linearly with the applied electric field is more suitable as the medium for the generation of elastic waves. Elasticity in a solid is concerned with the internal forces within it and displacement in solid from its equilibrium position [15]. The forces are expressed by stress T, while the displacements are expressed by strain S. The particle is an elementary region of a material much larger than the inter-atomic distance and much smaller than any characteristic elastic dimensions such as wavelength. Let us assume that in equilibrium state of solid, a particle is located at point $\mathbf{x} = (x_1, x_2, x_3)$ and displaced by an amount $\mathbf{u} = (u_1, u_2, u_3)$, where, the components u_1, u_2 and u_3 are the general components of coordinates x_1, x_2 and x_3, respectively. Thus the particle has been displaced to a new position $\mathbf{x} + \mathbf{u}$ as shown in figure 2.1. If $\mathbf{u}$ is independent of $\mathbf{x}$, there will be no internal

force since it simply represents displacement of the solid as a whole, and similarly there will be no internal force if the solid is rotated. The strain at each point can be defined as

$$S_{ij}(x_1, x_2, x_3) = \frac{1}{2}\left(\frac{\partial u_i}{\partial x_j} + \frac{\partial u_j}{\partial x_i}\right); \quad i, j = 1, 2, 3 \tag{2.1}$$

Thus the strain is related to the internal forces. The strain is a second rank tensor and symmetrical as $S_{ij} = S_{ji}$. The stress T is defined as internal stress in the material, i.e. force per unit area. The second-rank stress tensor is defined as T_{ij} (x_1, x_2, x_3) and is symmetric, i.e. $T_{ij} = T_{ji}$. According to Hooke's law, each component of stress is given by the linear combination of the strain components and is expressed as

$$T_{ij\,(mech)} = \sum_k \sum_l c_{ijkl} S_{kl} \; ; \quad i, j, k, l = 1, 2, 3 \tag{2.2}$$

where, c_{ijkl} is the fourth-rank stiffness tensor. These elements are the physical properties of the materials under consideration [1]

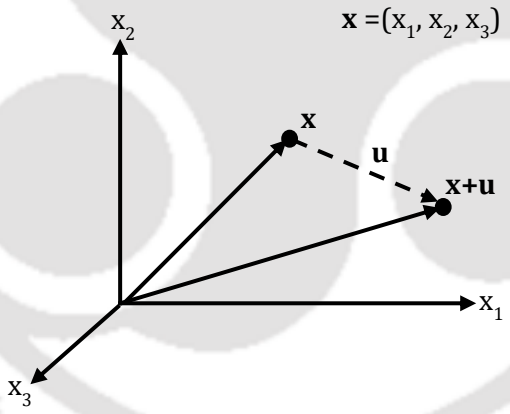

Figure 2.1 Particle positions in equilibrium and in deformed state of a solid body. The deformation of the solid is shown with dashed line [15].

SAW devices utilize the piezoelectricity phenomenon for the generation and detection of the acoustic waves. Pierre & Jacques Curie discovered the piezoelectricity phenomenon in 1880. The piezoelectricity is the ability of certain materials to generate electric charges in response to the applied mechanical stress. The molecular model of a piezoelectric crystal is given in figure 2.2. [79]. Before an external stress is applied to the material, the gravity centers of negative and positive charges of each molecule coincide. Thus

the external effects of the charges are reciprocally cancelled, as a result electrically neutral molecule appears. An external stress to the material deforms the internal structure and causes separation of positive and negative centers of the molecules, resulting in generation of dipoles. Eventually the facing dipoles inside the material are mutually cancelled and the total polarization at the surface of the piezoelectric material is the sum of individual polarizations as shown in figure 2.2 (b).

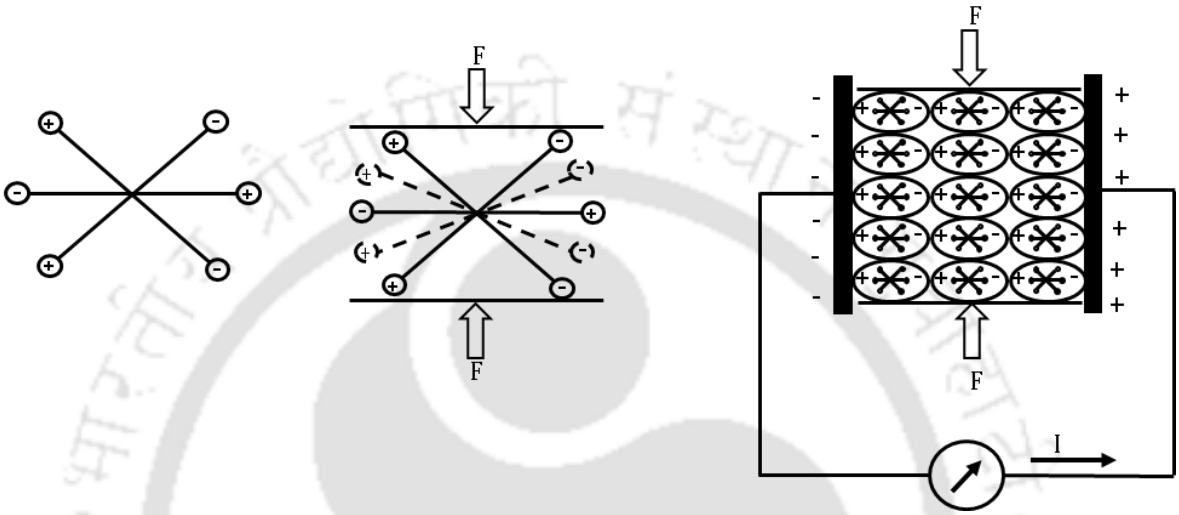

Figure 2.2 Molecular model of a piezoelectric material, (a) An unperturbed single molecule, (b) Molecule subjected to an external force *F*, (c) Polarization effects in the piezoelectric material.

Piezoelectricity occurs only in anisotropic materials whose internal lattice structure lacks a center of symmetry and is defined as a phenomenon which couples the elastic stress and strain to the electric field and displacement [11]. The stress, $T_{ij_{(elec)}}$ produced by the piezoelectric effect is given by

$$T_{ij_{(elec)}} = \sum_k e_{kij} E_k ; \quad i,j,k,l = 1,2,3 \tag{2.3}$$

where electric field $E_k = \frac{\partial v}{\partial x_k}$. Total stress T_{ij} is the sum of stresses due to the electric field and mechanical strain and can be expressed as

$$T_{ij} = \sum_k \sum_l c^E_{ijkl} S_{kl} - \sum_k e_{kij} E_k \tag{2.4}$$

The electric displacement can be expressed by electric field and permittivity tensor ε_{ij} of the dielectric medium. For a piezoelectric material, an additional electric field displacement

caused by the strain is developed due to the piezoelectric effect. The total electric displacement can then be given as

$$D_{ij} = \sum_j \varepsilon_{ij}^S E_j + \sum_j \sum_k e_{ijk} S_{jk} \tag{2.5}$$

where c_{ijkl}^E is the stiffness tensor for constant electric field (N/m^2), S_{kl} is the strain component, e_{ijk} is the piezoelectric tensor relating elastic stress to electric field (C/m^2), ε_{ij}^S is the permittivity tensor for constant stress (F/m), and E_j is the electric field vector (V/m) [11]. The equations (2.4) and (2.5) are known as piezoeletric constitutive relations. If the stress and strain are functions of time and position then Newton's law can be used to express the equation of motion

$$\rho \frac{\partial^2 u_i}{\partial t^2} = \sum_j \frac{\partial T_{ij}}{\partial x_j} \; ; \quad i,j = 1,2,3 \tag{2.6}$$

where ρ is the density, T_{ij} is the stress tensor, u_i is the displacement. In case of piezoelectric medium the speed of the elastic wave is five order less than electromagnetic waves. Hence the quasi static assumptions can be used to express the electric field.

$$E_i = -\frac{\partial V}{\partial x_i} \tag{2.7}$$

Substituting (2.4) in (2.6)

$$\rho \frac{\partial^2 u_i}{\partial t^2} = \sum_j \sum_k \left\{ e_{kij} \frac{\partial^2 \emptyset}{\partial x_j \partial x_k} + \sum_l c^E{}_{ijkl} \frac{\partial^2 u_k}{\partial x_j \partial x_l} \right\} \tag{2.8}$$

Since the piezoeletric material is assumed to be an insulator, there are no free charges, hence div D = 0 and therefore (2.5) is written as

$$\sum_j \sum_k \left\{ \varepsilon^S{}_{ij} \frac{\partial^2 \emptyset}{\partial x_i \partial x_j} + \sum_k e_{ijk} \frac{\partial^2 u_j}{\partial x_l \partial x_k} \right\} = 0 \tag{2.9}$$

The degrees of freedom (dependent variables) are the global displacements u_1, u_2, and u_3 in the global x_1, x_2, and x_3 directions, respectively and the electric potential V, can be obtained by solving equations (2.8) and (2.9) [11].

2.2 SAW device modelling

To obtain the dimensions of the IDT and optimum device performance, SAW devices are modelled using theoretical model or computer aided simulations before the fabrication of the device. For the estimation of SAW device performance and IDT designing, several theoretical models are used such as delta function model, impulse response model, equivalent circuit model, coupling of modes (COM) and P- matrix approach [11, 15, 79]. Using the models various device characteristics such as impedance parameters, admittance, coupling coefficient and bandwidth can be estimated.

2.2.1 Delta function model

The delta function is one of the basic models developed to predict the IDT response in the SAW device. It determines the transfer function of the IDT, giving relative insertion loss as a function of the frequency [15]. In this model, the complex electric field distribution between adjacent fingers of an excited IDT is modeled as a discrete number of delta function sources at the metal finger edges. Each finger has two delta function sources of electric field intensity, with amplitude proportional to the applied voltage. The voltage on the electrode fingers alternate in polarity. The model can be simplified by replacing the two delta sources at the edges of the fingers with one equivalent source at the center of each finger. The model does not consider energy, capacitance, and the electromechanical coupling coefficient of the materials, and cannot predict input/output impedance levels, and harmonic response.

2.2.2 Impulse response model

The impulse response method predicts the absolute amplitude and hence the power of SAW can be determined by considering the energy of the wave [15]. This method provides a deep perception about frequency scaling which is used in determining the apodization quantities for SAW devices. The impulse response is determined using Fourier transform to give the desired frequency response of the device. This model provides an information about the matching networks and circuit impedance which are not considered in delta function model [80, 81].

2.2.3 Equivalent circuit model

The response of SAW device in equivalent circuit model is described using a three-port model as shown in figure 2.3. The port 1 and 2 are the acoustic ports and are represented in the form

of transmission line, and the port 3 is the electrical port where the voltages are applied and sensed.

By applying a voltage to the IDT electric field is generated in SAW device as shown in figure 2.3(b). The distribution of the electric field can be approximated by cross-field model and in-line field model. In cross-filed model the electric fields are perpendicular to the substrate surface and in-line models the electric fields are parallel to the substrate surface.

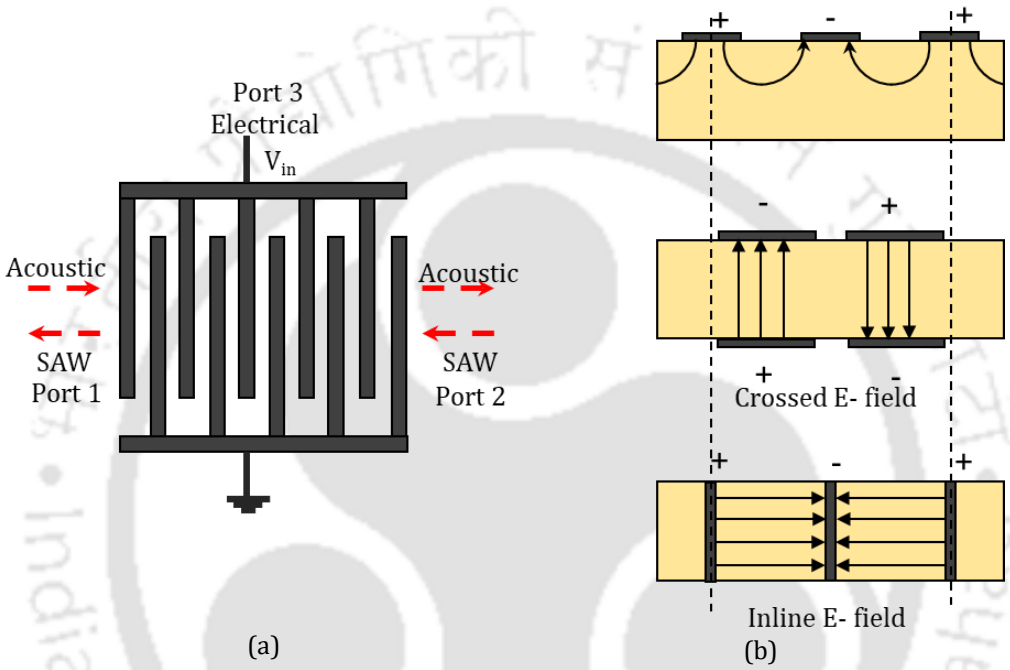

Figure 2.3 (a) IDT represented as a three-port network. Port 1 and 2 are electrical equivalents of acoustic port while port 3 is a true electrical port. (b) Directions of electric field lines in an electrically excited IDT with cross-field and inline-field approximations.

Using mason cross-field model, Smith et al. have formulated an equivalent circuit model for surface wave transducers [81]. In this model, the acoustic forces are represented as electric potentials and the SAW velocities as equivalent electric current. The IDT is represented as an equivalent three-port admittance network and is shown in figure 2.4.

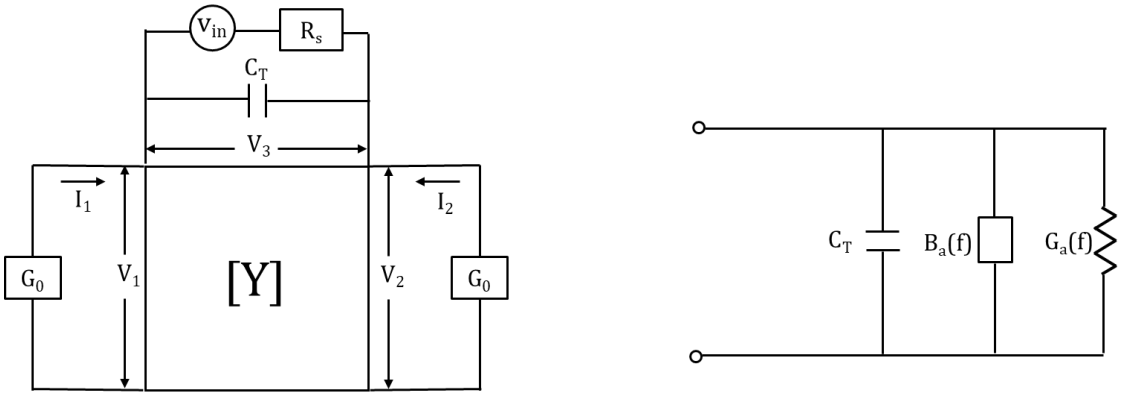

(a) (b)

Figure 2.4 (a) Three-port equivalent admittance network representation for an IDT in the crossed-field model. (b) Equivalent circuit representation of SAW IDT [81].

The admittance of SAW transmission lines G_0 is given as

$$G_0 = K^2 C_s f_0 \tag{2.10}$$

where f_0 is the synchronous frequency and C_s is the capacitance per finger pair and is expressed as $C_s = C_0 W$ where C_0 is the capacitance of one periodic section of IDT per unit length and K^2 is a measure of the surface wave coupling efficiency. The Y parameters of the 3-port network using the equivalent circuit of a period of an IDT can be expressed as

$$\begin{bmatrix} I_1 \\ I_2 \\ I_3 \end{bmatrix} = \begin{bmatrix} -jG_0 \cot N_p\theta & -jG_0 \csc N_p\theta & -jG_0 \tan(\theta/4) \\ jG_0 \csc N_p\theta & -jG_0 \cot N_p\theta & jG_0 \tan(\theta/4) \\ -jG_0 \tan(\theta/4) & jG_0 \tan(\theta/4) & j\omega C_T + 4jN_p G_0 \tan(\theta/4) \end{bmatrix} \begin{bmatrix} E_1 \\ E_2 \\ E_3 \end{bmatrix} \tag{2.11}$$

where C_T is the total capacitance of the IDT and is expressed as $C_T = N_p C_s$, N_p is the number of IDT pairs and $\theta = 2\pi f / f_0$ is the electrical transit angle in radian through one finger pair. The equivalent circuit representation of IDT is shown in figure 2.4 (b)

The input admittance $Y(f)$ is written as

$$Y(f) = G_a(f) + B_a(f) + j\omega C_T \tag{2.12}$$

$G_a(f)$ is the radiation conductance and is given by the relation

$$G_a(f) = G_a(f_0) \left| \frac{\sin X}{X} \right|^2 \tag{2.13}$$

$B_a(f)$ is the susceptance and is given by

$$B_a(f) = G_a(f_0)\,\frac{(\sin(2X)-2X)}{2X^2} \tag{2.14}$$

where, the radiation conductance at f_0 is

$$G_a(f_0) = 8K^2 f_0 C_s {N_p}^2 \tag{2.15}$$

and

$$X = N_p \pi (f - f_0)/f_0 \tag{2.16}$$

At center frequency, the radiation conductance is maximum and the susceptance passes through the zero. The equivalent circuit model is generally used in the design of IDT but the second order effects such as propagation losses, electrode resistance and electrode discontinuities are neglected. The IDT is designed such that its impedance should match the source impedance of 50 Ω. For a given piezoelectric material, the IDT with 50 Ω impedance at the operating frequency can be designed by choosing proper values of aperture of IDT (W) and number of pairs of IDT (N_p).

2.2.4 Coupling of modes (COM) model

COM model is widely used in designing of SAW devices. The model considers acoustic properties, wave amplitude and interaction between the waves but the depth of penetration of waves into the substrate is not considered. The coupling interaction between the two counter propagating waves from the IDT is represented in the form of differential equations [82]. As the wave propagates through the piezoelectric medium, charges are induced on the electrode due to inverse piezoelectric effect and it leads to a current flow through the electrodes. The COM model consists of three governing differential equations and are written as

$$\begin{aligned}
\frac{dR(x)}{d(x)} &= -j\delta R(x) + jkS(x) + j\alpha V \\
\frac{dS(x)}{d(x)} &= -jk^* R(x) + j\delta S(x) - j\alpha^* V \\
\frac{dI(x)}{d(x)} &= -2j\alpha^* R(x) - 2j\alpha S(x) + j\omega C V
\end{aligned} \tag{2.17}$$

where δ is the detuning parameter given as $\delta = 2\pi(f - f_0)/v - j\gamma$, k is the reflectivity due to perturbations, α is the transduction coefficient, C is capacitance per unit length, γ is

attenuation and v is the SAW velocity. The evaluation of the COM parameters are done either through numerical simulations or by performing experiments.

The COM analysis along with P-matrix formulation is often used for modeling the response of SAW devices. The P-matrix is a type of scattering matrix commonly used to describe the behavior of SAW gratings and transducers [83]. The figure 2.5 shows the P-matrix representation of an uniform IDT transducer and Ai_1 and Ai_2 represent the amplitudes of waves incident at ports 1 and 2 respectively. The amplitudes of waves leaving the transducer at these ports are represented by At_1 and At_2. W is the IDT aperture, N is the number of fingers in the IDT and $L_T = (2n-1)\lambda/4$ is the length of the transducer. Current and voltage are denoted by I and V respectively.

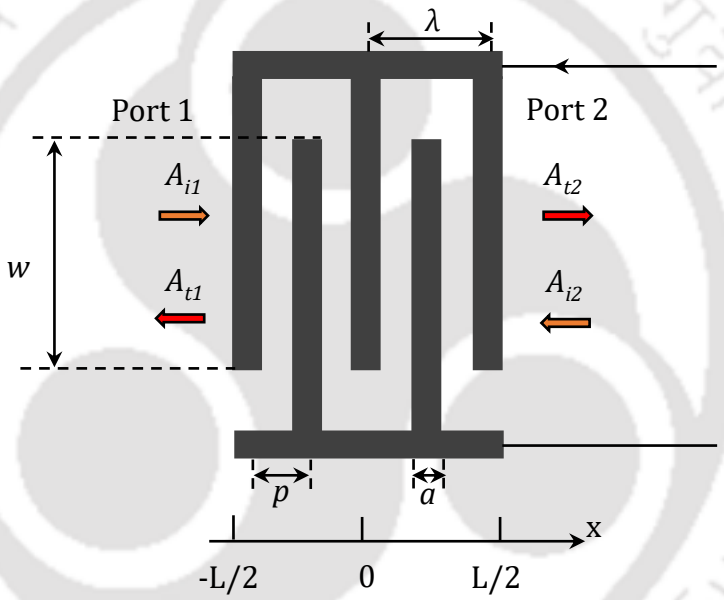

Figure 2.5 Schematic of IDT for P-matrix representation. The pitch p of the IDT is given as, $p = a/4 = \lambda/2$. A_i and A_t denote the amplitudes of incident and transmitted waves.

The P-matrix is defined as,

$$\begin{bmatrix} At_1 \\ At_2 \\ I \end{bmatrix} = \begin{bmatrix} P_{11} & P_{12} & P_{13} \\ P_{21} & P_{22} & P_{23} \\ P_{31} & P_{32} & P_{33} \end{bmatrix} \begin{bmatrix} Ai_1 \\ Ai_2 \\ V \end{bmatrix} \tag{2.18}$$

For a lossless non reflective transducer, with conditions of reciprocity, the elements of the P-matrix are

$$P_{11} = P_{22} = 0 \tag{2.19}$$

$$P_{12} = P_{21} = e^{-jkL} \tag{2.20}$$

$$P_{13} = -P_{31}/2 = j\overline{\rho_e}(k)\sqrt{\omega W \Gamma_s/2}\, e^{-jkL/2} \tag{2.21}$$

$$P_{23} = -P_{32}/2 = j\overline{\rho_e}(-k)\sqrt{\omega W \Gamma_s/2}\, e^{-jkL/2} \tag{2.22}$$

$$P_{33} = Y(\omega) = G_a(\omega) + jB_a(\omega) + j\omega C_T \tag{2.23}$$

P_{11} and P_{22} are the reflection coefficients of the IDT and are zero for the non-reflective transducers. P_{12} and P_{21} are the transmission coefficients, P_{33} represents the admittance of the IDT, P_{13} and P_{23} are the currents generated by the waves and are computed using $\overline{\rho_e}(k)$, which is the Fourier transform of electrostatic charge density in the IDT [84]. For a reflective transducer the P_{11} and P_{22} are written as

$$P_{11} = -c_{12}^{*}\frac{\sin(SL)}{D} \tag{2.24}$$

$$P_{22} = c_{12}\sin(SL)\frac{e^{-jk_0L}}{D} \tag{2.25}$$

where $c_{12} = \mathrm{r}_s/p$, r_s is the reflection coefficient of one finger, $s^2 = \delta^2 - |c_{12}^2|$, δ is the detuning factor, $D = s\cos(SL) + j\delta\sin(SL)$. These equations are important for designing the SAW devices.

2.3 Finite element method

The finite element method is numerical techniques used in engineering disciplines particularly in the areas of structural analysis, fluid dynamics and heat conduction analysis by solving the differential equations associated with these areas and provides the numerical solutions to the problems. Since the propagation of the waves in the piezoelectric medium is governed by the differential equations given in (2.8) and (2.9), FEM can be used to solve the equations along with complexities in geometry of the device, materials used and proper boundary conditions. This section explains about the basic procedures used in the formulations of FEM. The detailed descriptions about the FEM can be found in [85].

In FEM, initially the geometry of the structure is designed using either 2D or 3D coordinate system. The structure is assigned as a material in the simulation and the following material properties are provided. Elastic constants, permittivity values, piezoelectric coefficients, Young's modulus, density and Poisson's ratio of piezoelectric material, and Young's modulus, density and Poisson's ratio for IDT material. Appropriate boundary conditions are applied at the boundary of the structure. The geometry is divided into smaller domains called elements and can have different shapes like triangular, tetrahedral, quadrilateral or brick depending on the dimensions. The elements are connected at specific points called nodes. The output information in case of stress-strain analysis in piezoelectric material involves nodal and elemental information. The solutions to the primary unknown quantities like displacements in all directions, and voltage are determined at each node. These unknowns are called as degrees of freedom (DOF). In this thesis, the simulations and analyses of SAW devices are carried out by FEM using piezoelectric module of COMSOL Multiphysics software [86]. The software has well developed solvers, graphical user interface (GUI) and post-processing capabilities.

2.3.1 Approximations in FEM

Consider a one-port SAW resonator device having length, width and depth in terms of wavelength as 500λ, 50λ and 100λ respectively. To obtain a basic accuracy in FE simulations, the mesh in the geometry requires minimum ten elements per wavelength. For a piezoelectric simulation there are four unknowns to be solved namely three displacement components and potential. Therefore the total number of unknowns in this problem would be $(500 \times 50 \times 100) \times 10 \times 4 = 10^8$. Solving such large number of unknowns requires a powerful computing facility and takes large computational time. To reduce the computational complexity and time, the following valid approximations are made in the model.

Geometry can be reduced from three to two dimensions for Rayleigh waves as the profile of the wave is identical in the lateral direction and can be simulated by considering only the length and depth of the substrate ignoring the width. The IDT consists of a large number of periodically placed electrodes, therefore an infinite periodic boundary conditions with only one wavelength (λ) of the wave or antiperiodic boundary conditions with half wavelength ($\lambda/2$) of the wave can be used for device simulation. Since SAW carries energy mostly near the surface, only 5 to 10 wavelengths of the substrate depth can be considered, which reduces the number of calculations in solving a model.

2.3.2 SAW device simulation using FEM

Simulation of SAW devices using FEM plays a major role in studying the characteristics of the device before fabrication. Many researchers have reported simulations of SAW devices using FEM. Lerch *et al*. [87] presented an FEM scheme to calculate eigenmodes and dynamic response to mechanical and electrical excitations of 2D and 3D geometries of a piezoelectric transducer. FEM based analysis of acoustic waves propagating on layered SAW devices was performed by Ippolito *et al*. [88]. The FEM was used to study the effects of change in film properties on the mass sensitivity of SAW sensors [89]. FE simulation was used to simulate SAW delay line device coated with palladium thin film for sensing H_2 gas [90, 91]. Atashbar *et al*. simulated a SAW hydrogen sensor based on delay line and showed that FE simulation is a powerful tool to study the SAW propagation characteristics [90]. An FE simulation of SH-SAW delay line sensor with microcavities on the delay path was reported by Cular *et al*. [92]. Kabir *et al*. has developed an accurate two dimensional (2-D) FE simulation of a SAW device using COMSOL Multiphysics and the results was verified experimentally [93]. Thus the FE simulation is an effective method to analyze the device performance before fabrication. In this chapter 2D simulation of a conventional one-port SAW resonator is carried out using COMSOL Multiphysics to optimize the mesh settings, to obtain appropriate boundary conditions and to verify Rayleigh wave propagation and the settings will be followed in all the simulations in the thesis.

2.4 FE simulation of one-port SAW resonator device

In this section, an FE analysis of one-port SAW resonator device on Y cut Z propagation $LiNbO_3$ (YZ $LiNbO_3$) is presented and the results are discussed. YZ $LiNbO_3$ is used as a piezoelectric substrate that generates Rayleigh wave on the surface. The geometry and the boundary conditions used in the simulation of one-port SAW resonator are explained. Next, the mesh refinement process is described. The eigenmode analysis and the frequency response are performed to calculate the free surface velocity V_f, metallized surface velocity V_m, electromechanical coupling coefficient K^2, total displacement, admittance and quality factor Q of the device.

2.4.1 Simulation geometry

COMSOL Multiphysics is used to simulate a one-port SAW resonator with infinite number of IDT fingers on a YZ $LiNbO_3$ piezoelectric substrate using 2D geometry. The material properties of YZ $LiNbO_3$ such as elastic constants, stress constants, permittivity constants and

density are procured from [94] and are listed in Appendix A. A 2D piezo plain strain module is used in the simulation, which has degrees of freedom of u, v and V. Three devices having wavelength λ of 4 μm, 8 μm and 10μm are simulated. The substrate depth of 5λ is used in the simulation with bottom surface fixed. Aluminum IDT having finger width of $\lambda/4$ is made on the top surface of the resonator. The geometry used for 2D FE simulation is shown in figure 2.6.

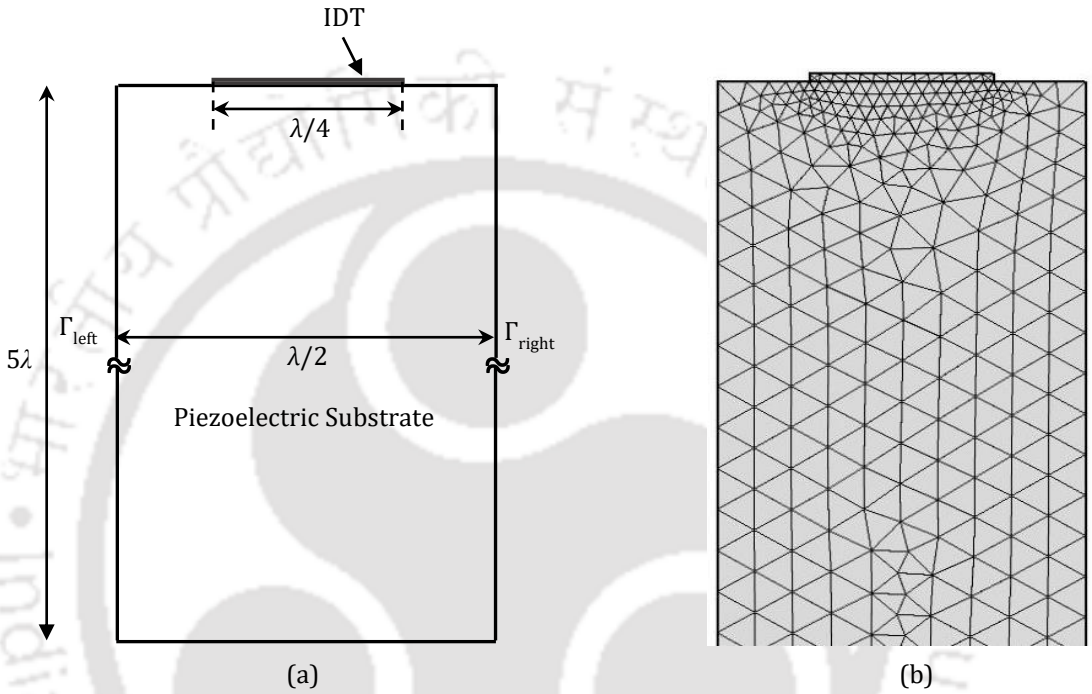

Figure 2.6 (a) Geometry used for 2D FE simulation (b) Refined mesh geometry with maximum element size of one by sixteenth of wavelength.

Due to the periodic nature of IDT, only one finger of IDT with appropriate boundary conditions is used in the simulation. Therefore, a section of resonator having width $\lambda/2$ is sufficient for the simulations with antiperiodic boundary conditions at the left and right surfaces (Γ_{left} and Γ_{right}) as follows.

$$u_l = -u_r$$

$$V_l = -V_r$$

where u_l and V_l are the displacement and potential at the left surface of the geometry, and u_r and V_r denote the displacement and potential at the right surface of the geometry. The stress-free boundary conditions are used in all boundaries except the bottom boundary of the device. The eigenmode analysis provided by the COMSOL Multiphysics is performed to obtain

the natural frequency of vibration of the structure. It calculates the homogeneous solutions of the differential equations involved and is used for the detailed analysis of the device.

2.4.2 Mesh refinement

The optimal mesh density giving sufficient accuracy is determined as follows. The maximum element size of the mesh is varied while keeping other parameters fixed and resonance frequency is obtained using eigen mode analysis. The mesh density is maximum at the top surface and the minimum element size, element growth rate and the resolution of narrow region are maintained at values 0.0004 μm, 1.3 and 0.9 respectively. The table 1 lists the number of elements per wavelength, resonance frequency and corresponding SAW velocities for λ of 4 μm, 8 μm and 10μm. It is observed that as the maximum element size decreases, the mesh is denser and the resonance frequency tends to stabilize after a certain value and is consider as the optimal mesh setting. The plot of phase velocity versus number of mesh elements in figure 2.7shows that the SAW phase velocity remains constant beyond mesh density of 16 per wavelength and the settings are used in all the simulations in the thesis.

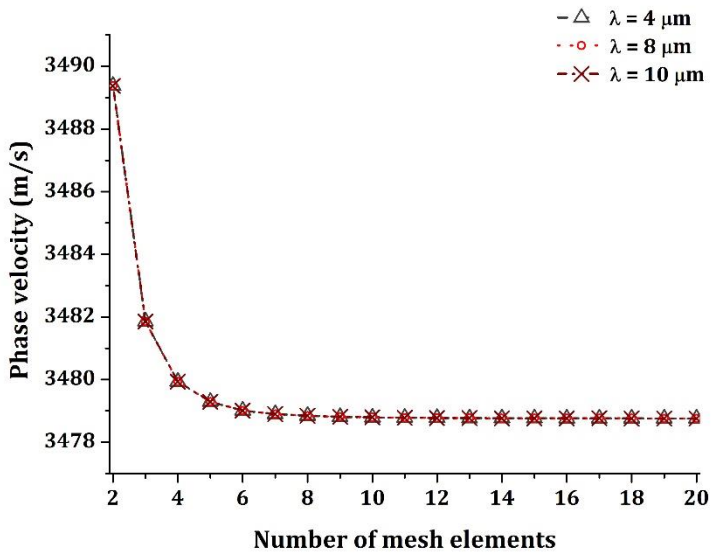

Figure 2.7 SAW phase velocity versus number of mesh elements for different values of λ.

Table 2.1 SAW phase velocity against number of mesh elements for different values of λ

No. of mesh element per wavelength a	λ = 4 μm		λ = 8 μm		λ = 10 μm	
	Frequency (MHz)	SAW Velocity (m/s)	Frequency (MHz)	SAW Velocity (m/s)	Frequency (MHz)	SAW Velocity (m/s)
2	872.344	3489.374	436.172	3489.374	348.937	3489.374
3	870.462	3481.848	435.231	3481.848	348.185	3481.848
4	869.984	3479.935	434.992	3479.935	347.993	3479.935
5	869.824	3479.294	434.912	3479.294	347.929	3479.294
6	869.753	3479.012	434.876	3479.012	347.901	3479.012
7	869.725	3478.900	434.863	3478.900	347.890	3478.900
8	869.711	3478.843	434.855	3478.843	347.884	3478.843
9	869.703	3478.811	434.851	3478.811	347.881	3478.811
10	869.698	3478.793	434.849	3478.793	347.879	3478.793
11	869.695	3478.782	434.848	3478.782	347.878	3478.782
12	869.694	3478.775	434.847	3478.776	347.878	3478.776
13	869.693	3478.770	434.846	3478.770	347.877	3478.770
14	869.692	3478.766	434.846	3478.766	347.877	3478.766
15	869.691	3478.764	434.846	3478.764	347.876	3478.764
16	869.691	3478.762	434.845	3478.762	347.876	3478.762
17	869.690	3478.761	434.845	3478.761	347.876	3478.761
18	869.690	3478.760	434.845	3478.760	347.876	3478.760
19	869.690	3478.760	434.845	3478.760	347.876	3478.760
20	869.690	3478.759	434.845	3478.759	347.876	3478.759

2.4.3 Analysis of one-port SAW resonator

The eigenmode analysis is performed to calculate free and metallized surface velocities of the Rayleigh SAW device and the electromechanical coupling coefficients K^2 is calculated using

$$K^2(\%) = 2\left(\frac{v_f - v_m}{v_f}\right) \times 100 \tag{2.26}$$

The free and metallized resonance frequencies of YZ $LiNbO_3$ for wavelength of 8 μm are obtained by applying electrical open and short boundary conditions at the substrate surface and are 434.845 MHz and 425.598 MHz respectively. From the resonance frequency the free velocity v_f and metallized velocity v_m are calculated using (1.1) and the calculated K^2 value for YZ $LiNbO_3$ is 4.3% .

The surface modes at resonance frequency are obtained with aluminum IDT fingers from the eigenmode analysis. The displacement profiles of the one-port SAW resonator at the resonance frequency f_r of 425.598 MHz up to a depth of about 2.5 λ inside the substrate are shown in figure 2.8. It is observed that the displacement is almost zero after a depth of 1.5 λ though the thickness of substrate used in the simulation is 5 λ.

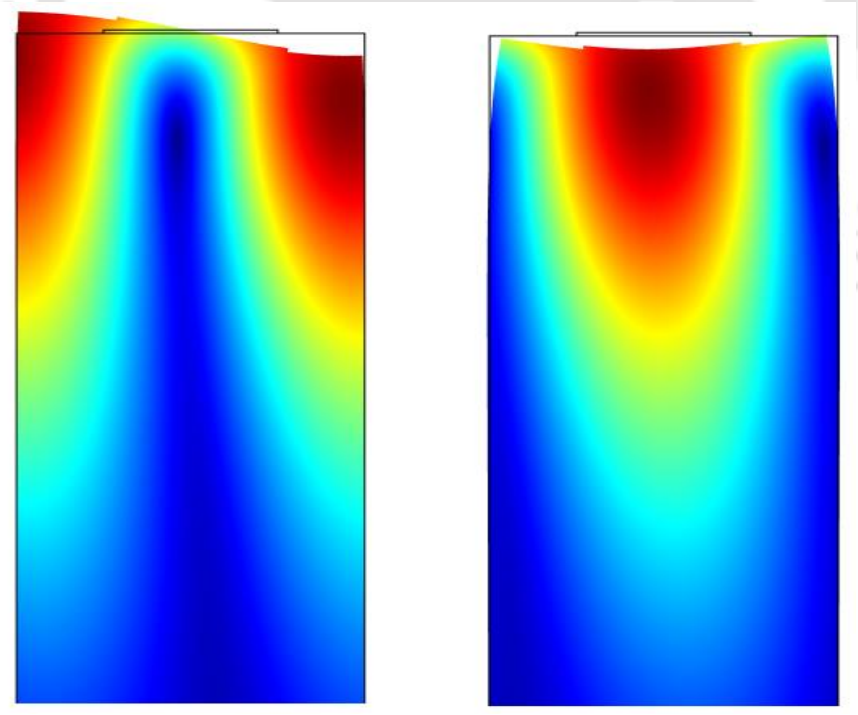

(a) (b)

Figure 2.8 Total displacement profile in SAW resonator (a) at eigenmode frequency of 425.598 MHz showing resonance mode (b) at eigenmode frequency of 429.938 MHz showing antiresonance mode.

The plot of longitudinal and transverse displacements versus substrate depth is shown in figure 2.9. The longitudinal displacement changes sign at a certain depth from the surface and the transverse displacement is dominant than the longitudinal displacement at the surface, and it confirms that Rayleigh wave is propagating on the surface of the device.

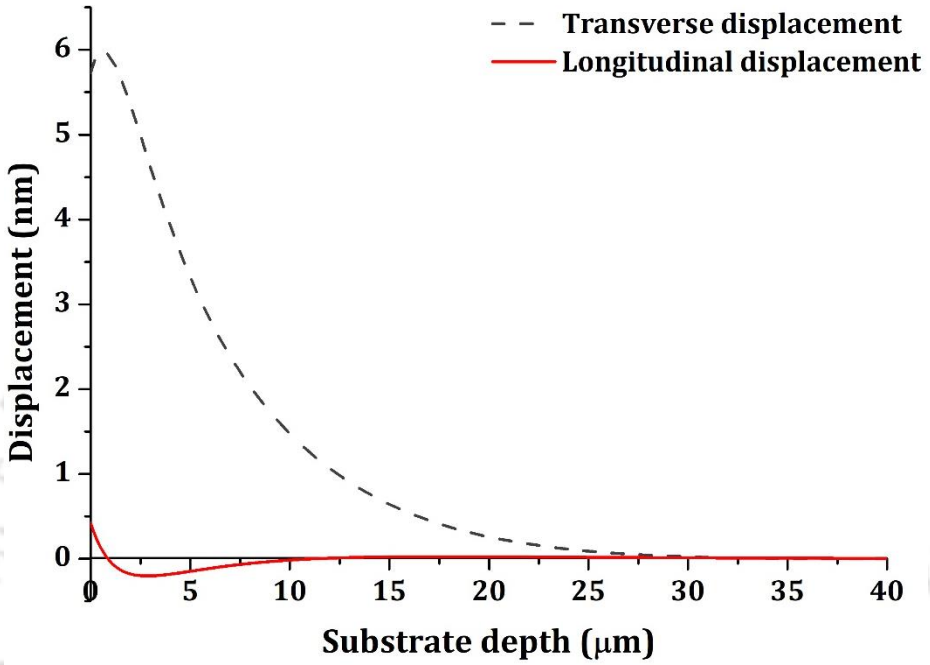

Figure 2.9 Plot of transverse and longitudinal displacements versus substrate depth at resonance frequency.

The frequency analysis of one-port SAW resonator is performed to confirm the resonance frequency of the device. The resonator operates at the wavelength of 8 μm. The frequency is varied in step size of 0.1 kHz to calculate the total displacement and harmonic admittance of the device. The resonance frequency of the device is determined from the admittance versus frequency plot and is the frequency for which the admittance is maximum and the susceptance crosses through zero. The total displacement and harmonic admittance versus frequency for SAW one-port resonator is plotted on figure 2.10. From the figure it is observed that resonance frequency of the device is at 425.598 MHz and At that frequency the total displacement is maximum at 30.75 μm and the harmonic admittance value is around 1.8×10^5 S. In practice, the device would show lower values of admittance due to attenuation, damping and finite aperture of IDT.

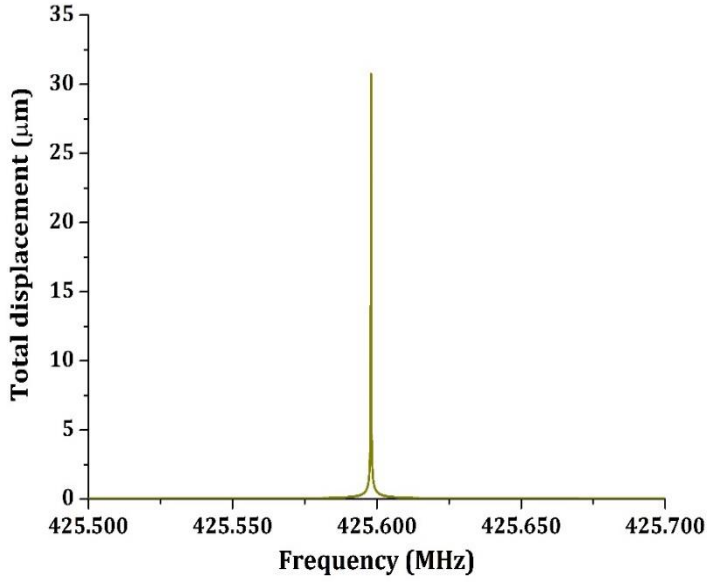

(a)

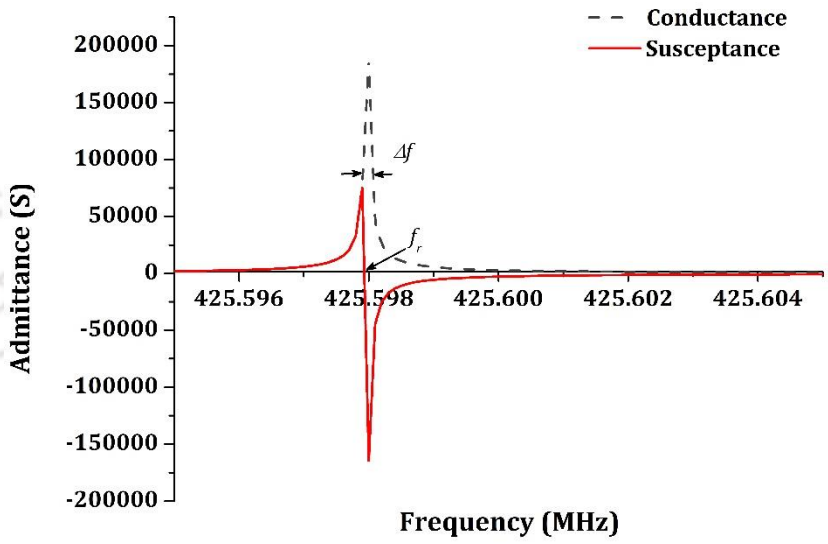

(b)

Figure 2.10 Plot of (a) Total displacement versus frequency and (b) Admittance versus frequency for one-port SAW resonator of λ = 8 μm.

The quality factor Q_r at resonance frequency of the conventional one-port SAW resonator is calculated from figure 2.10 (b) using the expression for quality factor given as

$$Q_r = \frac{f_r}{\Delta f} \tag{2.27}$$

where, Δf is the bandwidth at half of the peak-conductance [95, 96]. The quality factor of the conventional SAW resonator computed from simulation is 354665.

2.5 Operation of one-port SAW resonator sensor

The operation of SAW sensors are based on the change in the phase velocity and amplitude of the surface waves due to the presences of an entity in the propagation path. For chemical sensing, a sensing layer is coated on the transducer, the exposure of target analytes will change the properties of sensing layer and the quantitative information about the analyte is obtained by detecting these changes. A one-port SAW resonator configuration can be used for the excitation of the surface waves and detect the changes. In this configuration, sensing layer is deposited on the IDT and change in attenuation (α) and change in velocity (v) of the surface wave upon exposure to gases is measured. As the attenuation is affected by undesired electromagnetic interference, SAW sensor response is usually obtained in terms of velocity change and is evaluated by change in resonance frequency of the device [97]. The change in resonance frequency is related to change in velocity and is given as [98]

$$\frac{\Delta v}{v_0} = \frac{\Delta f}{f_0} \tag{2.28}$$

where v and f are the velocity and frequency of SAW wave in perturbed state whereas v_0 and f_0 are those in unperturbed state.

The measured change in SAW velocity and attenuation is influenced by the internal and external factors like mass-loading (m), electric (p_{elec}) factors (conductivity, permittivity etc.), mechanical (p_{mech}) factors (viscosity, elasticity), and environmental (p_{env}) factors (temperature, pressure, humidity etc.) to the propagating waves. A perturbation-based investigation has been made to evaluate the effect of these factors quantitatively. The net change in the velocity and attenuation is the sum of the perturbations caused by each and is given as [31, 10]

$$\frac{\Delta \gamma}{k_0} = \frac{\Delta \alpha}{k_0} - j\frac{\Delta v}{v_0} = \frac{\partial \gamma}{\partial m}\Delta m + \frac{\partial \gamma}{\partial p_{elec}}\Delta p_{elec} + \frac{\partial \gamma}{\partial p_{mech}}\Delta p_{mech} + \frac{\partial \gamma}{\partial p_{env}}\Delta p_{env} \tag{2.29}$$

where γ is the complex propagation coefficient of the propagating wave and k_0 is the wave number in unperturbed state.

In SAW chemical sensor the surface wave interact with sensing layer, the absorption of gases by the sensing film alters the density, viscoelastic properties and acoustoelectric properties of the sensing film causes variation in propagating velocity of the surface wave. The change in velocity due to change in mass and stiffness for a non-piezoelectric, non conducting, isotropic acoustically thin (h<<λ) layer is given as

$$\frac{\Delta v}{v_0} = (k_1 + k_2) f h \rho - k_2 f h \left\{ \frac{4G(K+G)}{{v_0}^2 (K+2G)} \right\} \tag{2.30}$$

where f is the operating frequency without the film, ρ is the density of the film, K and G are bulk and shear elastic modulii of the film, v_0 is the velocity of SAW, and h is the film thickness. k_1 and k_2 are material constants of the substrate. For example, Y-Z lithium niobate has k_1 = –3.775×10^{-8} m^{2}skg^{-1} and k_2 = –1.73×10^{-8} m^{2}skg^{-1} [99]

The response of SAW chemical sensor coated with viscoelastic polymer film was given by Martin et al. [100]. The change in attenuation and propagation velocity in SAW chemical sensor coated with polymer is described in following equations

$$\Delta\gamma/k_0 = \Delta\alpha/k_0 - j\,\Delta v/v_0 = \sum_{i=1}^{3} c_i \frac{\beta_i M_i}{\omega} \tanh(j\beta_i h_p)$$

$$\beta_i = \omega \sqrt{\frac{\rho_p - E_i/V_0^2}{M_i}} \qquad j = \sqrt{-1} \tag{2.31}$$

$$E_1 = \frac{4G(3K+G)}{3K+G}, E_2 = G, E_3 = 0$$

$$M_1 = M_2 = G, M_3 = K$$

where $k_0$and v_0 denote the unperturbed wave number and SAW velocity, respectively. $\Delta\gamma/k_0$ represents the fractional perturbation in the complex wave propagation factor per wavenumber, $\Delta\alpha/k_0$ is the change in attenuation per wave number, $\Delta v/v_0$ is the fractional change in propagation velocity. c is the SAW-film coupling parameter ρ_p is the polymer material density, and $h_p$is the polymer thickness. G and K denote the shear modulus and the bulk modulus of polymer. The exposure of the gas will vary density and thickness of the polymer sensing film and the variation for different concentrations due to absorption of the gas is given as [67]

$$\rho_p(c) = \frac{\rho_0 + k c_v}{\left(1 + \frac{k c_v}{\rho_v}\right)} \tag{2.32}$$

$$h_p(c) = h_0\left(1 + \frac{kc_v}{\rho_v}\right) \tag{2.33}$$

where c_v is the concentration of gas, k is the partition coefficient, ρ_0 density of the polymer film and ρ_v is the density of the target gas. The phenomenon of changes in thickness, density and elastic properties of a sensing medium is widely used in developing SAW chemical sensors.

The simulation of the proposed SAW devices by FEM using COMSOL Multiphysics is described below. The effect of trench depth on the resonance frequency is studied. In addition, the following sections include the simulation of gas sensor using proposed and conventional devices and the results are compared.

2.6 Summary

This chapter discusses a brief introduction to piezoelectricity followed by equations of motion, and solution to surface wave parameters for a piezoelectric substrate. The chapter presents modelling techniques such as delta function model, impulse response model, equivalent circuit model, coupling of modes (COM), P-matrix approach, and the FEM a numerical simulation method. The sensing mechanism for SAW devices used in sensing application is explained.

FE simulations of one-port SAW resonator configuration are performed using COMSOL Multiphysics to determine the free surface SAW phase velocity and optimal mesh density for the simulation. 2D simulation with periodic boundary conditions is simulated to study the surface modes generated in the structure. The eigenmode analysis is carried out to obtain the phase velocity and coupling coefficient. Harmonic admittance characteristics are obtained from frequency dependent analysis to identify the dominant surface mode generated in the structure. The quality factor of SAW resonator is calculated. The FE simulation is further extended to study the proposed SAW devices for gas sensing applications in the following chapters.

3

FE analysis of SAW resonator with trenches for sensing gases

The main objective of the research work in this thesis is to investigate structural changes in the conventional SAW devices for sensing applications leading to higher sensitivity. Two structures are prominently investigated. In the first structure a trench is made in the space between each IDT finger pair and the sensing material is placed inside the trench. The second structure employs high aspect ratio structures on the active surface and the sensing material is placed in the space between the high aspect ratio structures. This chapter presents the simulation of the first proposed structure. The pictorial representation of half periodic section of conventional and proposed one-port SAW resonator device is shown in figure 3.1. The second proposed structure is discussed in chapter 4.

In section 3.1 a one-port SAW resonator with trenches is simulated and optimal trench depth giving maximum change in resonance frequency for change in trench depth is determined. In section 3.2 the one-port SAW resonator with optimal trench depth is used to simulate dimethyl metha phospahate (DMMP) gas sensor using fluorinated bisphenol-containing polymer (BSP3) as the sensing material. DMMP is a typical simulant of organophosphate based chemical warfare agents such as sarin or soman and is commonly used for testing sarin in laboratory due to its low toxicity and similar chemical structure with sarin. Section 3.3 presents another gas sensor using palladium (Pd) as sensing material to sense hydrogen (H_2).

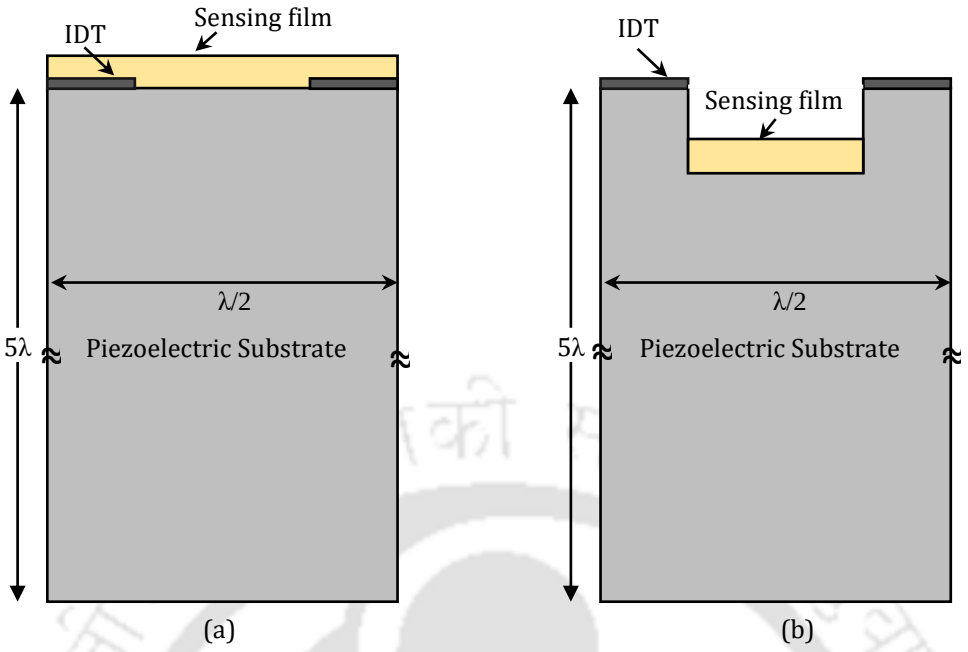

Figure 3.1 Pictorial representation of half period of SAW sensors using (a) conventional SAW device and (b) proposed SAW device with trenches.

3.1 2D Simulation of one-port SAW resonator with trenches

A one-port SAW resonator with trenches in the space between the IDT fingers can be designed by using a large number of IDT finger-pairs where multiple reflections occur between the fingers. This section presents 2D simulation of the proposed one-port SAW resonator device using COMSOL Multiphysics.

3.1.1 Structure of one-port SAW resonator with trenches

A one-port SAW resonator with infinite number of IDT fingers fabricated on piezoelectric substrate is considered in the simulation. A trench is made in the space between each finger pair. The resonator is considered as infinitely extended periodic structure of one unit cell, therefore a half unit cell with antiperiodic boundary conditions is used to model the proposed SAW one-port resonator. The 2D geometry structure of one-port SAW resonator with trenches is shown in figure 3.2.

3.1.2 Simulation methodology

A one-port SAW resonator with trenches having infinite number of IDT fingers is considered for the FE simulation. Owing to periodic nature of IDT structure, a half unit cell is used to model the proposed SAW resonator device and antiperiodic boundary conditions are applied.

The simulation is carried out using piezo module with plane strain mode provided in COMSOL Multiphysics [101]. The 2D geometry of a one-port SAW resonator with trenches considered in the simulation is shown in figure 3.2.

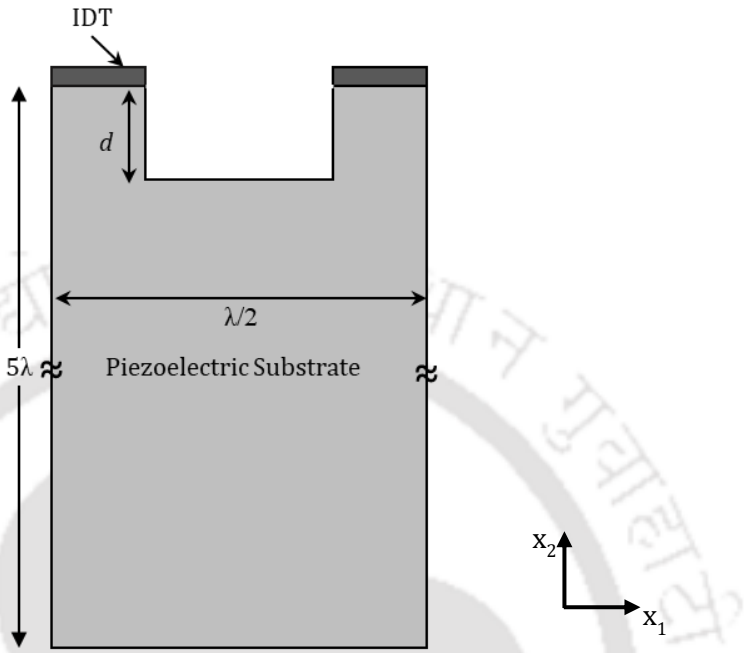

Figure 3.2 2D geometry of one-port SAW resonator with trenches used in simulation.

The dimensions used in the simulation are as follows: IDT finger width $\lambda/4$, electrode pitch $\lambda/2$, depth of the piezo-substrate 5 λ in $-x_3$ direction, and thickness of IDT fingers 0.05 µm. The YZ $LiNbO_3$ piezoelectric material is used as the piezo-substrate. The properties such as coupling matrix, elasticity matrix, relative permittivity and density of YZ $LiNbO_3$ piezo-substrate are taken from [102] and are given in Appendix A. A gold IDT having uniform thickness with metallization ratio of 0.5 is patterned on the substrate. The stress free boundary condition is used at the top surface of the substrate and bottom surface of the substrate is assumed to be fixed. Antiperiodic boundary conditions are applied in x_1 direction with sign inversion of variables at the boundaries. An extremely fine mesh with minimum element quality of 0.7 and the number of mesh elements of 16 per wavelength are used for the 2D simulation.

The eigenmode analysis is performed to obtain the resonance frequency by applying 0 V to the IDT fingers. The harmonic analysis is performed by applying an alternating voltage of 1 V to the IDT fingers to find the characteristics and parameters of the resonator.

3.1.3 Results and discussions

The results of simulation of the proposed one-port SAW resonator with trenches are discussed in this section. The effect of trench depth on the device resonance frequency is studied. The frequency analysis is performed to calculate the resonance frequency of the proposed device.

3.1.3.1 Effect of trench depth on resonance frequency

A simulation of proposed device is carried out to study the effect of trench depth (d) on resonance frequency for different values of λ. The depth is varied from 0.2 μm to $\lambda/2$ in steps of 0.1 μm. The plots of phase velocity versus normalized trench depth (d/λ) for λ of 8, 10, 12 and 14 μm are shown in figure 3.3(a). The phase velocity decreases with increase in trench depth for all values of λ. The corresponding plots of frequency versus normalized trench depth (d/λ) are shown in figure 3.3(b). The ratio of change in frequency to change in depth for each λ is calculated and plotted in figure 3.3(c).

Figures 3.3(b) and (c) show that the change in the resonance frequency is greater for smaller values of λ for a given change in trench depth, however it is important to note that the maximum change in frequency is at the trench depth of about 0.14λ in all the cases. It implied that the device designed to operate at the trench depth of 0.14λ will give maximum sensitivity for sensing applications. Therefore the trench depth of 0.14λ is considered in the following simulations.

3.1.3.2 Frequency analysis of proposed SAW resonator device

The frequency analysis of one-port SAW resonator with trenches is performed. The device is operating at the wavelength of λ = 8 μm. The dimensions used in the simulation are as follows: IDT finger width 2 μm ($\lambda/4$), electrode pitch 4 μm ($\lambda/2$), depth of the piezo-substrate 40 μm (5 λ) in $-x_3$ direction, thickness of IDT fingers 0.05 μm, trench depth of 1.1 μm (0.14λ). A potential of 1 V is applied at the IDT to obtain the harmonic admittance of the device. Figure 3.4 shows total displacement profile and plot of longitudinal and transverse displacements along the substrate depth of the proposed SAW one-port resonator for surface mode 0 and surface mode 1. The plots of longitudinal and transverse displacements along the substrate depth confirm that mode 0 is a Rayleigh mode and mode 1 is a vertically polarized mode.

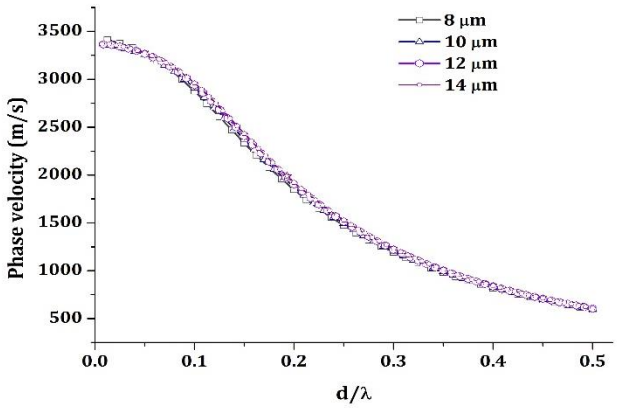

(a)

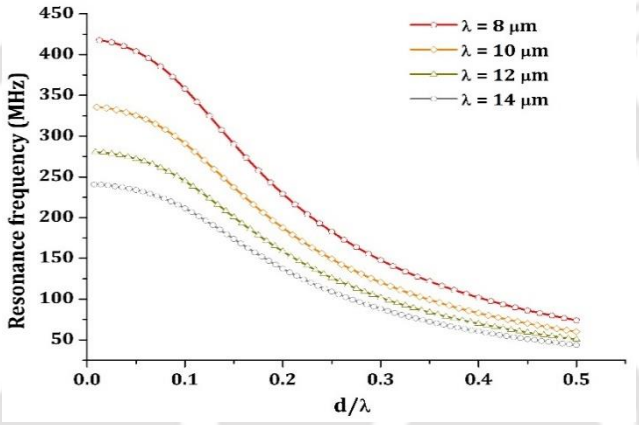

(b)

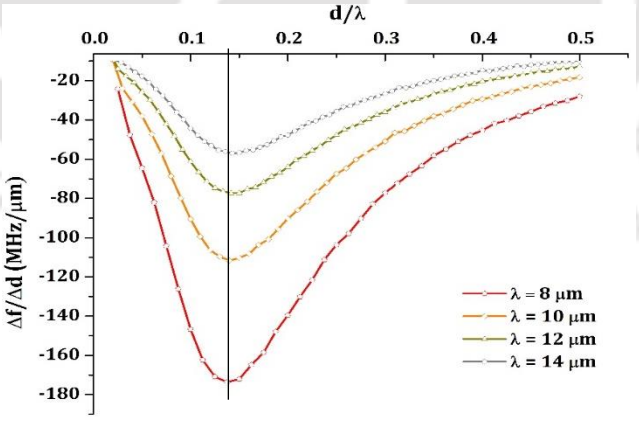

(c)

Figure 3.3 The plots of (a) phase velocity versus normalized trench depth, (b) resonance frequency versus normalized trench depth (c) ratio of change in frequency (Δf) to change in trench depth (Δd) versus normalized trench depth.

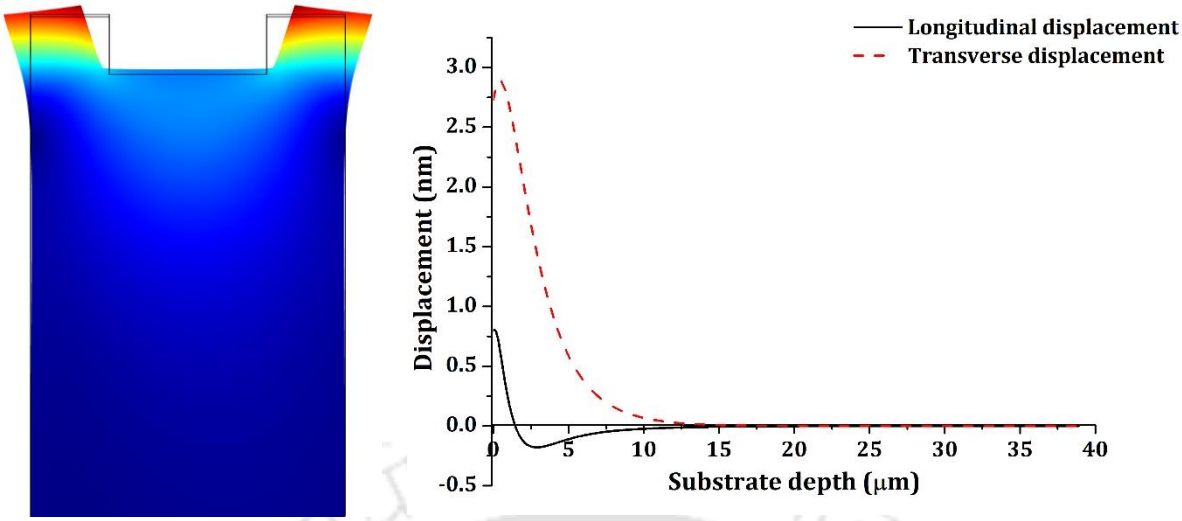

(a)

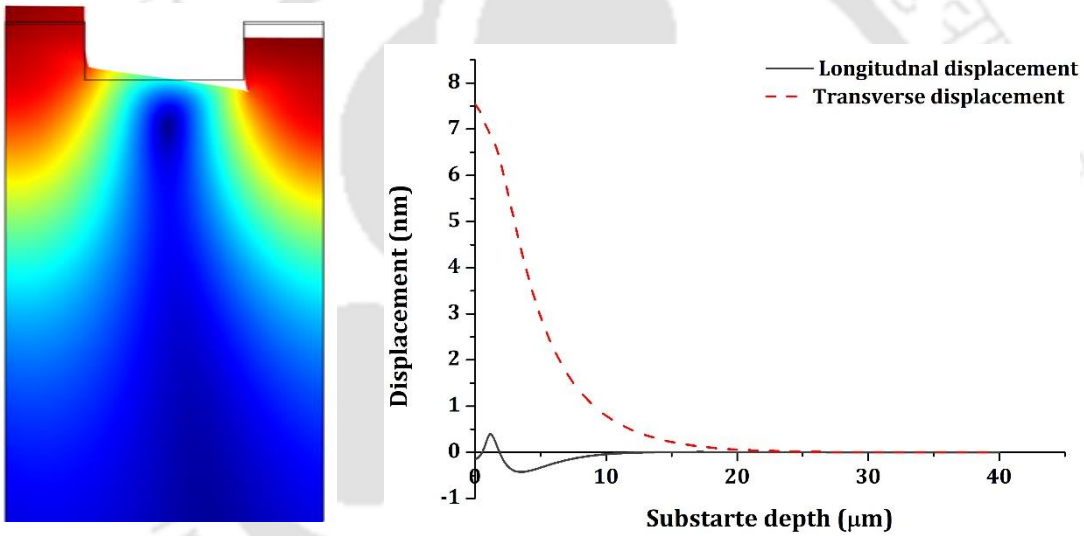

(b)

Figure 3.4 Total displacement profile and plot of longitudinal and transverse displacements along the substrate depth of the proposed SAW one-port resonator for (a) surface mode 0, (b) surface mode 1.

The figure 3.5 gives the admittance plot for the proposed one-port SAW resonator. From the plot it is observed that mode 0 is dominant and susceptance crosses zero at frequency of 308.041 MHz which is considered as the resonance frequency of the device.

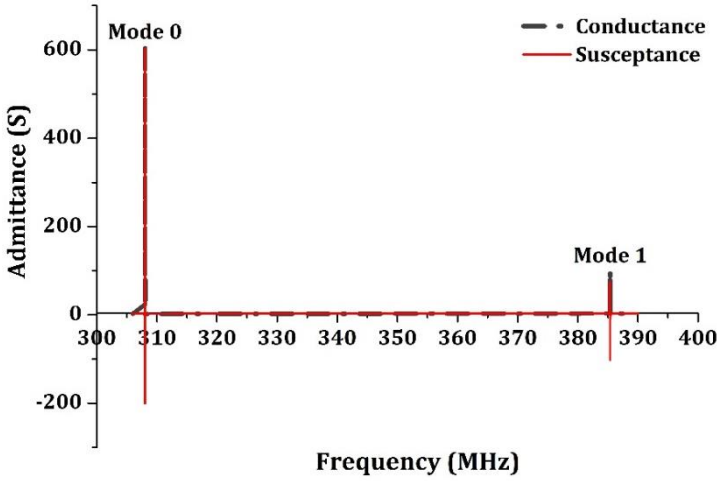

(a)

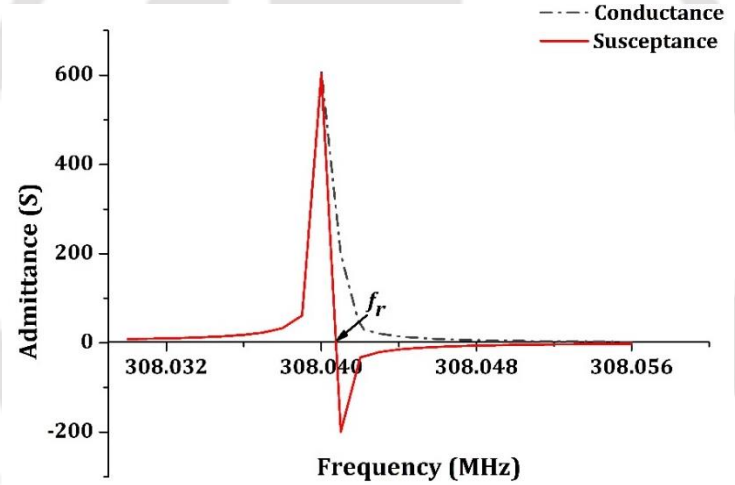

(b)

Figure 3.5 Frequency response for the proposed device showing (a) harmonic admittances for mode 0 and mode 1, (b) the resonance frequency f_r of dominant mode 0 at 308.041 MHz.

3.2 Simulation of one-port SAW resonator devices for sensing DMMP gas.

In this section, proposed and conventional one-port SAW resonators for sensing dimethyl metha phospahate (DMMP) gas are simulated and the results are compared. For proposed device, the sensing film is coated in the trench made in the space between the IDT, and for conventional device the sensing film is coated on the entire surface of the device. The exposure of gas will change the resonance frequency of the sensor as explained in section 2.5

and the shift in resonance frequency is measured as sensor response and related to the corresponding concentration of gas.

3.2.1 Simulation methodology

2D FE simulations of the proposed and conventional one-port SAW resonators for sensing DMMP gas are performed using COMSOL Multiphysics. The devices with large number of IDT fingers placed on YZ $LiNbO_3$ piezoelectric substrate are considered for the simulation. The periodic nature of the SAW resonator allows modeling the device using one unit cell with periodic boundary condition, which will reduce the size and computational complexity of the device. The geometries of half periodic sections of proposed and conventional SAW resonators with sign inversion of variables at the boundaries used in simulation are shown in figure 3.1. The piezo module with plain strain mode is used. The stress free boundary condition is used at the top surface of the substrate and bottom surface of the substrate is assumed to be fixed. The properties such as coupling matrix, elasticity matrix, relative permittivity and density of YZ $LiNbO_3$ piezo-substrate are taken from [102]. Since the energy in SAW is confined to a depth of about one wavelength from the wave propagation surface of the substrate, the substrate depth of 5λ is sufficient.

A gold IDT having uniform thickness of 50 nm with metallization ratio of 0.5 is patterned on the substrate and the fluorinated bisphenol-containing polymer (BSP3) is used as the sensing material. A trench in YZ $LiNbO_3$ substrate is made in the space between every adjacent IDT fingers and the BSP3 sensing film is placed at the bottom of the trench as shown in figure 1(a). The device is operating at frequency of about 310.42 MHz. The dimensions used in the simulation for the proposed device are as follows: the device wavelength λ = 8 μm, IDT finger width 2 μm ($\lambda/4$), electrode pitch 4 μm ($\lambda/2$), depth of the piezo-substrate 40 μm (5 λ) in $-x_3$ direction, and thickness of IDT fingers 0.05 μm. The trench depth of 1.1 μm (0.14λ) is used. The dimensions used for the conventional device are as follows: The device wavelength λ =11 μm, IDT finger width 2.8 μm ($\lambda/4$), electrode pitch 5.5 μm ($\lambda/2$), depth of the piezo-substrate 55 μm (5 λ) in $-x_3$ direction, and thickness of IDT fingers 0.05 μm. The device is operating at frequency of 311.4 MHz which is close to resonance frequency of the proposed device. An extremely fine mesh with minimum element quality of 0.7 and minimum number of 16 mesh elements per wavelength are used.

The properties of the BSP3 film and DMMP gas are reported in [3] and are used in our simulation. The density of BSP3 is 1.2 g/cm^3, and its G and K are $1.107\times10^{10} + i1.992\times10^{9}$ Pa and $1\times10^{10} + i1\times10^{10}$ Pa, respectively. The DMMP with density of 1.145 g/cm^3 is used. The

partition coefficient k of BSP3 towards DMMP is around 10^7. The experimental results on sensing DMMP gas using BSP3 film of thickness 76 nm are reported in [68], hence the following simulations are carried out with BSP3 film thickness of 76 nm.

The eigenmode analysis is performed to obtain the resonance frequencies of the proposed and conventional devices. The resonance frequency for each concentration of DMMP gas is recorded and the change in resonance frequency denoted as sensor response is calculated.

3.2.2 Results and Discussions

The simulation results of the proposed and conventional SAW one-port resonator sensors are presented below. The effect of change in sensing film thickness on resonance frequency of the proposed SAW one-port resonator sensor is studied. The sensor response (change in resonance frequency) of the proposed device due to absorption of DMMP gas is discussed and the results are compared with conventional device.

3.2.2.1 Effect of thickness of coated sensing film on sensor response

The simulation was performed to analyze the effect of thickness of coated sensing film (BSP3) on sensor response for the absorption of DMMP gas of various concentrations. The device geometry and parameters used in the simulation are explained in section 3.2.1. The figure 3.6 (a) shows the plot of sensor response versus DMMP gas concentration for initial BSP3 film thicknesses of 50 nm, 80 nm, 100 nm and 120 nm. The figure 3.6 (b) shows the sensor response versus initial BSP3 film thickness for different concentrations of DMMP gas. It is observed that the sensor response is almost linear with changes in height and concentration, consistent with the equations (2.30), (2.32) and (2.33).

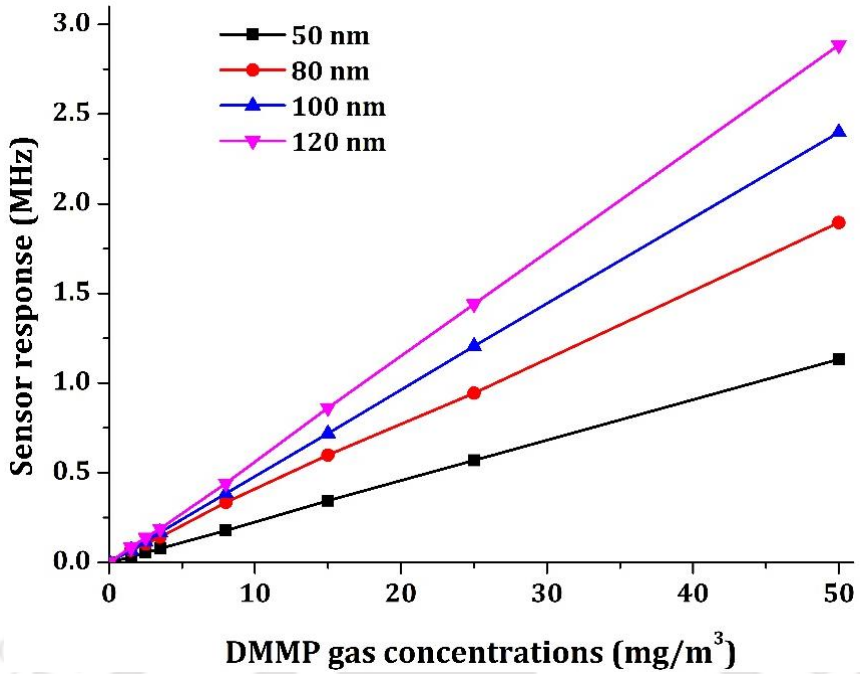

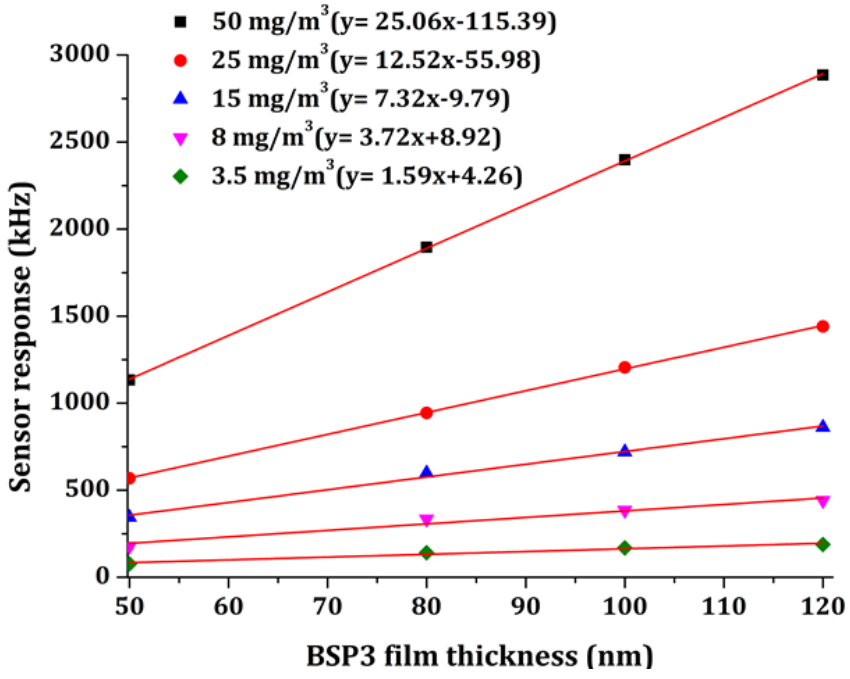

(b)

Figure 3.6 Effect of initial thickness of BSP3 film on sensor response (a) sensor response versus concentration of DMMP gas for different BSP3 film thicknesses (b) sensor response versus BSP3 film thickness for different DMMP gas concentrations. Equation of linear fit for each concentration is mentioned.

Table 3.1 compares the sensitivities of the proposed and conventional sensors for different thickness of BSP3 film

Table 3.1 Sensitivities of the proposed and conventional sensors

Initial thickness of BSP3 film	**Sensitivity of Proposed device**	**Sensitivity of Conventional device**
50 nm	22.66 kHz/mg/m^3	1.55 kHz/mg/m^3
80 nm	37.9 kHz/mg/m^3	2.64 kHz/mg/m^3
100 nm	47.96 kHz/mg/m^3	3.38 kHz/mg/m^3
120 nm	57.7 kHz/mg/m^3	3.95 kHz/mg/m^3

It is observed that the sensitivity of the SAW sensors increases with increase in thickness and the proposed device shows higher sensitivity, about 14 times greater than the conventional SAW sensor. However the higher thickness of sensing film leads to larger attenuation of SAW and in practice, affect the frequency stability of oscillators using the devices [68].

3.2.2.2 Sensor response

The simulation is carried out on the device of λ = 8 μm with 76 nm thick BSP3 film placed in the trench and resonance frequency is measured. The first two surface modes are observed at 310.419 MHz and 386.17 MHz, and the shapes of the eigenmodes are shown in figure 3.7.

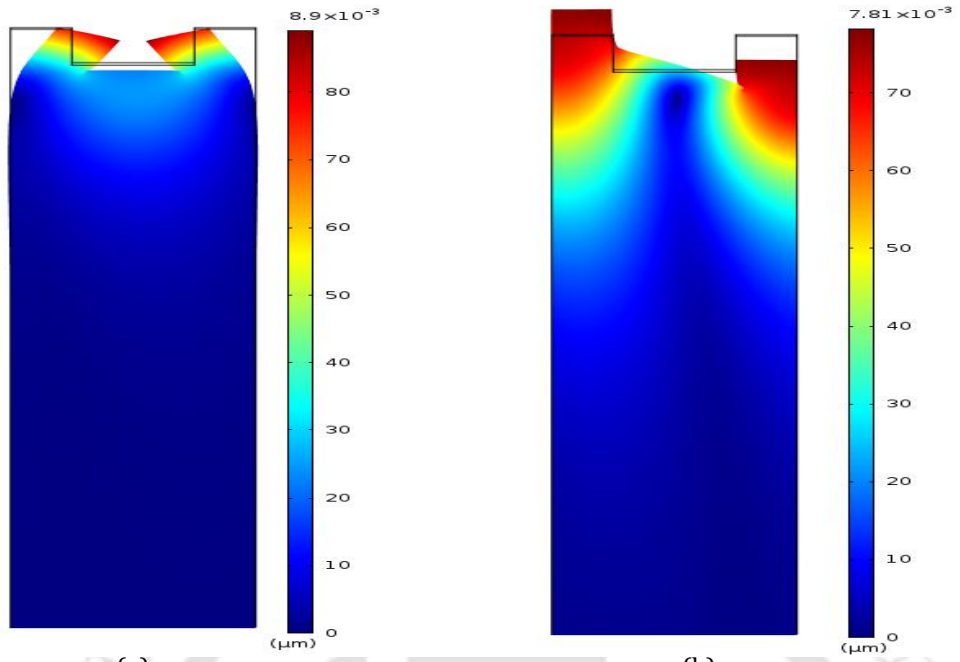

(a) (b)

Figure 3.7 Displacement profiles for (a) mode 0 and (b) mode 1 in proposed SAW device having λ 8 μm, trench depth 0.14λ and BSP3 film thickness 76 nm.

The frequency analysis is performed by assuming the potential of 1 V at the IDT to obtain the harmonic admittance of the proposed one-port SAW resonator device and the plot is shown in figure 3.8. From the plot it is observed that mode 0 is dominant and susceptance crosses zero at frequency of 310.419 MHz which is considered as the resonance frequency of the device.

The figure 3.9 shows the longitudinal and transverse displacements for mode 0 plotted against the substrate depth considered from the bottom of the trench. From the plots it is observed that the transverse displacement (1.45 nm) is dominant over the longitudinal displacement (0.19 nm) at zero depth and the longitudinal displacement changes sign at a depth of about 0.13λ, indicating that the surface wave propagating in the proposed device has properties close to Rayleigh wave [15].

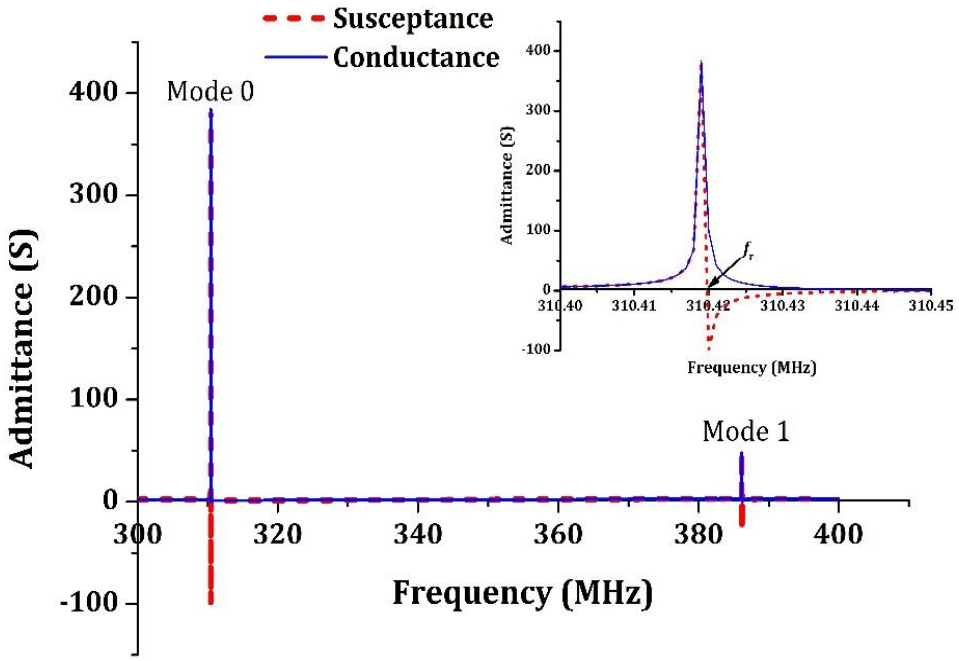

Figure 3.8 Frequency response for the proposed device shows the harmonic admittances for mode 0 and mode 1. The resonance frequency f_r (310.419 MHz) of dominant mode is marked.

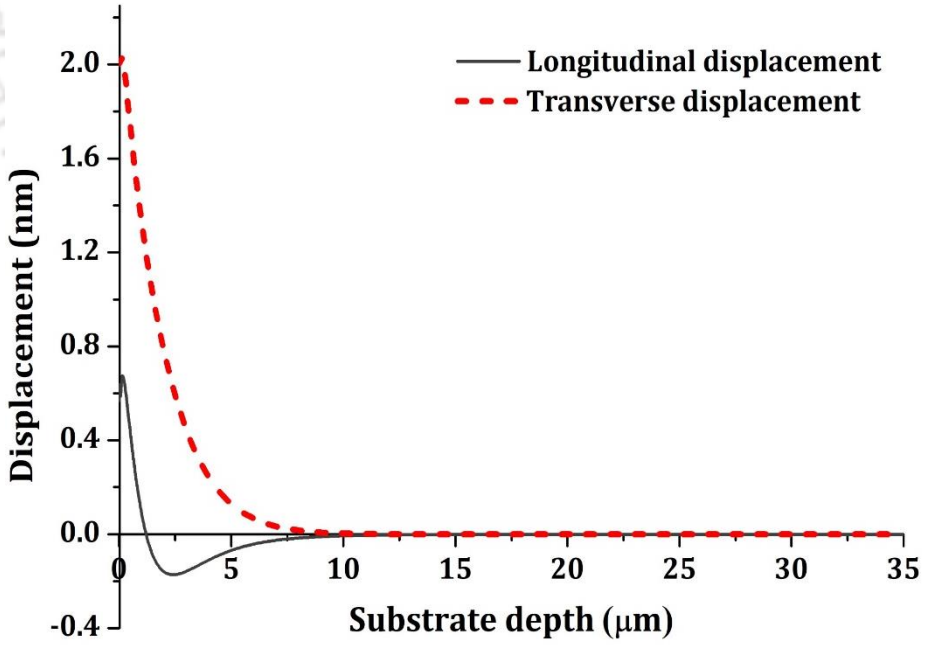

Figure 3.9 Plots of longitudinal and transverse displacements versus substrate depth for mode 0 in the proposed device.

The sensitivities of proposed and conventional SAW gas sensors are found from the shift in resonance frequency obtained using eigenmode analysis after absorption of gas into the sensing film. The BSP3 polymer of 76 nm thickness is used as the sensing film for the detection of DMMP gas and DMMP concentrations of 1.5, 2.5, 3.5, 8, 15, 25, 50 mg/m^3 are considered in the simulation. The changes in density and thickness of BSP3 film due to the absorption for each concentration of DMMP gas are calculated using (2.32) and (2.33). The resonance frequencies of proposed and conventional devices in absence of gas are close, at 310.42 MHz and 311.4 MHz, respectively. The resonance frequency for each concentration is noted and the shift in resonance frequency considered as the sensor response is calculated by subtracting the resonance frequency at 0 mg/m^3 from the resonance frequency at each concentration. The figure 3.10 shows the plot of sensor response versus concentration of DMMP gas using proposed and conventional SAW sensors.

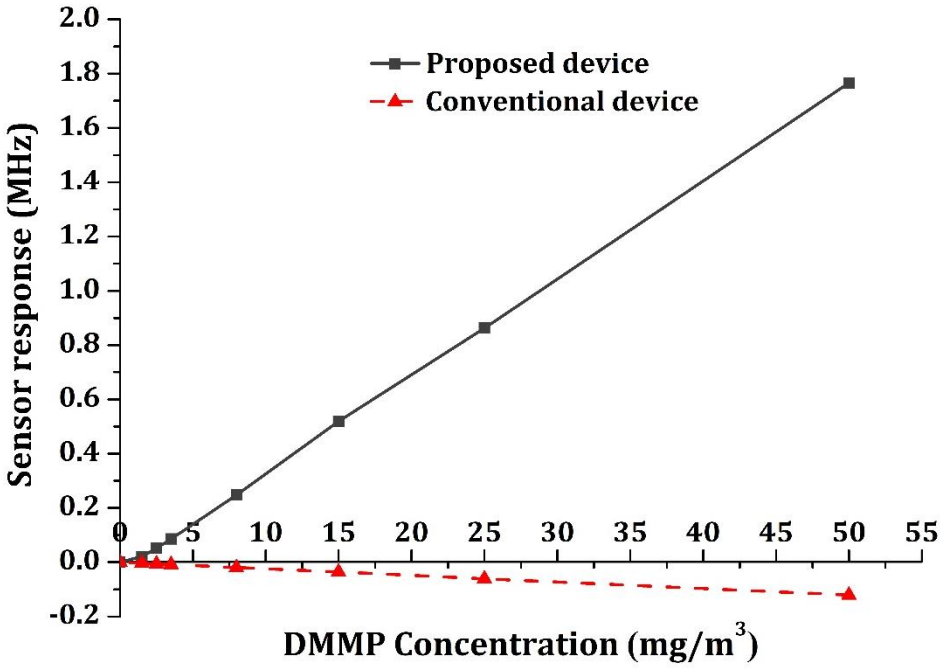

Figure 3.10 Plot of frequency shift versus concentration of DMMP gas for BSP3 film thickness of 76 nm using proposed and conventional SAW sensors.

The plot distinctly shows that with increase in gas concentration, the resonance frequency decreases in conventional device whereas it increases in proposed device. In addition, frequency shift in proposed device is about 14 times that in conventional device at higher concentrations. The response is almost linear for DMMP concentration range of 0 – 50 mg/m^3 for both devices and the sensitivity is calculated as approximately 35 kHz/mg/m^3 for proposed device and 2.4 kHz/mg/m^3 for conventional device.

The major factors affecting resonance frequency of the devices are the changes in density and thickness of sensing film due to the absorption of DMMP gas. The individual contributions of thickness and density variations in the sensor response of the proposed SAW gas sensor can be deduced from simulation. The effect of thickness change is calculated using (2.33) while keeping density constant and the effect of density change is calculated using (2.32) while keeping thickness constant. The figure 3.11 shows plot of frequency shift versus concentration of DMMP gas in three cases– only density change, only thickness change and change in both density and thickness.

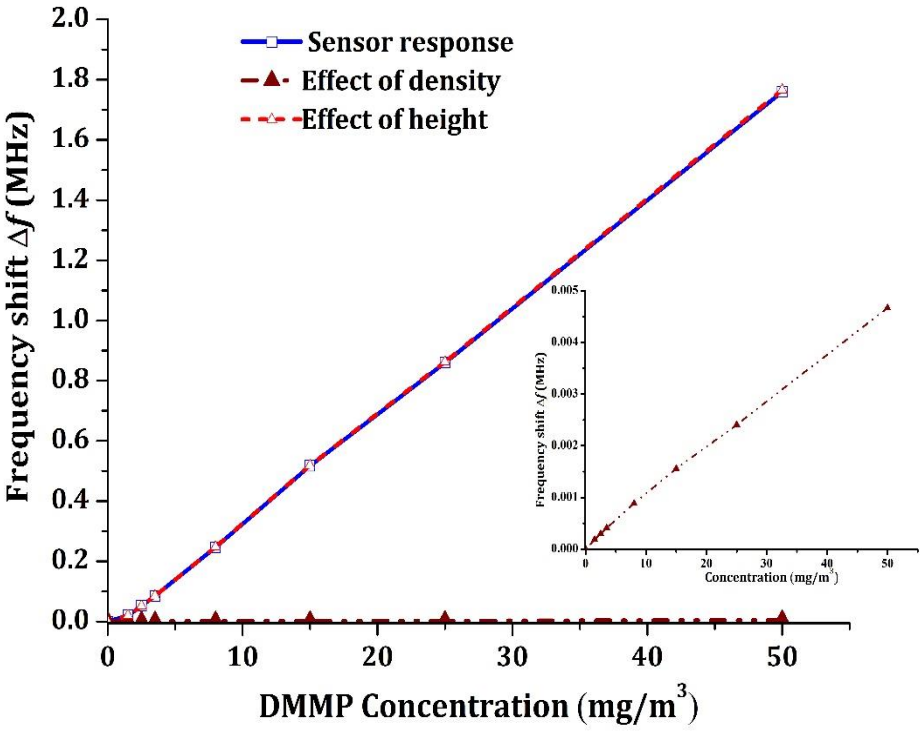

Figure 3.11 Plot of shift in resonance frequency versus concentration of DMMP gas for the proposed device in three cases with change in height, with change in density and change in both height and density.

From the plot, it is observed that the effect of density change is negligible and change in thickness is the major factor contributing to the sensor response. The effect of increase in thickness of sensing film also called swelling effect due to gas absorption is equivalent to decrease in trench depth causing shift in the operating point to the left in figure 3.3 (b) and resulting in the large increase in resonance frequency.

3.3 Simulation of proposed one-port SAW resonator device for sensing hydrogen gas.

In this section, proposed one-port SAW resonator for sensing hydrogen (H_2) gas using palladium (Pd) film is simulated. Pd film is coated at the bottom of the trench made between the IDT fingers. The absorption of Hydrogen (H_2) gas will change Pd film properties, which perturbs the SAW propagation velocity and results in change in resonance frequency of the device [91]. The shift in resonance frequency is obtained by subtracting the resonance frequency of the device in the absence H_2 from the resonance frequency in the presence of H_2 and is considered as sensor response.

3.3.1Simulation methodology

A 2D piezo module with plain strain mode in COMSOL 4.4 is used to simulate a one-port SAW resonator with infinite number of IDT fingers. The 2D geometry used for FE simulation is given in figure 3.12. The periodic nature of the SAW resonator allows modeling the device using one unit cell with periodic boundary condition, which reduces the size and computational complexity of the device. The half periodic section of proposed SAW resonator with sign inversion of variables at the boundaries is used in the simulation.

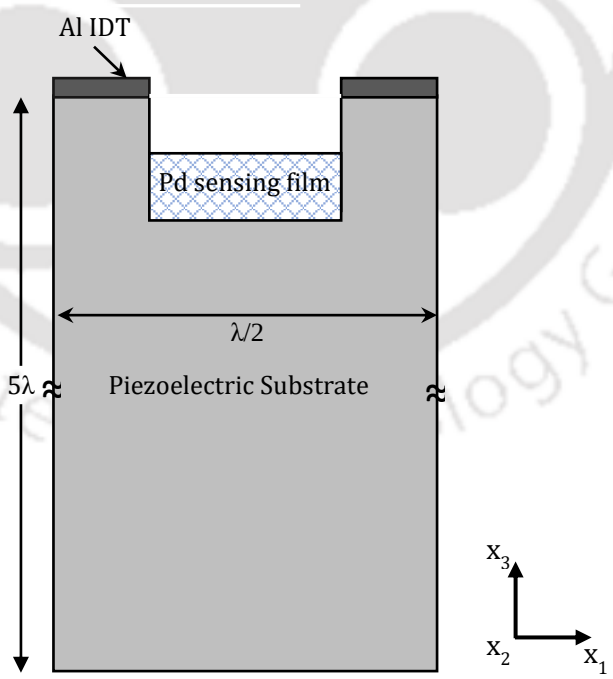

Figure 3.12 2D geometry of one-port SAW resonator with Pd in trenches used in simulation.

The dimensions used for simulation are as follows: finger width 4 μm, finger pitch 8 μm, depth of the substrate 64 μm (5λ). The thickness of IDT fingers is 0.05 μm. The trenches having width of 6 μm and depth of 4.8 μm (0.3λ) are used. The sensing film used for simulation has thickness of 2 μm as reported in [91]. The piezo-substrate of YZ $LiNbO_3$ material is used. The material properties of piezo-substrate such as elasticity matrix, coupling matrix, relative permittivity and density are referred from Ahmadi *et al*. [102]. The Eigenmode frequency calculation provided by COMSOL Multiphysics is used. An extremely fine mesh with minimum element quality of 0.7 and the number of mesh elements of minimum 16 per wavelength are used. The Eigen modes of the device are calculated with zero driven voltages at the IDT electrodes. The resonance frequency of the device is 132.87 MHz. The values of Young's modulus, density and thickness of Pd for different concentrations of hydrogen in Pd used for simulation [91] are given in table 3.1

Table 3.2 Material properties for the Pd at different hydrogen concentrations

Concentration (H_2/Pd)	Young's Modulus (GPa)	Density (kg/m^3)	Thickness (μm)
0.00	128.00	12020.00	2.000
0.05	126.20	12019.98	2.019
0.10	124.50	12008.57	2.038
0.15	123.00	11985.84	2.057
0.20	121.36	11951.94	2.076
0.30	118.50	11851.50	2.114
0.37	116.83	11756.33	2.141
0.43	115.00	11659.35	2.163
0.50	113.73	11529.29	2.190

3.3.2 Results and Discussions

The FE simulations are performed for various concentrations of H_2 gas and resonance frequency is calculated. The resonance frequency of the device without H_2 absorption is at 132.87 MHz and is taken as reference value. Subtracting the resonance frequency calculated for various concentrations of H_2 gas from the reference value gives the shift in resonance frequency and is considered as sensor response. The sensor response for various concentrations of H_2 gas is shown in figure 3.13.

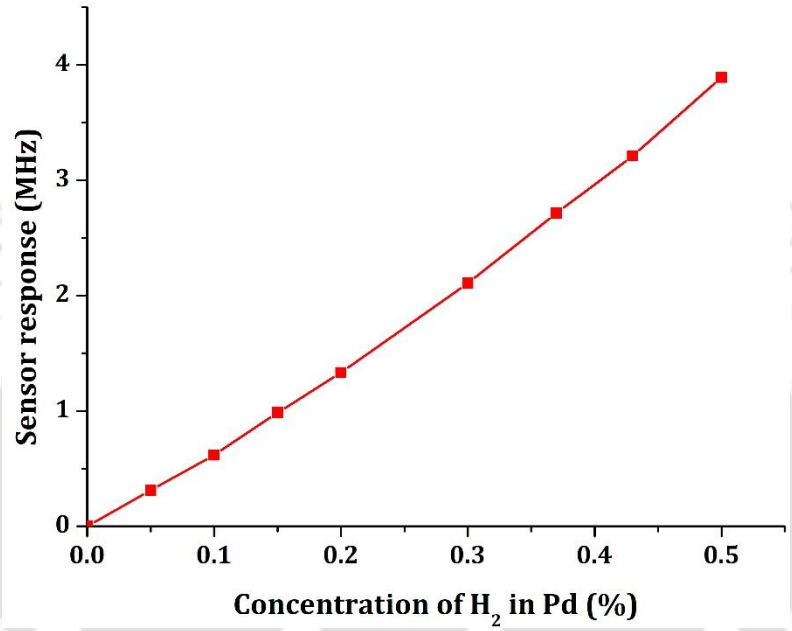

Figure 3.13 Plot of sensor response versus concentration of H_2 in Pd.

An increase in resonance frequency with increase in H_2 concentartion is observed in the proposed device using Pd sensing film. As dicussed in detail in section 3.2.2.2 for sensing DMMP gas, the increase in Pd thickness called swelling effect due to H_2 gas absorption leads to decrease in trench depth resulting in the large increase in resonance frequency, about 3% for H_2 concentration of 0.5%. The Pd sensing film thickness of 2 μm is used in the simulation as the H_2-Pd data is available. A 2 μm thick Pd sensing film in the trench of trench depth 2.2 μm has shifted the operating point to extreme left in Fig. 3.3 (b) and the change in Pd thickness goes beyond a small linear perturbation on the operating point leading to nonlinear response.

3.4 Summary

This chapter presents the simulation of one-port SAW resonator with trenches made in the space between the IDT fingers and its application in gas sensing. A 2D FE analysis of proposed SAW one-port SAW resonator using COMSOL Multiphysics is carried out to determine the harmonic admittance and resonance frequency. The effect of trench depth on the resonance frequency is studied. It is observed that the resonance frequency decreases with increase in trench depth and the maximum change in resonance frequency occurs at trench depth of 0.14λ for YZ $LiNbO_3$ piezoelectric substrate.

2D FE simulations of proposed and conventional SAW one-port resonator devices for sensing Dimethymethaphosponate (DMMP) are carried out. The fluorinated bisphenol-containing polymer (BSP3) is used as a sensing material for the detection of DMMP gas. In the proposed SAW sensor, BSP3 film is placed at the bottom of the trench having depth of 0.14λ made in the space between the IDT fingers. Initially the effect of sensing film thickness on resonance frequency of the device for fixed trench depth is studied by using different BSP3 film thicknesses. It is observed that as the thickness of BSP3 film increases, the trench depth decreases which leads to increase in the resonance frequency of the device. Though higher thickness of BSP3 film gives higher sensitivity, it leads to greater attenuation of SAW. BSP3 film thickness of 76 nm is used in the simulations of proposed and conventional devices for detection of DMMP gas and results are compared. An increase in resonsce frequency is observed in proposed device while decrease in resonance frequency is observed in conventional device for the same concentrations of DMMP gas. The swelling of BSP3 film in the trench due to absorption of DMMP gas will decrease the effective trench depth in the proposed sensor and leads to increase in resonance frequency in accordance with the effect of trench depth mentioned above. A positive shift is observed in the proposed sensor response and shows a sensitivity of approximately 35 kHz/mg/m^3 which is about 14 times greater than that of conventional device.

An FE simulation of proposed SAW one-port resonator device for sensing hydrogen gas (H_2) is carried out. The palladium metal (Pd) is used as a sensing material for the detection of H_2 gas. The Pd film of 2 μm is placed at the bottom the trench having depth of 4.8 μm made in the space between IDT fingers. An increase in resonance frequency is observed in proposed device with increase in concentrations of H_2 gas. The swelling of Pd film in the trench due to absorption of H_2 gas will decrease the effective trench depth in the proposed sensor and lead to increase in resonance frequency.

4

FE analysis of SAW resonator with HAR structures for sensing gases

This chapter presents the second structure proposed in the SAW devices for sensing applications leading to higher sensitivity. The first structure discussed in chapter 3 has shown higher sensitivity for gas sensing compared to the conventional SAW device, however it requires fabrication of trenches of precise depth in the substrate. The structure proposed in this chapter involves developing high aspect ratio (HAR) structures on the substrate to achieve the effect observed in the first structure without making trenches in the substrate. Two types of high aspect ratio structures are analyzed, i) using thick IDT fingers and ii) using SiO_2 HAR structures covering IDT fingers.

Initially FE analysis of one-port SAW resonators with thick IDT is carried out using COMSOL Multiphysics and its application in sensing dimethymethaphospohnate (DMMP) gas is simulated using fluoroalcholpolysiloxane (SXFA) as sensing material. The second structure simulated is a one-port SAW resonator with SiO_2 HAR structures covering IDT fingers and it is used to sense DMMP gas using SXFA sensing film, trichloroethylene (TCE) vapor using Polyisobutylene (PIB) as sensing material and H_2 gas using Pd as sensing material. The sensitivities obtained using the two proposed devices are compared with that of conventional SAW devices. The fabrication and testing of SAW one-port resonator devices with SiO_2 pillars and experimental results of sensing TCE and H_2 gases are presented in chapter 5.

4.1. Analysis of one-port SAW resonator with thick IDT

A one-port SAW resonator with infinite number of thick IDT fingers is considered. The characteristics of the proposed resonator are studied by simulation. The simulation methodology, geometry used for simulation, and results are discussed below.

4.1.1. Simulation methodology

2D piezo module using plain strain mode in COMSOL Multiphysics 4.4 is used to simulate a one-port SAW resonator with infinite number of thick IDT. A 2D geometry used for simulation

is shown in figure 4.1. Due to the periodic nature of the IDT structure, the periodic boundary condition is used which allows the devices to be modelled using half spatial period of IDT with sign inversion at the boundaries. The SAW wavelength (λ) of 8 μm is used for simulation. The dimensions used for simulation are as follows: finger width 2 μm (λ/4), finger pitch 4 μm (λ/2) and depth of the substrate 40 μm (5λ). Different types of IDT metals such as gold(Au), sliver (Ag), Aluminium (Al) and Nickel (Ni) having width of 2 μm are used to make IDT over the piezo-substrate and the height (h_{IDT}) is varied from 0.1 μm to 4 μm (λ/2). Y cut Z propagation lithium niobate (YZ $LiNbO_3$) material is used as piezo-substrate. The material properties of piezo-substrate such as elasticity matrix, coupling matrix, relative permittivity and density are referred from Ahmadi *et al* [102]. Appropriate boundary conditions are applied. Rayleigh wave propagates perpendicular to the IDT electrodes and there is no displacement along the x_2 direction. Thus the top surface of the substrate is kept stress free and bottom of the substrate is assumed fixed. Extremely fine mesh with mesh element size of 0.5 μm is used. The periodic boundary condition is applied to left and right sides of the device as given in Hamodon *et al.* [103]. The eigenmodes of the device are calculated with zero driven voltages at the IDT electrodes.

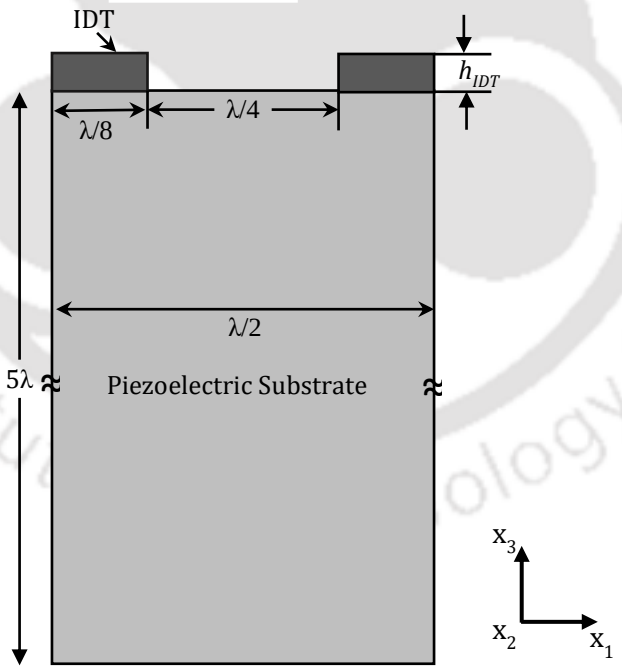

Figure 4.1 Geometry of proposed SAW resonator with thick IDT.

4.1.2 Results and discussions

To study the effect of IDT thickness on resonance frequency an eigenmode analysis of one-port SAW resonator with thick IDT is carried out. The thickness of IDT is varied from 0.1 μm to 4 μm (λ/2) with step size of 0.1 μm and resonance frequency at each thickness is observed. Different metals such as Ag, Au, Al and Ni are used to make IDT. The resonance frequency of the device versus normalized thickness of IDT for different metals is shown in figure 4.2(a). From the plot, it is observed that as the thickness of IDT increases, the resonance frequency decreases for a given IDT metal due to mass loading effect and the results are consistent with theoretical results on SAW devices having HAR Ni IDT structure on piezo-substrates reported by Laude et al. [104, 105, 106]. For a fixed thickness of IDT, the resonance frequency of the device is lower for higher density materials. The rate of change of frequency with respect to thickness of IDT is plotted in figure 4.2(b). It is observed that IDT thickness at which change in frequency is maximum varies with IDT material. IDT thickness required for maximum change in frequency is smaller for higher density materials. The fabrication of thick Ni electrode on lithium niobate piezoelectric substrate is reported in [105] and is considered as IDT material. The thickness at which maximum change in frequency occurred for Ni IDT is at 0.1λ (0.8 μm) and is used as the IDT thickness in the following simulations.

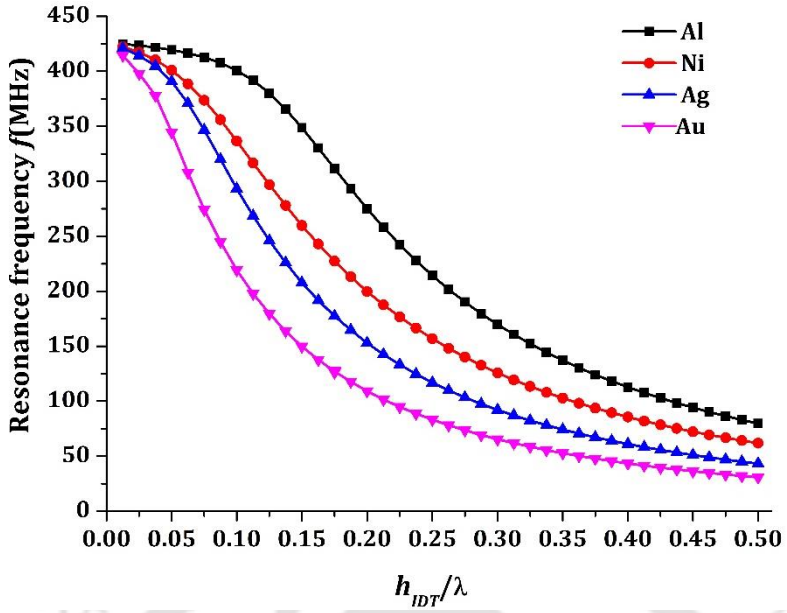

(a)

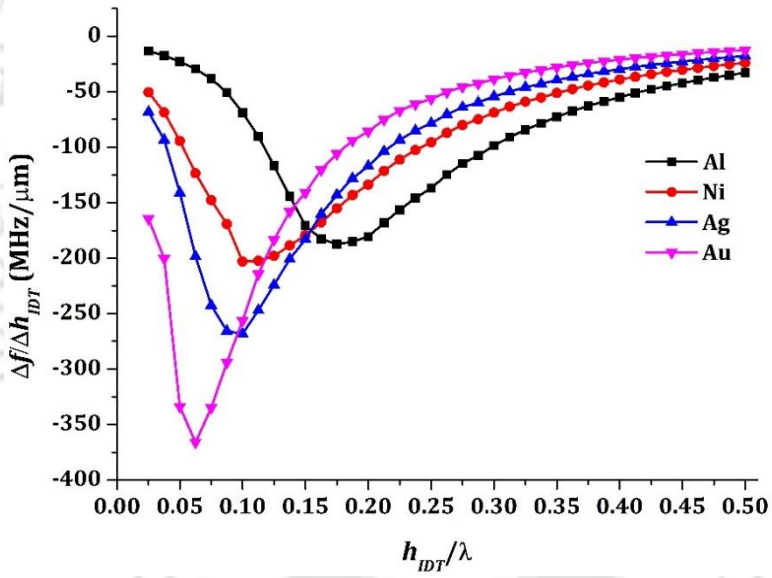

(b)

Figure 4.2 Plots of (a) Resonance frequency versus normalized IDT thickness for different metals, (b) Rate of change of frequency with respect to IDT thickness versus normalized IDT. thickness

The frequency analysis of one-port SAW resonator with thick Ni IDT is performed. The dimensions used in the simulation are as follows: wavelength 8 μm (λ), IDT finger width 2 μm ($\lambda/4$), electrode pitch 4 μm ($\lambda/2$), depth of the piezo-substrate 40 μm (5 λ) in $-x_3$ direction. The IDT thickness of 0.8 μm (0.1 λ) as discussed above is used. A potential of 1 V is applied at the IDT to obtain the harmonic admittance of the device. The plots of displacement and

harmonic admittance versus frequency of the proposed one-port SAW resonator device is shown in figure 4.3.

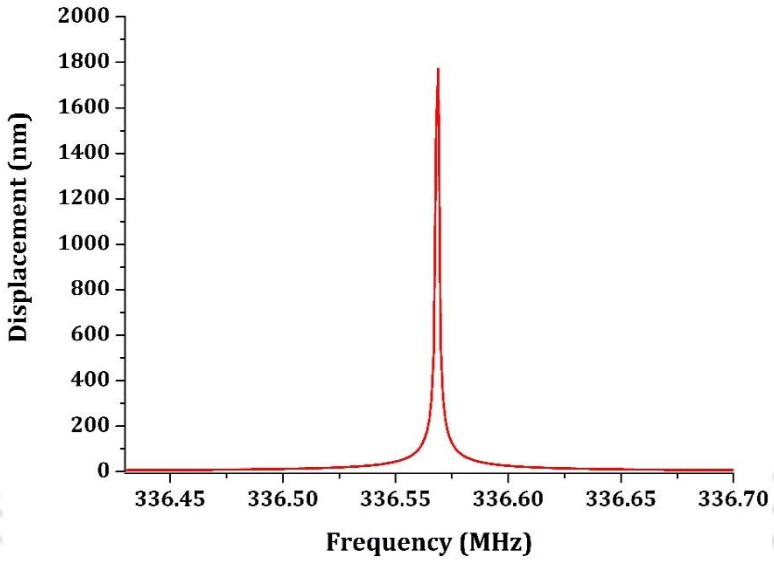

(a)

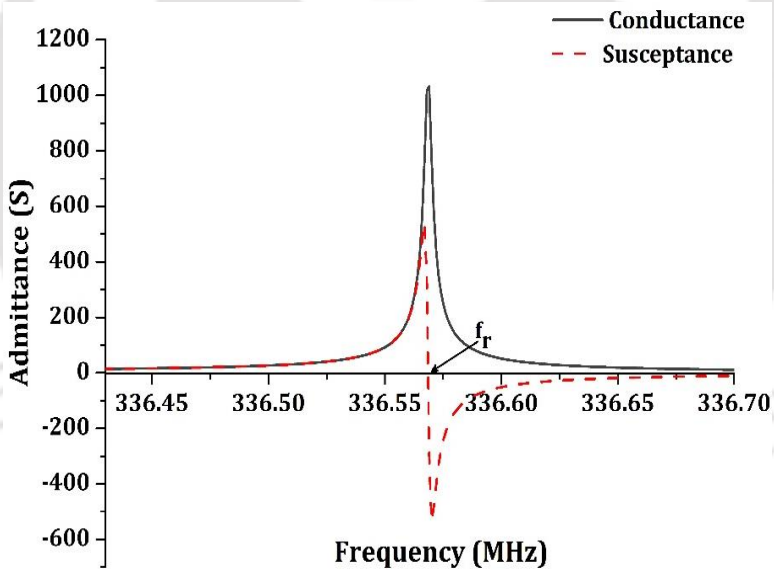

(b)

Figure 4.3 Results of simulation of the one-port resonator with thick Ni IDT. (a) Plot of total displacement versus frequency, (b) Plot of harmonic admittance versus frequency.

4.2. Analysis of one-port SAW resonator with thick IDT for sensing DMMP gas

The proposed and conventional SAW one-port resonator configurations are simulated in COMSOL Multiphysics to sense dimethylmethylphosphonate (DMMP) gas using fluoroalcoholpolysiloxane (SXFA) film as sensing medium. The resonance frequency of the device is noted in the presence and absence of the gas. The sensitivity is obtained from the resonance frequency shift for various concentrations of DMMP gas. The sensitivities of the proposed SAW sensor and a conventional SAW sensor are compared.

4.2.1 Simulation methodology

2D FE simulations of the proposed and conventional SAW devices for sensing DMMP gas are performed using COMSOL Multiphysics. The one-port SAW resonator having single thick IDT with infinite number of IDT fingers is considered. The periodic nature of the SAW resonator allows modeling the device using one unit cell with periodic boundary condition, which will reduce the size and computational complexity of the device. The geometries of half periodic sections of proposed and conventional SAW resonators with sign inversion of variables at the boundaries used in simulation are shown in figure 4.4. The piezo module with plane strain mode provided in COMSOL Multiphysics is used. The stress free boundary condition is used at the top surface of the substrate and bottom surface of the substrate is assumed to be fixed. The properties such as coupling matrix, elasticity matrix, relative permittivity and density of YZ $LiNbO_3$ piezo-substrate are taken from [102]. Since the energy in SAW is confined to a depth of about one wavelength from the wave propagation surface of the substrate, the substrate depth of 5λ is considered.

A Ni IDT having uniform thickness of 0.8 μm with metallization ratio of 0.5 is patterned on the YZ $LiNbO_3$ substrate and SXFA is used as the sensing material. The SXFA sensing film is placed in the space between the thick IDT fingers as shown in figure 4.4(b). The device is operating at frequency of about 336.708 MHz. The dimensions used in the simulation for the proposed device are as follows: the device wavelength λ = 8 μm, IDT finger width 2 μm ($\lambda/4$), electrode pitch 4 μm ($\lambda/2$), depth of the piezo-substrate 40 μm (5 λ) in $-x_3$ direction. The dimensions used for the conventional device are as follows: Wavelength λ =10 μm, IDT finger width 2.5 μm ($\lambda/4$), electrode pitch 5 μm ($\lambda/2$), depth of the piezo-substrate 50 μm (5 λ) in $-x_3$ direction, thickness of IDT fingers 0.05 μm. The device is operating at frequency of 339.334 MHz which is close to resonance frequency of the proposed device. An extremely fine mesh

with minimum element quality of 0.7 and the number of mesh elements of minimum 16 per wavelength are used.

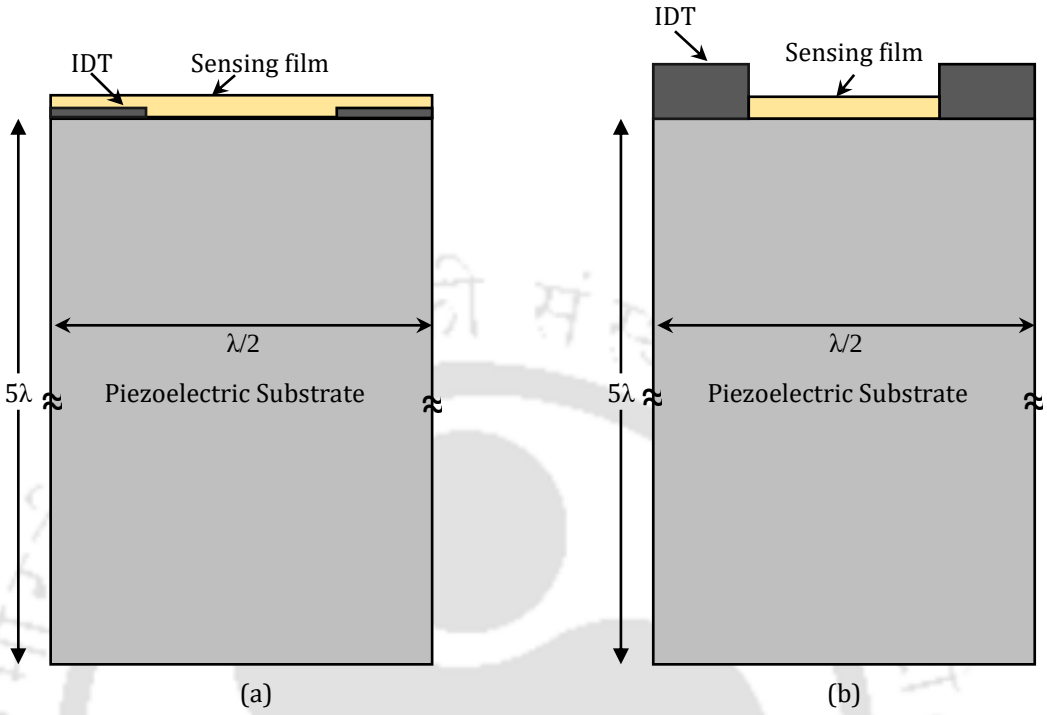

Figure 4.4 2D geometries of one-port SAW resonators used in simulation (a) sensing film over the IDT (conventional device) (b) sensing film between the thick IDT (proposed device).

In this simulation, fluoroalcoholpolysiloxane (SXFA) is a used as a sensing material and the target gas is DMMP. The properties of the SXFA film and DMMP gas are reported in [107] and are used in the simulation. The density of SXFA is 1.447 g/cm^3, and its G and K are $9.3\times10^9 + i1.2\times10^9$ Pa and $10\times10^9 + i0$ Pa, respectively. DMMP with density of 1.145 g/cm^3 is used. The partition coefficient k of SXFA towards DMMP is around $10^{6.4}$. The SXFA film of thickness 65 nm is used in simulations. The eigenmode analysis is performed to obtain the resonance frequency of the proposed and conventional devices. The absorption of DMMP gas changes the properties of the SXFA sensing film, which perturbs the SAW velocity and results in change in the resonance frequency of the device. The resonance frequency for each concentration of DMMP gas is recorded and the shift in resonance frequency is calculated.

4.2.2 Results and discussions

The simulation is carried out on the device of λ = 8 μm with 65 nm thick SXFA film placed in the space between thick IDT fingers and resonance frequency is measured. The first two

surface modes are observed at 336.708 MHz and 372.757 MHz, and the shapes of the eigenmodes are shown in figure 4.5.

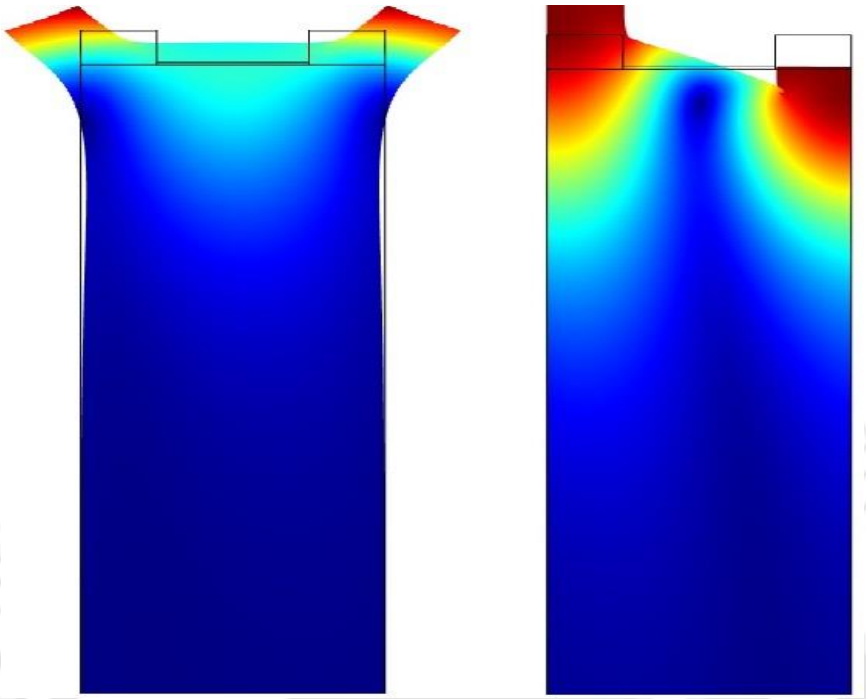

(a) (b)

Figure 4.5 Total displacement profile of the proposed SAW one-port resonator with 65 nm thick SXFA film between IDT fingers of 0.8 μm thickness at (a) surface mode 0, and (b) surface mode 1.

The frequency analysis is performed by assuming the potential of 1 V at the IDT to obtain the harmonic admittance of the proposed one-port SAW resonator device and the plot is shown in figure 4.6. From the plot it is observed that mode 0 is dominant and susceptance crosses zero at frequency of 336.708 MHz which is considered as the resonance frequency of the device.

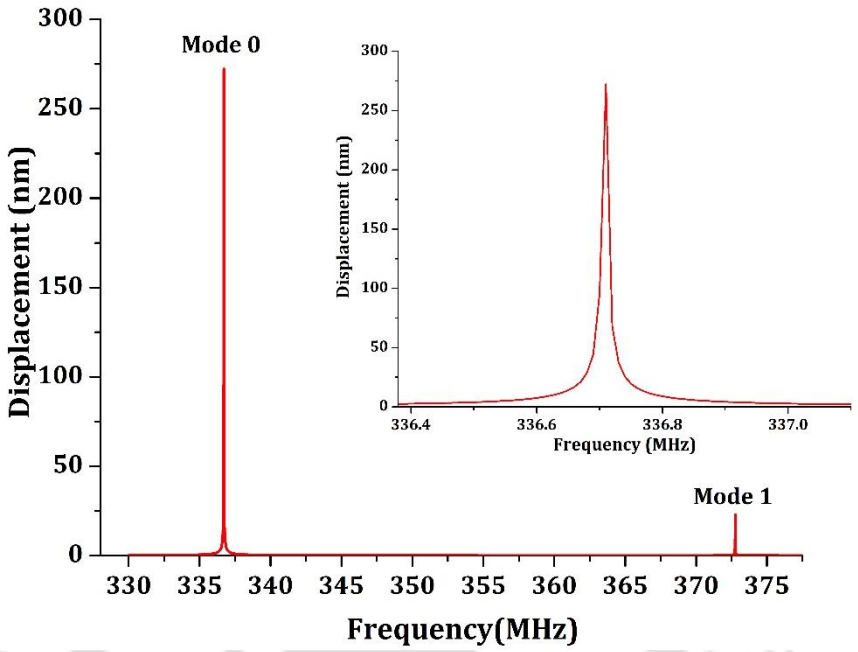

(a)

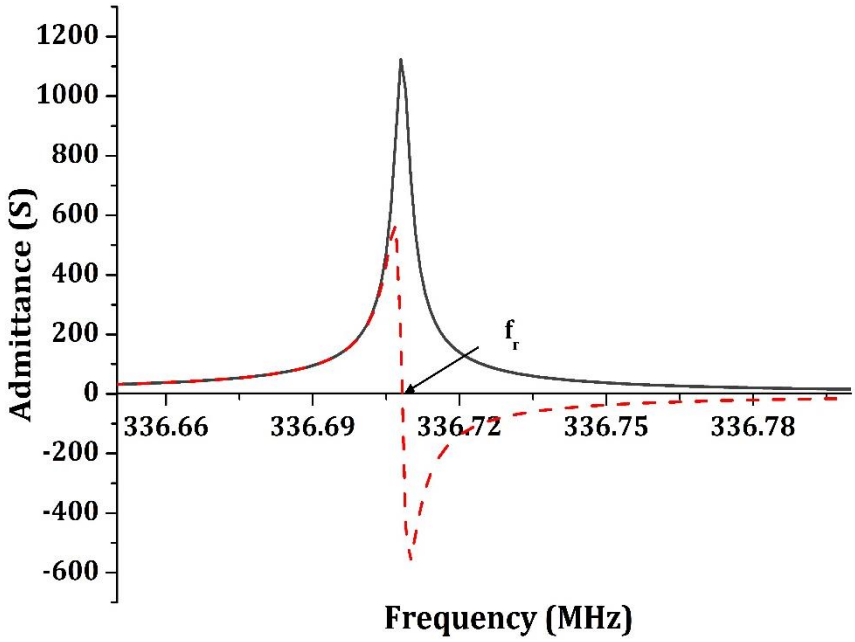

(b)

Figure 4.6 Results of simulation of one-port resonator with SXFA between the thick Ni IDT. (a) Plot of total displacement versus frequency (b) Plot of harmonic admittance versus frequency at mode 0.

The figure 4.7 shows the longitudinal and transverse displacements for mode 0 plotted against the substrate depth. From the plots it is observed that the transverse displacement is dominant over the longitudinal displacement at zero depth and the longitudinal displacement

changes sign at a depth of about 0.17λ, indicating that the surface wave propagating in the proposed device has properties close to Rayleigh wave [15].

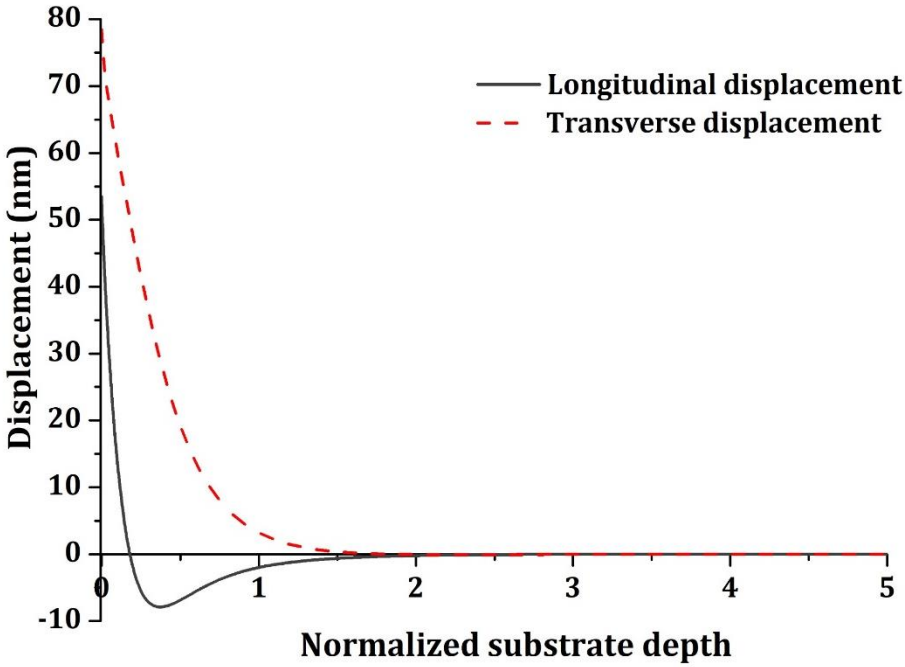

Figure 4.7 Plots of longitudinal and transverse displacements versus substrate depth for mode 0 in the proposed device.

The sensitivities of proposed and conventional SAW gas sensors are found from the shift in resonance frequency obtained using eigenmode analysis after absorption of gas into the sensing film. The SXFA polymer of 65 nm thickness is used as the sensing film for the detection of DMMP gas and DMMP concentrations from 0 to 100 mg/m^3 are considered in the simulation. The change in density and thickness of SXFA film due to the absorption of each concentration of DMMP gas is calculated using (2.32) and (2.33). The resonance frequencies of proposed and conventional devices in absence of gas are close, at 336.708 MHz and 339.334 MHz, respectively. The resonance frequency for each concentration is noted and the shift in resonance frequency considered as sensor response is calculated by subtracting the resonance frequency at 0 mg/m^3 from the resonance frequency at each concentration. The figure 4.8 shows the plot of sensor response versus concentration of DMMP gas using proposed and conventional SAW sensors.

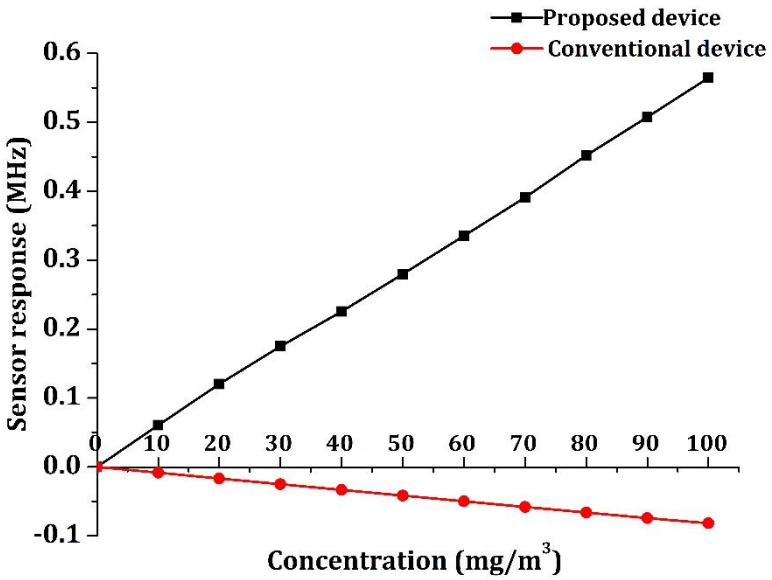

Figure 4.8 Plot of sensor response versus concentration of DMMP gas for SXFA film thickness of 65 nm using proposed and conventional SAW sensors.

The plot distinctly shows that with increase in gas concentration, the resonance frequency decreases in conventional device, corroborated by experimental results reported by Singh et al. [8], whereas it increases in proposed device. In addition, frequency shift in proposed device is about 7 times that in conventional device. The response is almost linear for DMMP concentration range of 0 – 100 mg/m^3 for both the devices and the sensitivity is calculated as approximately 5.64 kHz/mg/m^3 for proposed device and 0.82 kHz/mg/m^3 for conventional device.

The changes in density and thickness of sensing film due to absorption of DMMP gas are the major factors affecting resonance frequency of the devices. The individual contribution of thickness and density variations in sensor response of the proposed SAW gas sensor can be deduced from simulation. The effect of thickness change is calculated using (2.33) while keeping density constant and the effect of density change is calculated using (2.32) while keeping thickness constant. The figure 4.9 shows frequency shift versus concentration of DMMP gas in three cases– only density change, only thickness change and change in both density and thickness.

From the plot, it is observed that the effect of density change is negligible and change in thickness is the major factor contributing to the sensor response. The effect of increase in thickness also called swelling effect due to gas absorption is equivalent to decrease in

effective thickness of IDT resulting in shifting the operating point to the left in figure 4.2 (a) and the large increase in resonance frequency is observed.

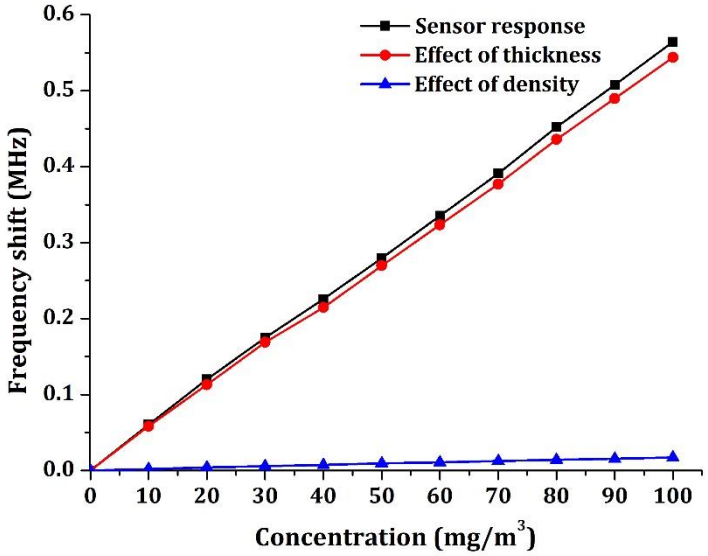

Figure 4.9 Plot of shift in resonance frequency versus concentration of DMMP gas for the proposed device with change in film thickness and with change in density. The combined effect of change in film thickness and density is also included.

4.3. Analysis of one-port SAW resonator with SiO_2 HAR structures over IDT

A one-port SAW resonator with infinite number of IDT fingers with HAR structure made of silicon dioxide (SiO_2) covering the IDT fingers is considered. The characteristics of the resonator are studied by simulation. The simulation methodology, geometry used for simulation, and results are discussed below.

4.3.1. Simulation methodology

2D piezo module using plain strain mode in COMSOL Multiphysics 4.4 is used to simulate a one-port SAW resonator with infinite number of IDT fingers having SiO_2 HAR structure over each finger. The geometry used for simulation is shown in figure 4.10. Due to the periodic nature of the IDT structure, the periodic boundary condition is used which allows the devices to modelled using half spatial period of IDT with sign inversion at the boundaries. The SAW wavelength (λ) of 8 μm, 10 μm, 12 μm, 16 μm and 20 μm are used in the simulation. The dimensions used for simulation are as follows: finger width λ/4, finger pitch λ/2, depth of the

substrate 5λ and thickness of fingers 0.05 μm. Each IDT finger is covered with SiO_2 HAR structure of width λ/4 and its height (h_{SiO_2}) is varied from 0.06λ to 0.5λ. Y cut Z propagation lithium niobate (YZ $LiNbO_3$) material is used as piezo-substrate. The material properties of piezo-substrate such as elasticity matrix, coupling matrix, relative permittivity and density are referred from Ahmadi *et al* [102]. Appropriate boundary conditions are applied to the model in the simulation as follows. The top surface of the substrate is kept stress free and bottom of the substrate is assumed fixed.

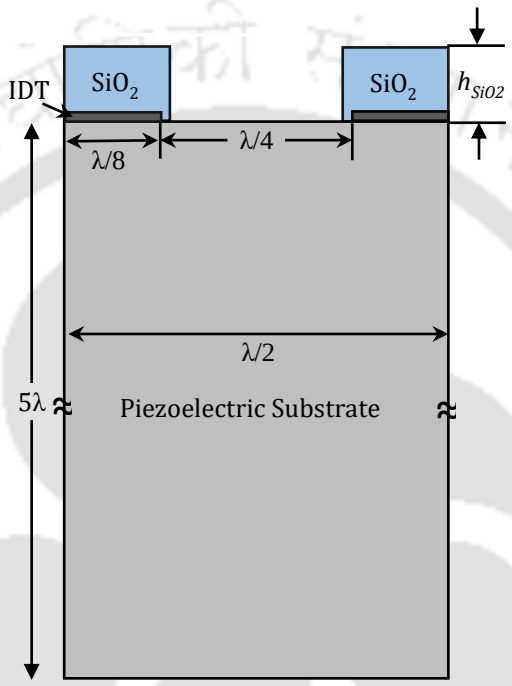

Figure 4.10 Geometry of SAW one-port resonator with SiO_2 HAR structure over IDT.

An extremely fine mesh with minimum element quality of 0.7 and the number of mesh elements of minimum 16 per wavelength are used for all the simulations. The periodic boundary condition is applied to left and right sides of the device as given in Hamodon *et al.* [103]. The eigenmodes of the device are calculated with zero driven voltages at the IDT electrodes.

4.3.2 Results and discussions

To study the effect of height of SiO_2 HAR structure on the resonance frequency, an eigenmode frequency analysis of one-port SAW resonator with SiO_2 HAR structure over IDT without sensing film is carried out for different values of λ. The h_{SiO_2} is varied from 0.06λ to 0.5λ and eigenmode frequency at each height is observed. The plots of frequency versus normalized SiO_2 HAR structure height (h_{SiO_2}/λ) for λ of 8, 10, 12, 16 and 20 μm are shown in figure 4.11(a).

The rate of change of frequency with respect to h_{SiO_2} for each λ is calculated and plotted in figure 4.11(b).

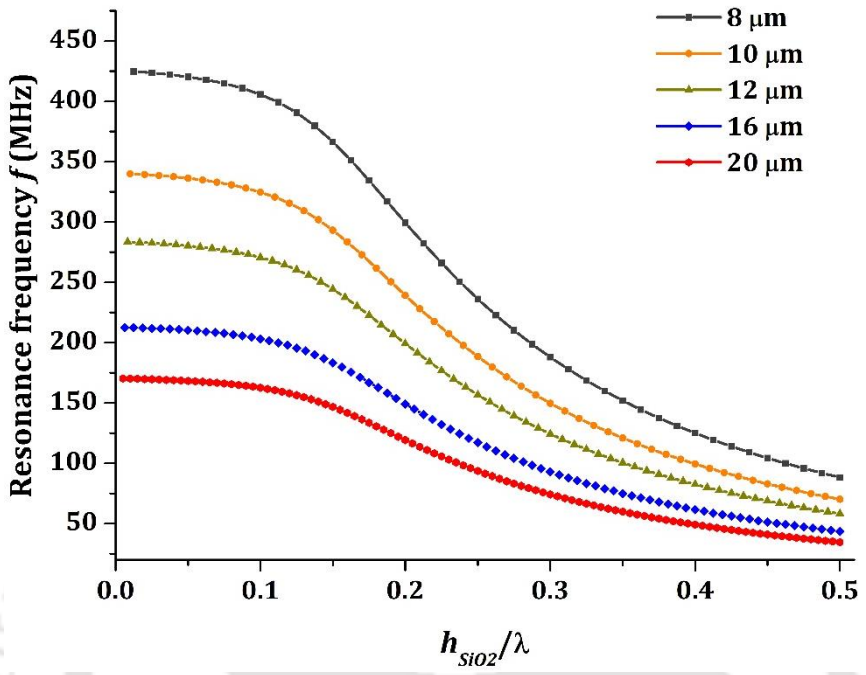

(a)

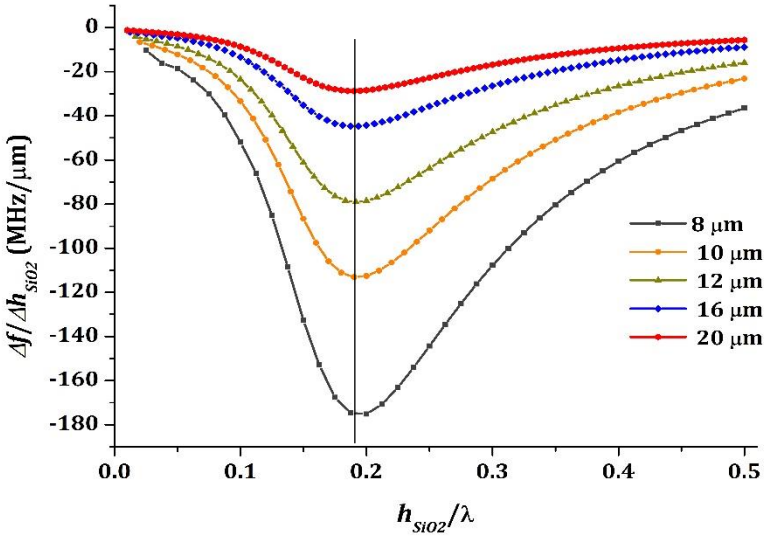

(b)

Figure 4.11 The plots of (a) Resonance frequency versus normalized height of SiO_2 HAR structure (h_{SiO_2}/λ), (b) Rate of change of frequency with respect to h_{SiO_2} versus h_{SiO_2}/λ.

Figure 4.11 shows that the change in the resonance frequency is greater for smaller values of λ for a given change in h_{SiO_2}, however the maximum change in frequency is at h_{SiO_2} of about 0.19λ in all the cases. Therefore, h_{SiO_2} of 0.19λ is considered in the following simulations.

4.4 Simulation of one-port SAW resonator with SiO_2 HAR structures for sensing gases

The simulations of one-port SAW resonators with SiO_2 HAR structure covering the IDT finger with sensing film coated in the space between the fingers as shown in figure 4.12(a) for sensing DMMP gas, trichloroethylene (TCE) organic vapor and hydrogen (H_2) gas are carried out. The SXFA, polyisobutylene (PIB) and palldium (Pd) are used as sensing materials for the detection of DMMP, TCE and H_2 gas respectively. The resonance frequency is calculated using eigenmode frequency analysis in COMSOL Multiphysics. The change in resonance frequency of the SAW device for various concentrations of gas is plotted. The sensitivity of the gas sensor using proposed SAW device is compared with that using conventional SAW device.

4.4.1 One-port SAW resonator with SiO_2 HAR structure over IDT for sensing DMMP gas

The DMMP gas sensors using SXFA film as the sensing medium in proposed and conventional one-port SAW resonators are simulated in COMSOL Multiphysics. The resonance frequency of the device is noted in the presence and absence of DMMP gas. The sensitivity is obtained from the resonance frequency shift for various concentrations of DMMP gas. The sensitivities with the proposed SAW device and that with conventional SAW device are compared.

4.4.1.1 Simulation methodology

2D FE simulations of the proposed and conventional devices for sensing DMMP gas are performed using COMSOL Multiphysics. The one-port SAW resonator having SiO_2 HAR structure covering each IDT finger with infinite number of fingers is considered. The periodic nature of the SAW resonator allows modeling the device using one unit cell with periodic boundary condition, which will reduce the size and computational complexity of the device. The geometries of half periodic sections of proposed and conventional SAW resonators are shown in figure 4.12, and sign inversion of variables at the boundaries is used in the simulation. The piezo module with plane strain mode provided in COMSOL Multiphysics is used. The stress free boundary condition is used at the top surface of the substrate and bottom surface of the substrate is assumed to be fixed. The properties such as coupling matrix, elasticity matrix, relative permittivity and density of YZ $LiNbO_3$ piezo-substrate are taken

from [102]. Since the energy in SAW is confined to a depth of about one wavelength from the wave propagation surface of the substrate, the substrate depth of 5λ is considered.

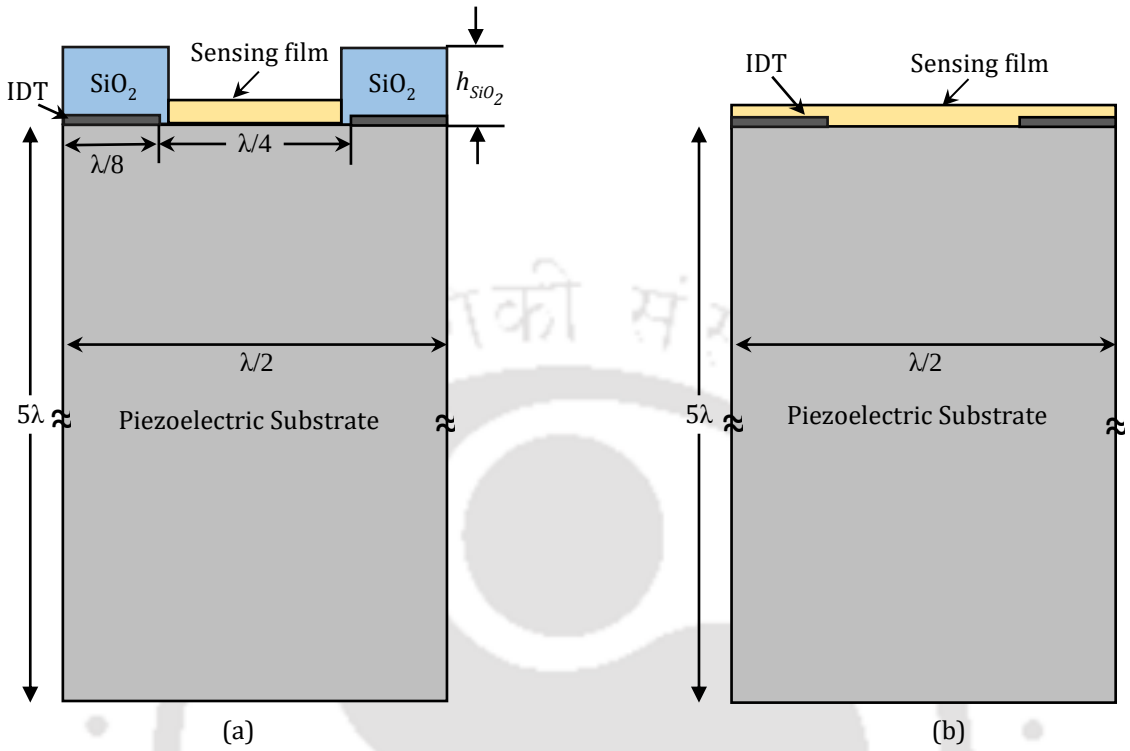

Figure 4.12 2D geometries of one-port SAW resonators used in the simulation with (a) sensing film between the fingers covered with SiO_2 HAR structures (proposed device), (b) sensing film over the IDT (conventional device).

IDT made of aluminium having uniform thickness of 0.05 μm with metallization ratio of 0.5 is patterned on the substrate. In the proposed device SXFA sensing film is placed in the space between fingers covered with the SiO_2 HAR structures as shown in figure 4.12 (a). The dimensions used in the simulation for the proposed device are as follows: Wavelength λ = 8 μm, IDT finger width 2 μm ($\lambda/4$), electrode pitch 4 μm ($\lambda/2$), depth of the piezo-substrate 40 μm (5 λ) in $-x_3$ direction and SXFA film thickness 65 nm. The resonance frequency of the proposed device is about 315.479 MHz. The dimensions used for the conventional device are as follows: Wavelength λ =10.8 μm, IDT finger width 2.7 μm ($\lambda/4$), electrode pitch 10.4 μm ($\lambda/2$), depth of the piezo-substrate 54 μm (5 λ) in $-x_3$ direction and thickness of SXFA film covering the entire device 65 nm. The resonance frequency of the conventional device is about 314.862 MHz which is close to the resonance frequency of the proposed device. An extremely fine mesh with minimum element quality of 0.7 is used and the number of mesh elements is minimum 16 per wavelength. The properties of the SXFA film and DMMP gas are given in section 4.2.1. The eigenmode analysis is performed to obtain the resonance

frequency of the proposed and conventional devices. The resonance frequency for each concentration of DMMP gas is recorded and the shift in resonance frequency is calculated.

4.4.1.2 Results and discussions

The first two surface modes for the proposed device are observed at 315.479 MHz and 403.616 MHz, and the shapes of the eigenmodes are shown in figure 4.13.

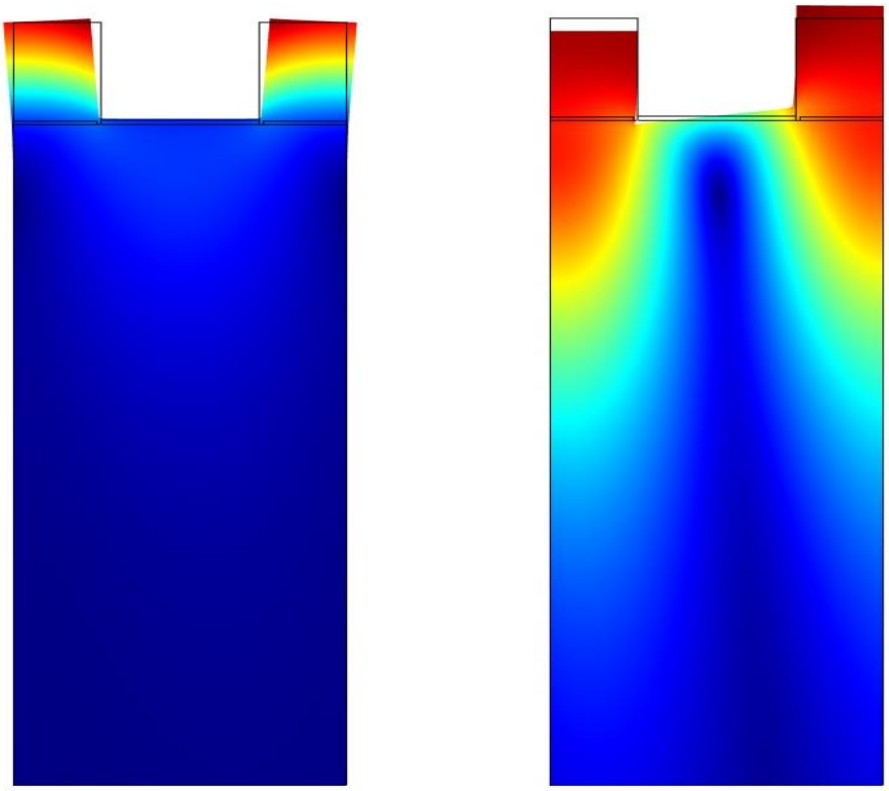

Figure 4.13 Total displacement profiles of the proposed one-port SAW resonator with SiO_2 HAR structure at (a) surface mode 0, and (b) surface mode 1.

The frequency analysis is performed by assuming the potential of 1 V at the IDT to obtain the harmonic admittance of the proposed one-port SAW resonator device and the plots of displacement and harmonic admittance are shown in figure. 4.14. From the plot it is observed that mode 0 is dominant and susceptance crosses zero at frequency of 315.479 MHz which is considered as the resonance frequency of the device.

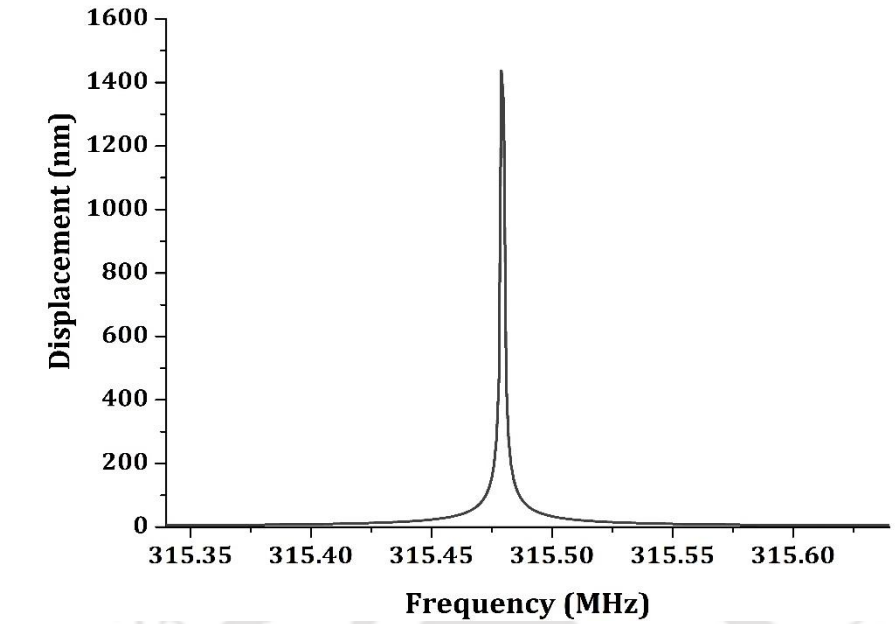

(a)

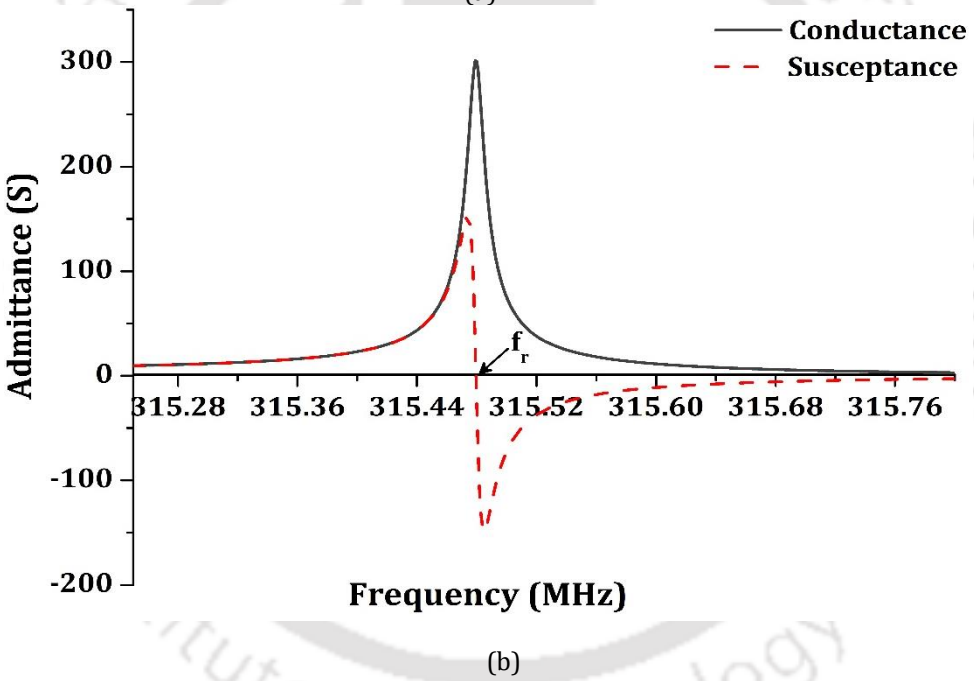

(b)

Figure 4.14 Results of simulation of one-port SAW resonator with SXFA between the fingers covered with SiO_2 HAR structure at mode 0. (a) Plot of total displacement versus frequency, (b) Plot of harmonic admittance versus frequency.

The figure 4.15 shows the longitudinal and transverse displacements for mode 0 plotted against the substrate depth. From the plot it is observed that the transverse displacement is dominant over the longitudinal displacement at the surface and the longitudinal displacement changes sign after a certain depth, indicating that the surface wave propagating in the proposed device has properties close to Rayleigh wave [15].

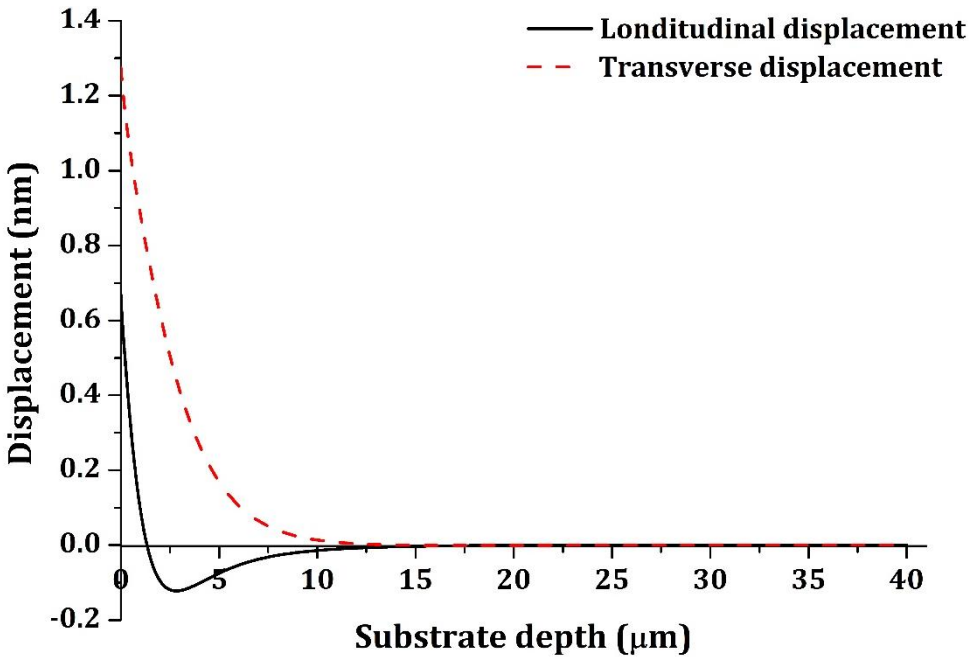

Figure 4.15 Plots of longitudinal and transverse displacements versus substrate depth for mode 0 in the proposed device.

Eigenmode frequency analysis of proposed one-port SAW resonator with SXFA sensing film for the detection of DMMP gas is carried out. The changes in density and thickness of sensing film due to absorption of DMMP gas for the concentration of 0 mg/m^3 to 100 mg/m^3 are calculated using (2.32) and (2.33) and used in the simulation. The h_{SiO_2} of 3 μm and SXFA thickness of 65 nm are used for simulation and the eigenmode frequency in the absence of DMMP vapor is at 315.479 MHz which is taken as the reference value. The shift in frequency is measured by subtracting reference value from the resonance frequency after absorption of DMMP gas. The conventional one-port SAW resonator with SXFA sensing film over IDT is simulated. The SXFA thickness of 65 nm is used for simulation and the eigenmode frequency in absence of DMMP gas is at 314.862 MHz which is taken as the reference value for conventional device. The shift in frequency in presence of DMMP gas is calculated as above. The plot of shift in frequency versus concentration of DMMP gas is shown in figure 4.16. The plot distinctly shows that with increase in gas concentration, the resonance frequency decreases in conventional device, substantiated by experimental results reported by Singh et al. [108], whereas it increases in proposed device. In addition, frequency shift in proposed device is about 8.5 times that in conventional device. The response is linear for DMMP gas concentration range of 0 – 100 mg/m^3 for both the devices and the sensitivities are calculated

as approximately 6.15 kHz/mg/m^3 for proposed device and approximately 0.72 kHz/mg/m^3 for conventional device.

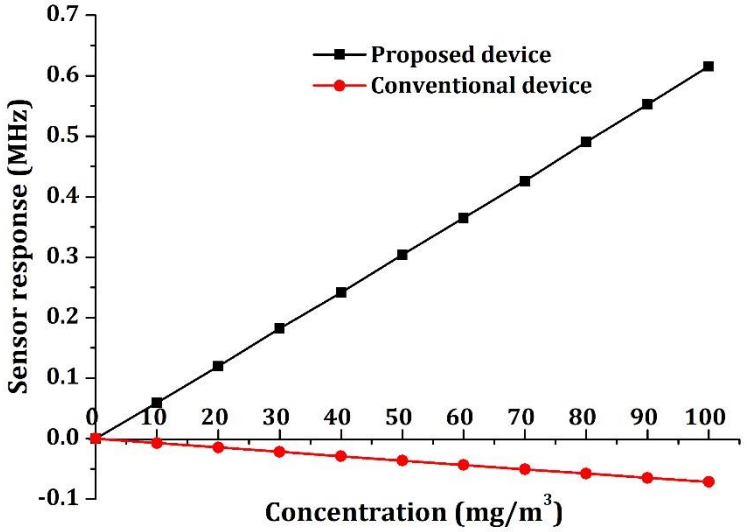

Figure 4.16 Plot of sensor response versus concentration of DMMP gas for SXFA film thickness of 65 nm using proposed and conventional SAW devices.

The change in resonance frequency of the devices is mainly due to the combined effect of change in density and thickness of sensing film by absorption of DMMP gas. The individual contributions of thickness and density variations in sensor response however can be deduced from simulation.

The effect of thickness change is calculated using (2.33) while keeping density constant, and the effect of density change is calculated using (2.32) while keeping thickness constant. The plots of frequency shift versus concentration of DMMP gas in figure 4.17 show three cases– effect of density change, effect of thickness change and combined effect of change in density and thickness. From the plot, it is observed that the effect of density change is negligible and change in thickness is the major factor contributing to the sensor response. The effect of increase in thickness also called swelling effect due to gas absorption is equivalent to decrease in the height of SiO_2 HAR structure resulting in shifting the operating point to the left in figure 4.11(a) and the large increase in resonance frequency is observed .

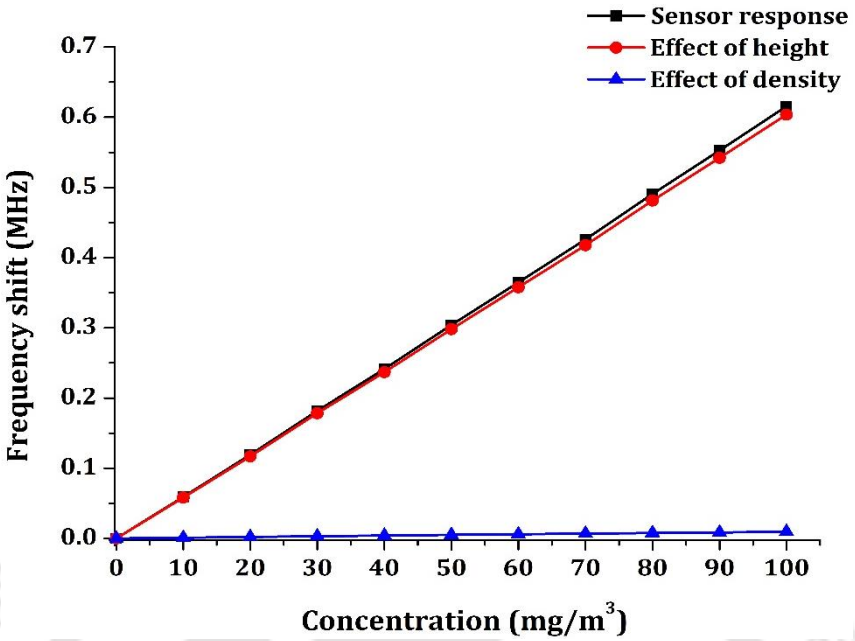

Figure 4.17 Plots of shift in resonance frequency versus concentration of DMMP gas for the proposed device with change in height and with change in density. The combined effect of change in height and density is also included.

4.4.2 One-port SAW resonator with SiO_2 HAR structure over IDT for sensing organic vapor

The trichloroethylene (TCE) vapor sensor using polyisobutylene (PIB) film as the sensing medium in proposed one-port SAW resonator is simulated in COMSOL Multiphysics. The resonance frequency of the device is noted in the presence and absence of TCE vapor. The sensitivity is obtained from the resonance frequency shift for various concentrations of TCE vapor.

4.4.2.1 Simulation methodology

2D FE simulations of the proposed device for sensing TCE organic vapor are performed using COMSOL Multiphysics. The geometry, boundary conditions and meshing used in this simulation are as explained in section 4.4.1.1. IDT made of aluminium having uniform thickness of 0.05 μm with metallization ratio of 0.5 is patterned on the substrate. In the proposed device PIB sensing film is placed in the space between fingers covered with the SiO_2 HAR structures as shown in figure 4.12 (a). The dimensions used in the simulation for the proposed device are as follows: Wavelength λ = 20 μm, IDT finger width 5 μm ($\lambda/4$), electrode

pitch 10 μm ($\lambda/2$), depth of the piezo-substrate 100 μm (5 λ) in $-x_3$ direction and PIB film thickness 0.67 μm.

In this simulation PIB is a used as a sensing material and the target gas is TCE vapor. The properties of the PIB film and TCE vapor are adapted from [109, 110] and are as follows. The density of PIB is 918 kg/m^3, and its G and K are $1\times10^9 + i50\times10^6$ Pa and $1\times10^{10} + i0$ Pa, respectively. The density of TCE is 5.866 kg/m^3. The partition coefficient k of PIB towards TCE is around $10^{2.3994}$. The eigenmode analysis is performed and the resonance frequency of the proposed device is found to be about 137.446 MHz. The absorption of organic vapor changes the properties of the PIB sensing film, which perturbs the SAW velocity and results in change in the resonance frequency of the device. The resonance frequency for each concentration of TCE vapor is recorded and the shift in resonance frequency is calculated.

4.4.2.2 Results and discussions

Eigenmode frequency analysis of proposed one-port SAW resonator with PIB sensing film for the detection of TCE is carried out. The changes in density and thickness of sensing film due to absorption of TCE for the concentration of 0 mg/m^3 to 100 mg/m^3 are calculated using (2.32) and (2.33) and used in the simulation. The h_{SiO_2} of 3.5 μm and PIB thickness of 0.67 μm are used for simulation and the resonance frequency in the absence of TCE vapor is at 137.446 MHz which is taken as the reference value. The shift in frequency is measured by subtracting reference value from resonance frequency after absorption of TCE vapor. The plot of shift in frequency versus concentration of TCE vapor is shown in figure 4.18.

The plot distinctly shows that with increase in gas concentration, the resonance frequency increases in proposed device. The response is almost linear for TCE vapor concentration range of 0 – 100 mg/m^3 and the sensitivity is calculated as approximately 249 Hz/mg/m^3 for proposed device.

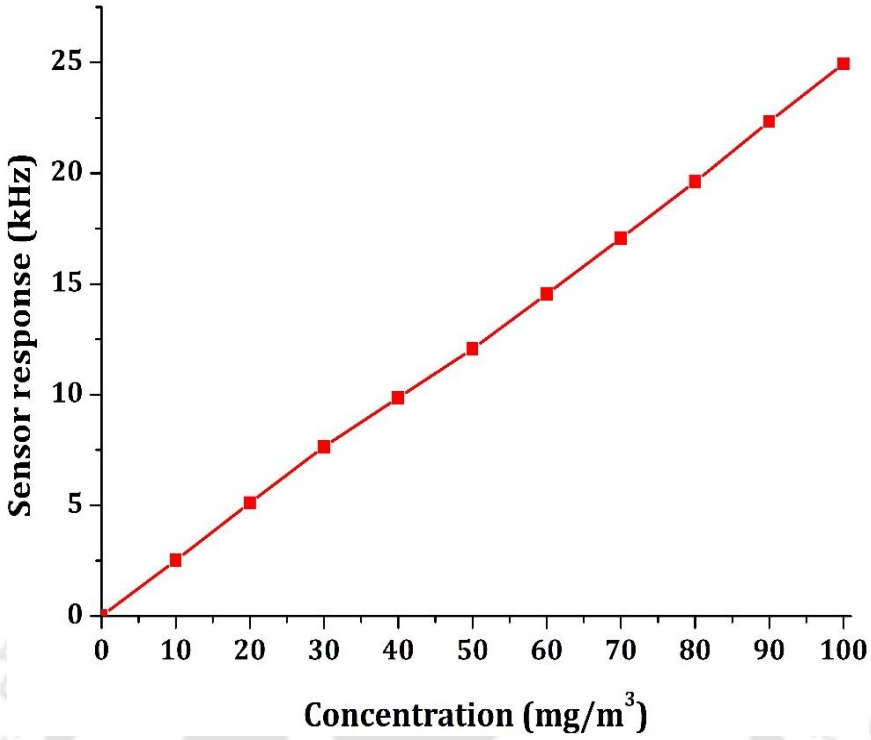

Figure 4.18 Plot of sensor response versus concentration of TCE vapor for PIB film thickness of 0.67 μm using proposed SAW device.

4.4.3 One-port SAW resonators with SiO_2 HAR structure over IDT for sensing hydrogen gas

In this section, proposed one-port SAW resonator for sensing hydrogen (H_2) gas is simulated in COMSOL Multiphysics. A palladium metal film (Pd) is used as the sensing medium and is placed in the space between fingers covered with the SiO_2 HAR structures as shown in figure 4.19. The absorption of H_2 gas will change Pd film properties, and perturbs the SAW propagation velocity and results in change in resonance frequency of the device. The shift in resonance frequency is obtained by subtracting the resonance frequency of the device in the absence H_2 from the resonance frequency in the presence of H_2 and is considered as the sensor response. The sensitivity is obtained from the resonance frequency shift for various concentrations of H_2 gas.

4.4.3.1 Simulation methodology

A 2D piezo module with plain strain mode in COMSOL 4.4 is used to simulate a one-port SAW resonator with infinite number of fingers covered with SiO_2 HAR structures. The 2D geometry of half periodic section of proposed SAW resonator used in FE simulation is given in figure

4.20. The periodic nature of the SAW resonator allows modeling the device using half unit cell with antiperiodic boundary condition at the boundaries is used.

The dimensions used for simulation are as follows: Wavelength (λ) 20 μm, finger width 5 μm, finger pitch 10 μm, and depth of the substrate 100 μm (5λ). The thickness of IDT fingers is 0.05 μm. The h_{SiO_2} having width of 5 μm and height of 5 μm is used. The sensing film used for simulation has thickness of 2 μm as reported in [91]. The piezo-substrate of YZ $LiNbO_3$ material is used and the material properties such as elasticity matrix, coupling matrix, relative permittivity and density are referred from Ahmadi *et al*. [102]. An extremely fine mesh with minimum element quality of 0.7 and the number of mesh elements of minimum 16 per wavelength is used. From eigenmode frequency analysis provided by COMSOL Multiphysics the resonance frequency of the device is at about 138.64 MHz. The values of Young's modulus, density and thickness for different concentrations of hydrogen in palladium used for simulation are given in table 3.1.

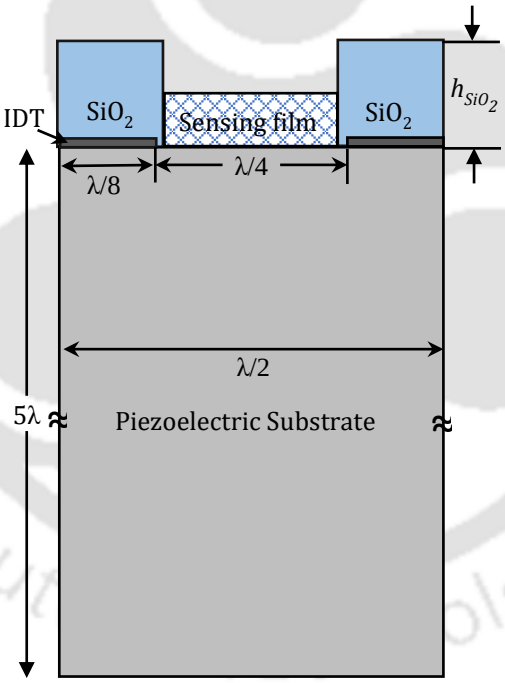

Figure 4.19 2D geometry of proposed one-port SAW resonator with Pd between fingers covered with SiO_2 HAR structures used in simulation.

4.4.3.2 Results and discussions

FE simulation is performed for various concentrations of H_2 gas in Pd and resonance frequency is calculated. The resonance frequency of the device without H_2 absorption is at 138.64 MHz and is taken as the reference value. Subtracting the resonance frequency

calculated for various concentrations of H_2 gas from the reference value gives the shift in resonance frequency for particular H_2 gas concentration and is considered as the sensor response. The plot of sensor response for various concentrations of H_2 gas in Pd is shown in figure 4.20.

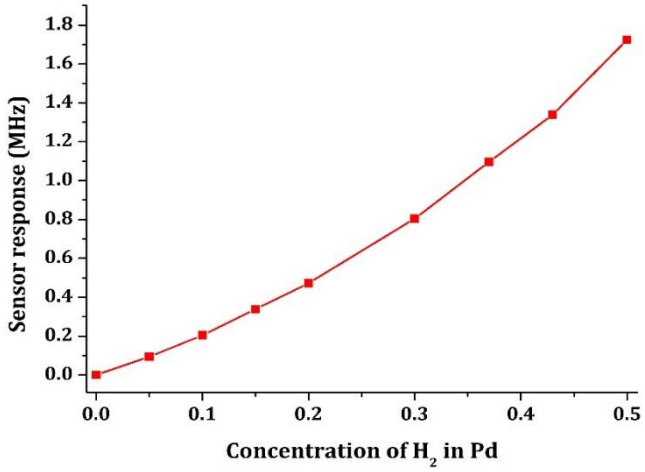

Figure 4.20 Plot of shift in resonance frequency versus concentration of H_2 in Pd.

An increase in resonance frequency is observed for increase in H_2 concentartion in the proposed device using Pd sensing film. The cause of increase in resonance frequency has been explained in detail in section 4.2.2. and is about 1.8 MHz for H_2 concentration of 0.5%.The Pd sensing film thickness of 2 μm is used in the simulation as the H2-Pd data is available. A 2 μm thick Pd sensing film in the trench of trench depth 2.2 μm has shifted the operating point to extreme left in Fig. 3.3 (b) and the change in Pd thickness goes beyond a small linear perturbation on the operating point leading to nonlinear response.

4.5 Summary

This chapter presents the simulations of two structures of one-port SAW resonator i) with thick IDT and ii) with high aspect ratio SiO_2 structures covering IDT fingers and their application in sensing gases.

For thick IDT configuration, the effect of IDT thickness on the resonance frequency for Ag, Au, Al and Ni as IDT metals is studied. It is observed that, in general the resonance frequency decreases as the thickness of IDT increases due to the usual mass loading effect, and for a fixed thickness of IDT, the resonance frequency of the device is lower for a higher density

material. This structure is used to simulate sensing of DMMP gas using SXFA sensing film placed in the space between thick Ni IDT fingers. The results are compared with that of an identical conventional SAW device with SXFA sensing film coated on entire device including IDT. An increase in resonance frequency is observed in proposed device while decrease in resonance frequency is observed in conventional device for the same concentrations of DMMP gas. The proposed device shows a sensitivity of approximately 5.64 kHz/mg/m^3 which is about 7 times greater than that of conventional device. It is observed that the swelling of SXFA film due to absorption of DMMP gas decreases the effective thickness of IDT in the proposed sensor and leads to increase in resonance frequency as noted above.

A 2D FE analysis of proposed second structure of one-port SAW resonator with SiO_2 HAR structure covering the IDT fingers is carried out. The effect of SiO_2 height on the resonance frequency for different wavelengths is studied. It is observed that the resonance frequency decreases with increase in SiO_2 height and the height of SiO_2 at which maximum change in resonance frequency occurs is at 0.19λ for YZ $LiNbO_3$ piezoelectric substrate.

The FE simulations of second structure used for sensing DMMP gas using SXFA sensing film coated in the space between IDT fingers is carried out. The results are compared with that of an identical conventional SAW device with SXFA sensing film coated on entire device including IDT. An increase in resonance frequency is observed in proposed device while decrease in resonance frequency is observed in conventional device for the same concentrations of DMMP gas. The swelling of SXFA film due to absorption of DMMP gas will decrease the effective height of SiO_2 HAR structure in the proposed sensor and lead to increase in resonance frequency. The proposed device shows a sensitivity of approximately 6.15 kHz/mg/m^3 which is about 8.5 times greater than conventional device. Comparing the SiO_2 HAR structure with thick IDT structure for sensing DMMP gas, the former structure shows a little higher sensitivity.

The SiO_2 HAR structure has been investigated for different gas sensing applications. TCE vapor sensor using PIB as sensing material in the space between IDT fingers covered with SiO_2 HAR structure is simulated. The resonance frequency increases with increase in concentration of TCE vapor as observed in case of DMMP gas and the sensitivity is approximately 249 Hz/mg/m^3. In another FE simulation for sensing H_2 gas, PIB is replaced by Pd and similar effects are observed.

5

Fabrication and characterization of SAW one-port resonator with SiO_2 HAR structure for sensing gases

This chapter describes the fabrication process of the proposed SAW devices, characterization of fabricated devices, experimental set up and results of experiments performed using fabricated devices. Several one-port SAW resonators with SiO_2 HAR structures over IDT fingers have been fabricated. Experiments are carried out to sense two gases, viz. H_2 gas and TCE vapour. For sensing H_2 gas, Pd is coated as the sensing material in the space between HAR structures on the fabricated devices. For sensing TCE vapor, PIB is used as the sensing material in another set of the fabricated devices. The experimental set up and the results of experiment are presented in each case.

5.1. Fabrication of one-port SAW resonator

The devices have been fabricated in Indian Institute of Science, Bangalore under Indian Nano Users Program (INUP). The process steps involved in the fabrication of SAW one-port resonator are the layout design, mask preparation, photolithography, and metal deposition on the wafer and lift-off. YZ $LiNbO_3$ substrate is used due to its reasonably high K^2 and low insertion loss. Single side polished $LiNbO_3$ wafers of 4" diameter are ordered from Roditi International, U.K. IDT dimensions with desired 50 Ω impedance are designed using equivalent circuit model for one-port resonators.

5.2. Process flow

The process involved in fabrication of the proposed one-port SAW resonator for sensing applications is illustrated in figure 5.1. A YZ $LiNbO_3$ wafer is cleaned and the IDT pattern with specified dimensions is transferred in the photoresist-coated wafer using photolithography. Chromium followed by gold are deposited on the substrate through e-beam evaporation

method, and IDT on the surface of the substrate is formed using lift-off process. On the fabricated SAW devices SiO_2 is deposited on the surface using plasma enhanced chemical vapor deposition (PECVD).The second stage photolithography is performed followed by dry etching of SiO_2 to form HAR structures over the IDT fingers. A third stage photolithography is performed and the sensing film is coated on photoresist. The device is dipped in the acetone for removing sensing film present over the pillars and retaining sensing film between HAR structures.

5.2.1 Design of SAW device

The SAW devices are graphically designed using CleWin software. A bi-layered design is chosen to accomplish the layout of both the IDT structure and patterned SiO_2 layer. Figure 5.2 shows the arrangement of one-port SAW resonator with design pattern of SiO_2 HAR structure present above IDT on a 3" wafer. Bond pads are designed according to the dimensions of conventional GSG probes with 100 µm pitch to facilitate the characterization of fabricated SAW devices using RF probe station and network analyzer. External square bond pads of 2 mm × 2 mm are also designed for wire connection and soldering if required. The width of the bus bar connecting the fingers of the IDT is of 50 µm. Table 5.1 lists all the sizes and dimensions used for the fabrication of SAW devices. IDT finger width, pitch, and aperture are denoted by *a*, *p*, and *W,* respectively. *Np* is the number of finger pairs in the IDT. A minimum spacing of 3 mm is provided between adjacent devices to ensure the possibility of dicing of the processed wafer.

Table 5.1 Dimensions used for the fabrication of one port SAW resonators

Resonator devices	*a*	*p*	*W*	*Np*
Device 1 (λ = 20 µm)	5 µm	10 µm	2.4 mm	30
Device 2 (λ = 60 µm)	15 µm	30 µm	7.5 mm	30

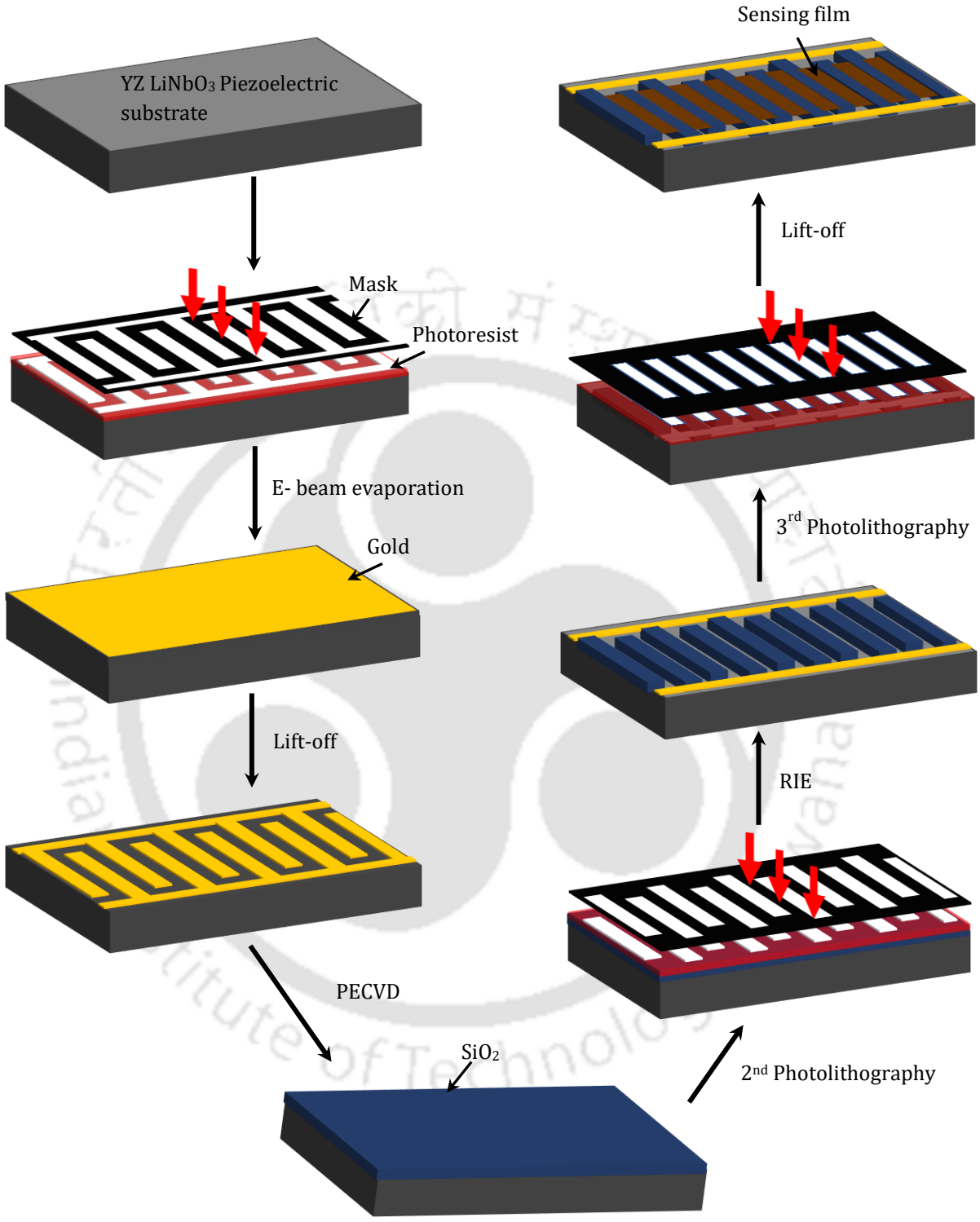

Figure 5.1 Process flow for fabrication of SAW device and SiO_2 HAR structures and deposition of sensing film.

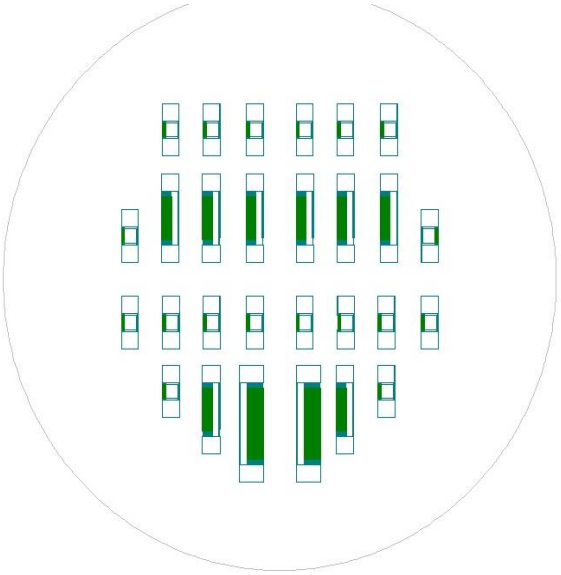

Figure 5.2 Mask layout designed using Clewin software for SAW resonator with SiO_2 HAR structure and sensing film.

5.2.2 Preparation of Mask

4" chrome mask plates with 3" active area are prepared using laser writer μPG 501 (Heidelberg Instruments, Germany). Each chromium coated mask plate with positive photoresist is loaded into the laser writer and the desired dimensions are patterned using a standard lens. The chrome mask plates are developed using MF-26A developer (MicroChem, USA). The exposed chromium region is etched using chrome etchant solution. The unwanted photo-resist is removed using acetone, followed by piranha cleaning process for 30 s.

5.2.3 Photolithography for IDT

The wafer is cleaned using acetone and isopropyl alcohol (IPA) then rinsed with deionized (DI) water and dried using dry N_2 gas. The wafer is placed in the hot plate for 1 min at 110°C to remove the excess water content in the wafer after cleaning. A photoresist AZ 5214E was applied over the polished surface of the wafer via spin coating for 40 s at 4000 rpm. It produces photoresist thickness of about 1.4 μm. The resist is soft baked on a hot plate for 1 min at 110°C and left for cooling. The wafer with photoresist is placed in the mask aligner MJB4 (SUSS MicroTech) with 4-inch substrate chuck. The parameters such as wafer thickness, wedge correction, separation between mask plate and wafer, and alignment of the substrate are performed manually. Now the wafer is exposed to UV light with dosage of 45 $mJcm^{-2}$ for 5 s to transfer the pattern in the mask to the photoresist. The wafer is then immersed in the

developer solution MF-26A for 18 s to get the IDT pattern. While developing, the sample is inspected using optical microscope to avoid over-development or under-development of features on the resist.

Table 5.2 Parameters used in lithography process for IDT design

	Photolithography	
Process Involved	**Temperature**	**Time**
Wafer cleaning (YZ $LiNbO_3$)	Room temperature	5 mins
Dehydration bake (YZ $LiNbO_3$)	110°C	10 mins
Spin coating (AZ 5214E) (4000 rpm)	Room temperature	40 s
Soft bake	110°C	60 s
UV exposure (dosage 45mJ/cm2)	Room temperature	5 s
Developer (MF-26A)	Room temperature	18 s

5.2.4 Metal Deposition and Lift-off

After the photolithography the gold is deposited over the entire patterned wafer using E-beam evaporation technique. To improve the adhesion between gold and $LiNbO_3$ substrate, a thin chromium layer of 10 nm is deposited before the deposition of gold. A thin gold film of 80 nm thickness is used as electrode material for the IDT structure. The E- beam evaporation parameters used for the deposition of chromium and gold are listed in Table 5.3.

Table 5.3 Parameters used in E-beam evaporator for metal deposition

	E- Beam Evaporator	
Specifications	**Gold (Au)**	**Chromium (Cr)**
Thickness	80 nm	10 nm
Base pressure	3.3×10^{-6} Torr	3.3×10^{-6} Torr
Deposition pressure	4×10^{-6} Torr	4×10^{-6} Torr
Rotation speed	10 rpm	10 rpm
Deposition rate	2 Å/s	1 Å/s
Deposition time	105 mins	105 mins

The etching or lift-off techniques can be used for the development of IDTs. For a small feature size (< 5 µm) lift-off process is more suitable for developing a uniform IDT pattern because precise control of etching time is challenging to realize small feature size. Therefore the lift-off process is used in the development IDT in the proposed SAW resonator devices. After metal deposition, the samples are dipped in dish containing acetone, and the dish is placed in ultra-sonication for 15 minutes. Acetone removes the resist as well as the metal layer deposited over it, leaving the patterned metal electrodes on the surface. Once the lift-off is completed, the wafer is washed with IPA and DI water to remove any metal debris remaining on the surface of the wafer. The accuracy and resolution of UV lithography process limits the feature size of the IDT to minimum 5 µm. The devices with IDT finger width of 5 µm and 15 µm are fabricated.

5.3 Fabrication of SiO_2 HAR structures

The process steps involved in the fabrication of SiO_2 HAR structure over the IDT fingers of SAW one-port resonator are the layout design, deposition, mask preparation, photolithography, and etching. The fabrication facility allows depositing SiO_2 of thickness up to 3.5 µm and is considered as height of HAR structure for the device. The layout design and the preparation of the mask for the SiO_2 pillars are explained in section 5.2.1 and 5.2.2.

5.3.1 Deposition of SiO_2

The SiO_2 layer is deposited over the wafer containing one-port SAW resonator devices using plasma enhanced chemical vapor deposition (PECVD) process using PlasmaLab machine (Oxford Instruments,UK). The wafer is kept on the sample holder on a silicon carrier wafer along with some support pieces so that the wafer does not move during deposition. The deposition is uniform and a small sample wafer piece is kept at the side of the main wafer to measure the thickness of SiO_2 layer. The recipe for PECVD process is shown in Table 5.4. The deposition rate was 40 nm min^{-1}, and the machine was used for about 150 min to acquire a thickness of about 3.5 μm as verified by the profilometer.

Table 5.4 Parameters used in PECVD deposition of 3.5 μm thick SiO_2

Deposition rate	Gases	Pressure	RF power	Time
40 nm/min	SiH_4 : 8.5 sccm N_2O : 710 sccm N_2 : 163 sccm	998 mTorr	10 W	150 mins

5.3.2 Photolithography for SiO_2 HAR structure

The second stage photolithography process is carried out to ensures that the resist will stay only over the IDT fingers and remaining portion is etched out. The wafer with SiO_2 layer is cleaned with acetone, IPA, and DI water, and baked at 110 ^oC for 10 min. Negative photoresist AZ nLOF 2070 is spin-coated on the wafer at 3000 rpm for 40 s. After soft baking the wafer is placed in the mask aligner to match the pattern and exposed to UV light with dosage of 65 mJ cm^{-2}. Post baking is done at 110^oC for 90 s to have the cross-links in UV-exposed areas of the resist. The wafer is dipped in MF-26A developer solution for 15 s to remove the unexposed areas but retain exposed portions. The resist is then hard baked at 110^oC for 3 min.

5.3.3 Etching of SiO_2

Wet etching method is used to etch the SiO_2 layer. The negative photoresist protects the SiO_2 present over the IDT fingers and the rest of SiO_2 is etched. The wet etching process is done by dipping samples in 13:2 BHF solution for 30 min. The etch rate of SiO_2 is about 120 nm min^{-1}. After completion of wet etching, the negative resist present over the SiO_2 is removed using

TechniStrip NI555 resist remover. The image of wafer containing the fabricated devices is shown in figure 5.3 (a). From output of profilometer shown in figure 5.3 (b), the height of SiO_2 HAR structure is found to be 3.57 µm uniform over the IDT fingers and atleast 3 µm between fingers where profilometer tip has not reached the bottom because of high aspect ratio of the structure.

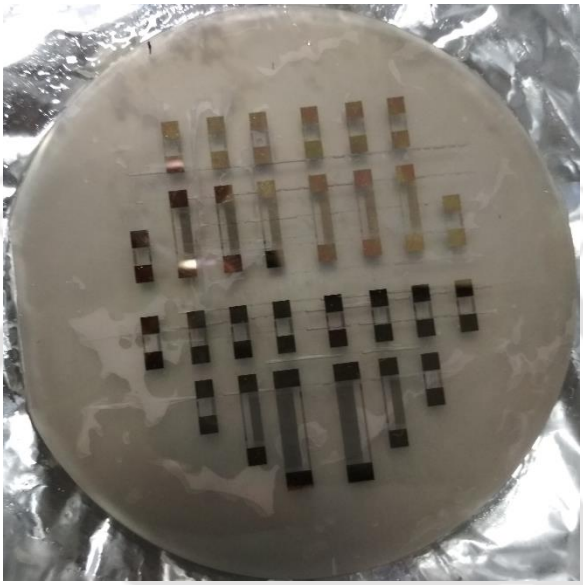

(a)

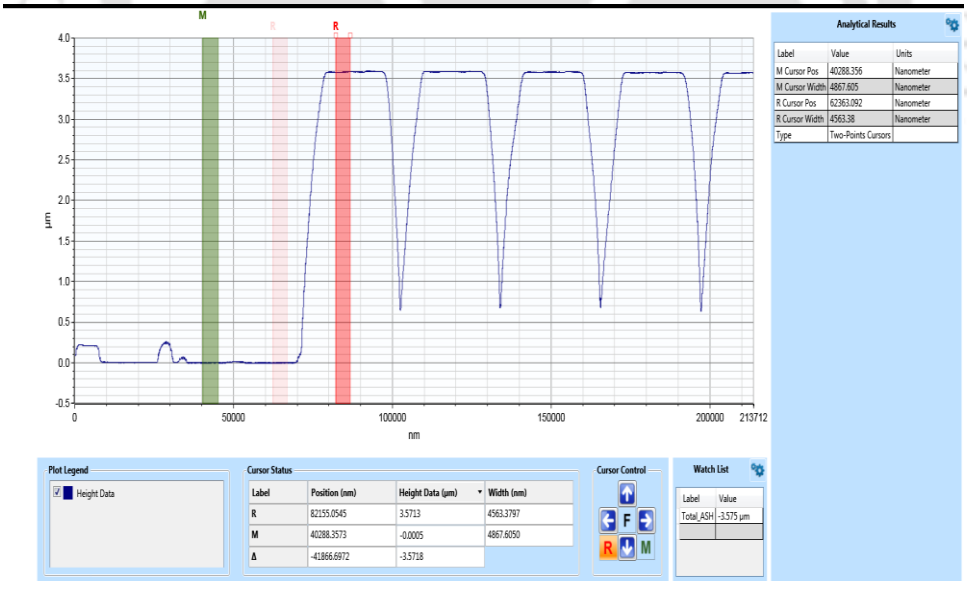

Figure 5.3 (a) Photo of wafer containing fabricated devices with SiO_2 HAR structures (b) measurement of height of SiO_2 HAR structure using dektak profilometer with 5 µm tip.

5.4 Testing of fabricated devices for sensing H_2 using Pd

The fabricated one-port SAW resonator devices with SiO_2 HAR structure have been employed for gas sensing applications. This section discusses about sensing H_2 gas using Pd sensing film in the space between HAR structures. The process of coating Pd and experimental setup used for sensing H_2 gas are described. The results of sensing H_2 gas at various concentrations using the fabricated devices are presented.

5.4.1 Coating of Pd film between SiO_2 HAR structures

Photolithography is required to ensure that resist will stay on entire surface of the device except in the space between SiO_2 HAR structures. The wafer with SiO_2 HAR structure over the IDT is cleaned with acetone, IPA and DI water followed by dehydration bake at 110°C for 10 min. A positive photoresist S1813 is spin coated on the wafer at 4000 rpm for 40 s. The wafer is then soft-baked and placed in the mask aligner to match the pattern and is exposed to UV with dosage of 45 mJ cm^{-2} for 5 s. The wafer is dipped in the MF-26A solution for 40 s and the pattern is developed.

The palladium (Pd) metal is used as the sensing film for the detection of H_2 gas. Pd is coated over the wafer using RF sputtering. The sputtering parameters for the deposition of Pd are listed in the table 5.5.

Table 5.5 RF sputtering parameters used for deposition of 200 nm thick Pd

RF Sputtering	
Target material	Palladium (Pd)
Power	90 W
Temperature	Room temperature
Gas used	Ar
Target to substrate distance	7 cm
Pressure	8×10^{-6} Torr
Pre sputter time	3 mins
Deposition time	5 mins

After Pd deposition, the samples are dipped in acetone, and ultra-sonication is done for 15 minutes for aiding the lift-off process. The acetone removes the photoresist along with the Pd coated over the photoresist, leaving Pd on the surface between the HAR structures. The sample is then cleaned using IPA and DI water to remove the Pd debris remaining on the surface. The figure 5.4 (a) shows the optical image of fabricated device having finger width of 15 μm, figure 5.4 (b) shows the optical image of fabricated device having finger width of 5 μm, and figure 5.4 (c) shows the output of optical profilometer used to measure thickness of the Pd film.

5.4.2 Dicing

A semi-automatic wafer dicer (MTI Corporation) is used to dice the devices. The back side of the wafer containing the fabricated devices was coated with Crystal-Bond-509 gel and is placed on a glass plate. By heating at 120°C for 5 min, the gel becomes viscous, and the wafer gets stuck on the glass plate upon cooling. The glass plate with the attached wafer is then placed on the wafer dicer machine. The blade used for cutting is 0.3 mm thick. The samples are cut at a rate of 8 mm /s and devices are diced out. Once dicing is completed, the wafer is kept on the hot plate at 130°C so that the gel melts and devices can be taken out. The separated devices are cleaned with acetone, IPA, and DI water.

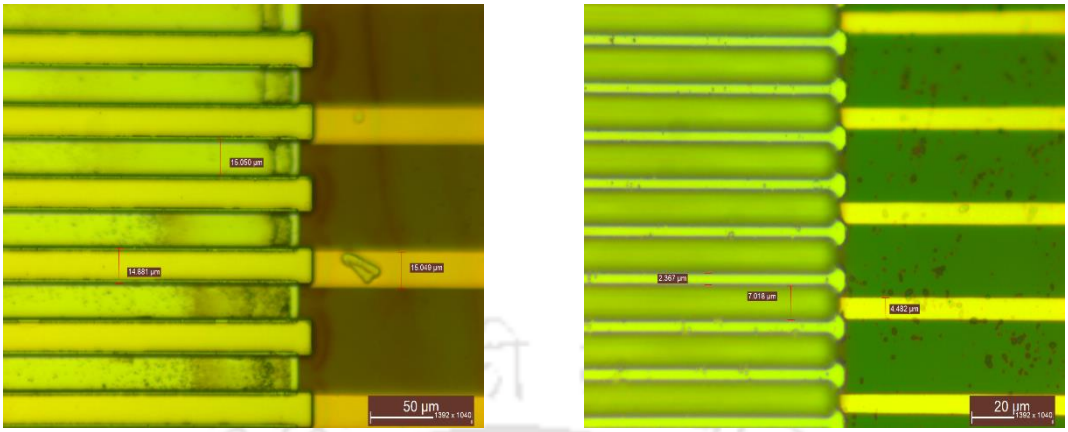

(a) (b)

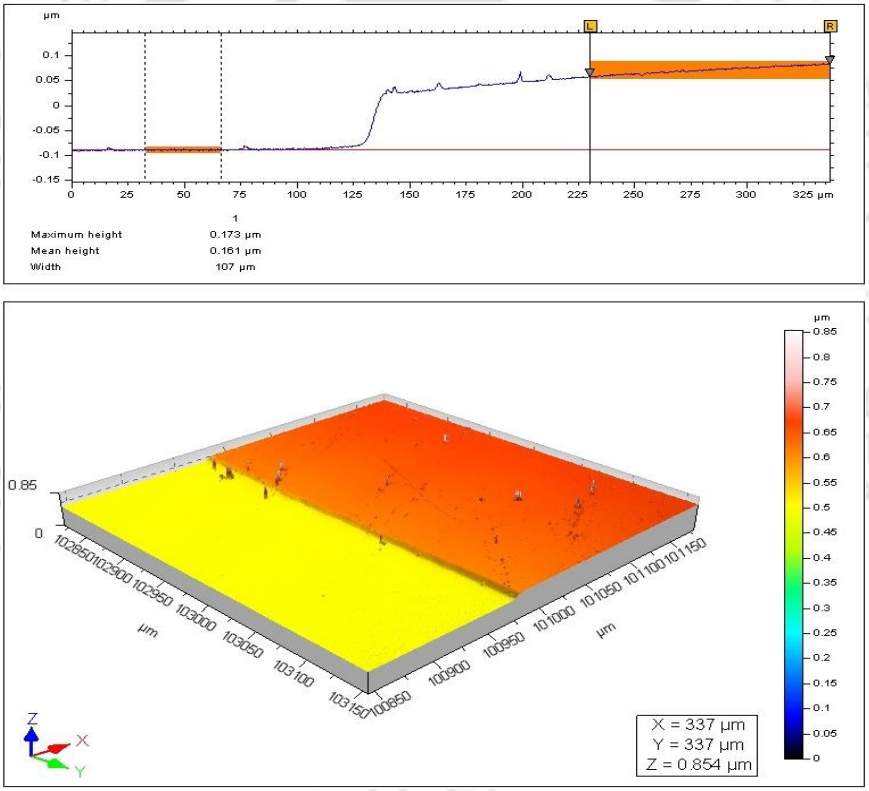

(c)

Figure 5.4 Optical images of fabricated devices having SiO_2 HAR structures with Pd sensing film, (a) the device having finger width of 15 µm and (b) the device having finger width of 5 µm. (c) Pd thickness measurement using optical profilometer.

5.4.3 Experimental setup

Figure 5.5 shows the block diagram and photos of the experimental setup used for sensing H_2 gas. The experimental set up consists of three mass flow controllers (MFCs) (MC-5SLPM-D, MCS-5SCCM-D and MCS-500SCCM_D) having different maximum flow rates, mixing chamber, controlled environmental chamber and network analyzer. H_2 gas is used as analyte and N_2 is used as purge gas. MFCs are used in the system for controlling the gas concentrations from ppb to pure and maintaining a steady flow rate.

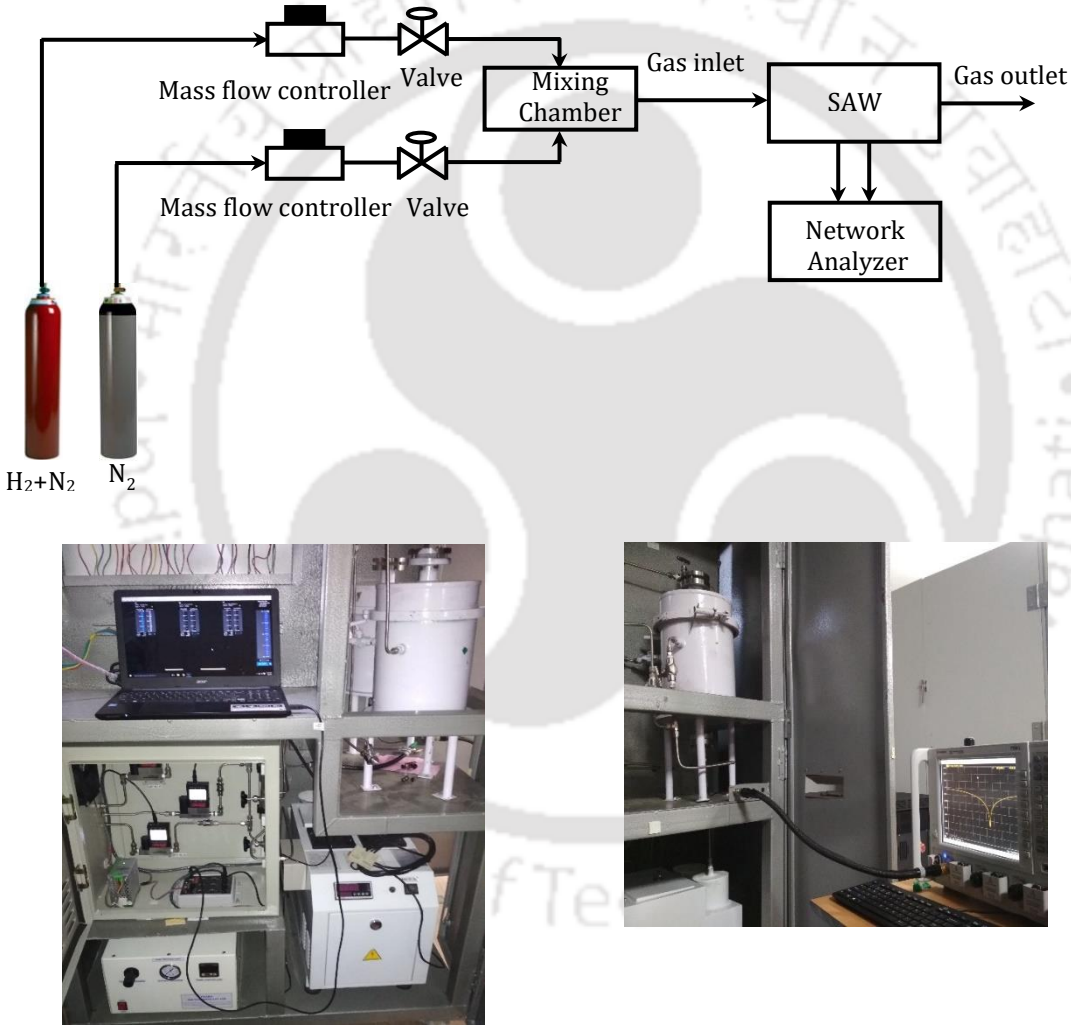

Figure 5.5 Block diagram and photos of the experimental setup employed for sensing H_2 gas using fabricated devices.

The MFCs are controlled using flow vision software to mix H_2 with N_2 to obtain range of concentrations of H_2 gas from 0 % to 3 %. The gases flowing through the MFCs are mixed in

the mixing chamber and passed through a controlled environmental chamber where the device to be tested is placed.

5.4.4 Device characterization

The fabricated device are characterized by measuring scattering parameters (S-parameters) using network analyzer. S-parameters are normally measured as a function of frequency and are measured using network analyzer Keysight PNA-L N5232A. Network analyzer with all the test leads and terminations are calibrated using calibration kit.

An IDT structure of SAW device is designed in such a way that the input impedance of the device will close to 50 Ω . However, due to fabrication imperfections and inconsistencies, the impedance of the device will not be 50 Ω. A circuit is required in between the signal source and the SAW device to match the impedances so that the maximum power from the source is transferred to the SAW device. Generally, a two-component L-section matching network is used at the input of the SAW device [11] . The L-section matching network can be designed by using a combination of series and parallel reactance. The matching circuit designed for SAW device is shown in figure 5.6. The device is connected to network analyzer without matching circuit to calculate the load impedance Z_L at the operating frequency. The required values of capacitor and inductor for the load impedance are calculated and implemented in the circuit.

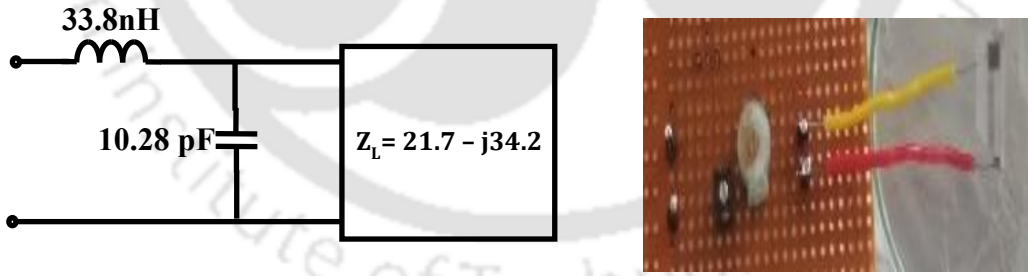

Figure 5.6 Matching circuit for SAW device.

The S_{11} curve for the fabricated one-port SAW resonator having SiO_2 HAR structure with Pd sensing film is obtained using network analyzer to measure the resonance frequency. The resonance frequency of the device fluctuates between ± 1 kHz depending on the external noise, vibrations and test fixture stability. The figure 5.7 shows the S_{11}-parameter curves for fabricated device for different concentration of H_2 gas.

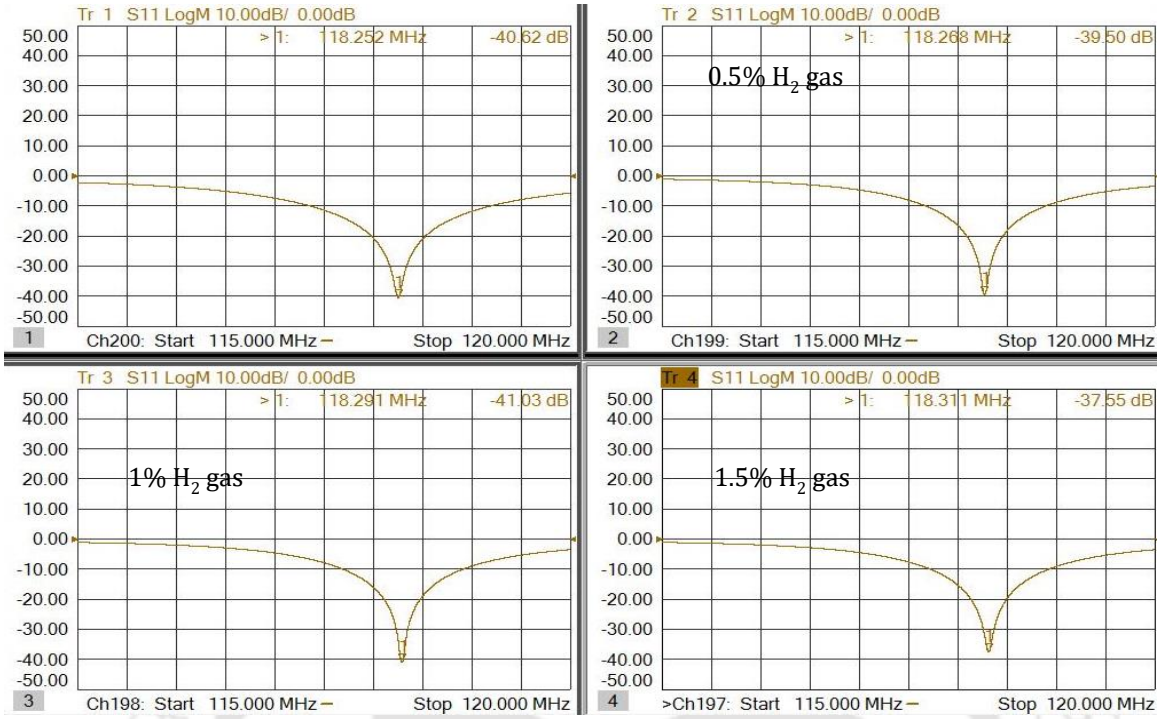

Figure 5.7 S11-parameter curves for fabricated device without H_2 gas and with H_2 gas concentrations of 0.5%, 1% and 1.5%.

5.4.5 Experimental results

The responses of a SAW device having finger width of 5 µm coated with 167 nm thick Pd film in the space between the SiO_2 HAR structures is tested at room temperature in absence of H_2 gas. The resonance frequency is observed at 118.252 MHz as shown in figure 5.7. The different concentrations of H_2 ranging from 0.5% to 3% are passed into the controlled environmental chamber. Desired concentration of H_2 gas is achieved by mixing it with N_2 gas. The flow rate is kept at 0.5 SLPM. The sensor response ($\Delta f = f_c - f_0$) is calculated by subtracting the resonance frequency (f_c) in presence of H_2 gas from resonance frequency before passing H_2 gas (f_0). The results show that the frequency shifts of 20.3 kHz, 38.4 kHz, 56.7 kHz, 83 kHz, 99.9 kHz and 110 kHz are obtained for H_2 concentrations of 0.5%, 1%, 1.5%, 2%, 2.5% and 3% mixed with N_2, respectively. The plots of S_{11} parameter and sensor response for different concentrations of H_2 (in %) are shown in figure 5.8.

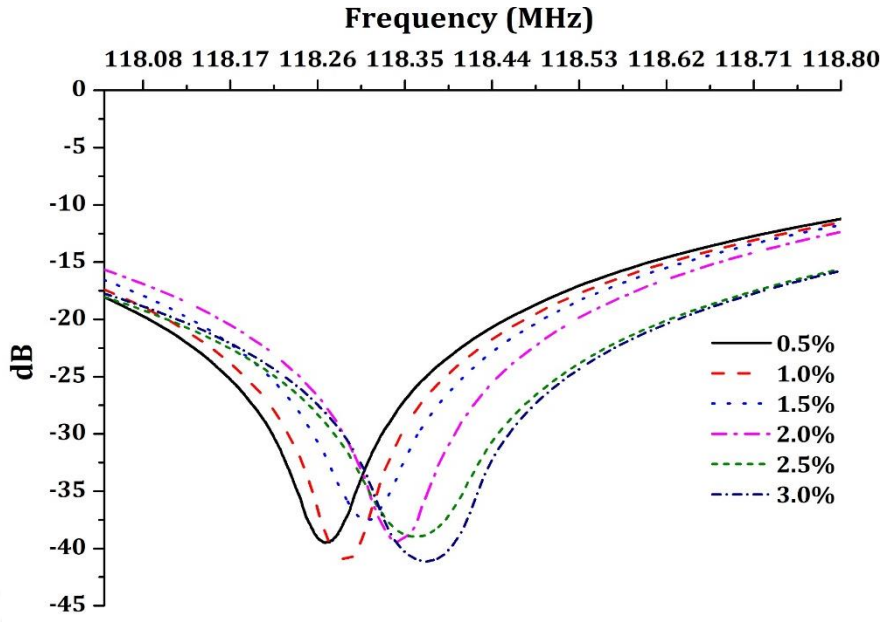

(a)

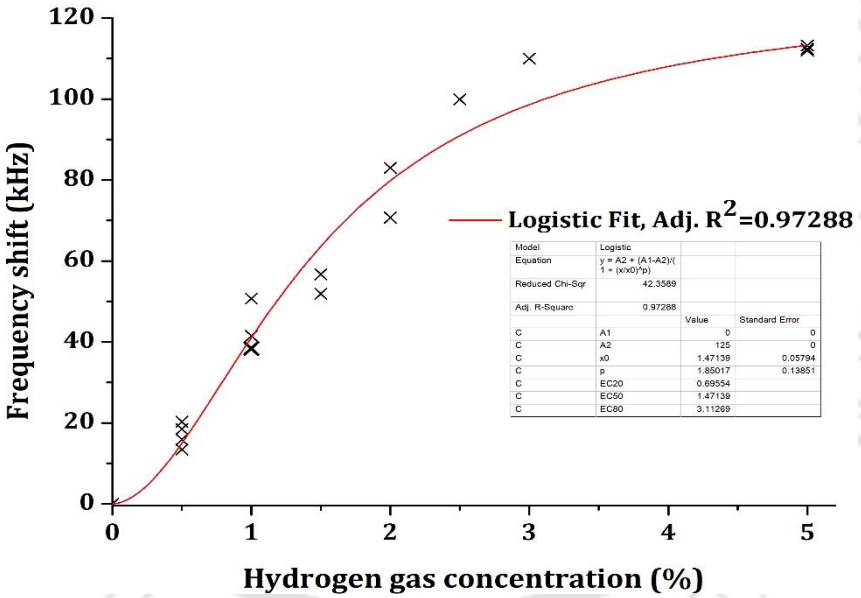

(b)

Figure 5.8 Plot of sensor response (a) S_{11} parameter for different concentrations of H_2 gas (b) frequency shift versus H_2 gas concentration (in %).

The distinct observation from the plot of experimental results is that the resonance frequency of the fabricated proposed device increases with increase in concentration of H_2, which is supported by the simulation results given in section 4.4.3.2. The response is nonlinear and tends to saturate at higher concentrations of H_2. A sensitivity of approximately 30 kHz/% equivalent to 3 Hz/ppm of H_2 is obtained at 0.5 % of H_2 from the experiment. The limit of

detection (LOD) is defined as three times the noise level per sensitivity [77]. For the noise level of about 3 kHz observed in the experiment, the calculated LOD is 3000 ppm.

5.4.6 Comparison with simulated results

For comparison, the simulation for sensing H_2 gas concentration using SAW device of dimensions of the fabricated device is carried out. The dimensions of simulated device are λ of 20 μm, SiO_2 HAR structure height of 3.5 μm and Pd film of thickness 0.16 μm. However the data of density and Young's modulus of Pd for H_2 absorption is available in [91] for H_2 concentration of 0 to 0.5%, and the experiments have been carried out for H_2 concentration of 0.5% and above. Therefore the plot of experimental results given in figure 5.8 (b) is extrapolated using sigmoid (logistic function) best fit for estimation of the values below 0.5% concentration. Figure 5.9 shows the plots of experimental and simulation results for concentration from 0 to 0.5% of H_2 gas.

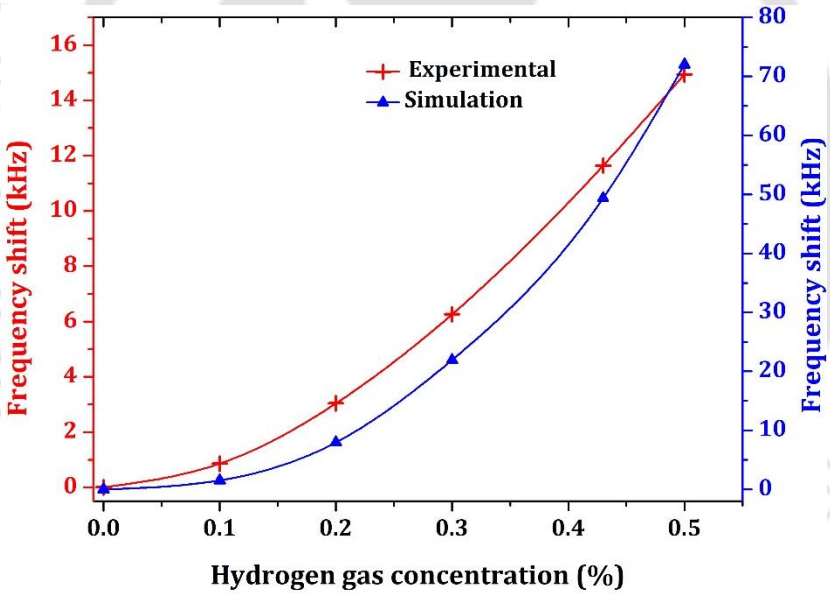

Figure 5.9 Plots of frequency shift vs hydrogen gas concentration by experiment and by simulation.

From the plots it is observed that the resonance frequency increases rapidly with increase in concentration of H_2 up to 0.5 %. The sensitivity obtained is broadly 144 kHz/% from the simulation and 30 kHz/% from experiment. The lower sensitivity observed in the experimental plot can be attributed to following reasons. As seen in the optical image of the fabricated device given in figure 5.4 (b), the width of SiO_2 HAR structure is approximately 7 μm instead of 5 μm reducing space for Pd deposition which has width of approximately 2.4

μm instead of 5 μm. It has resulted in the reduction in device resonance frequency from 134.76 MHz to 118.25 MHz, in addition to about 50% reduction in Pd area which is the main reason for reduced sensitivity. Another factor contributing to lower sensitivity can be the delay of about one year between the fabrication of the devices at Indian Institute of Science, Bangalore and the experiments for sensing H_2 gas carried out in our institute after the controlled gas sensing setup is installed.

5.4.7 Comparison with recently reported SAW H_2 gas sensors

The comparison of sensitivity of the fabricated device with recently reported SAW based H_2 gas sensors is given in table 5.6.

Table 5.6 Comparison of sensitivity of the fabricated device with recently reported work on SAW based H_2 gas sensors.

Year/Author	Device/Substrate	Sensing Material	*f* (MHz)	Sensitivity (Hz/ppm)	LOD
2014/Viespe	Delay line/ Quartz	Nanoporous Pd and ZnO layer,	70	0.31 (pd), 0.01 (ZnO)	50 ppm (pd), 316 ppm(ZnO)
2015/Marcu and Viespe	Delay line/ Quartz	Nanowires and Nanofilm of ZnO	69.4	0.062 (nanowires), 0.01 (films)	0.01%
2017/Yang et al.	Delay line/ 128° Y X $LiNbO_3$	Pd/SnO_2 bilayer	99.8	57.9 (115.9 kHz towards 2000ppm of H_2 @175°c)	
2017/Marcu and Viespe	Delay line/ Quartz	Pd, ZnO, Pd/ZnO	69.5	0.29 (Pd), 0.15 (ZnO), 0.51 (Pd/ZnO)	105 ppm (Pd), 216 ppm (ZnO), 59 ppm (Pd/ZnO)
2017/Ha et al.	Delay line/ AIN-Si	Nanocomposite Pd-graphene	126.54	5 (25 kHz for 0.5% of H_2)	
2018/Miu et al.	Two-port resonator/ ST X Quartz	Nanoporous Pd/WO_3 bilayer	69.5	0.13	4540 ppm
This work	One-port resonator/ Y Z $LiNbO_3$	Pd film	118.25	2.98 (14.9 kHz for 0.5% of H_2)	3000 ppm

Viespe has used a 70 MHz delay line SAW device with nanoporous Pd sensing film and reported a sensitivity of 0.31 Hz/ppm. In a H_2 sensor based on 69.5 MHz SAW delay line, Marcu and Viespe reported sensitivities of 0.29 Hz/ppm, 0.15 Hz/ppm and 0.51 Hz/ppm using Pd, ZnO and Pd/ZnO sensing films respectively. Ha et al. used a nano composite Pd – graphene sensing film in a SAW delay line operating at 126.5 MHz to sense H_2 gas and reported a sensitivity of 5 Hz/ppm. Miu et al. developed a 69.5 MHz two-port SAW resonator coated with nanoporous Pd/WO_3 bilayer sensing film for sensing H_2 gas and reported a sensitivity of 0.13 Hz/ppm. Summarizing, the researcher have used conventional SAW devices and modified sensing films to improve the sensitivity of the sensor. In this work, the SAW device has been modified by having SiO_2 HAR structure in a one-port SAW resonator and pure Pd film in the space between HAR structures to sense H_2 gas. For the fabricated device operating at 118.25 MHz the sensitivity observed is 4 Hz/ppm and is higher than the reported SAW H_2 gas sensors at room temperature except the device using nanocomposite Pd-graphene.

5.5 Testing of fabricated devices for sensing TCE vapor using PIB

Some of the fabricated devices are used to detect TCE vapor by coating PIB sensing film between the SiO_2 HAR structures. The processes involved in the fabrication of proposed SAW devices are mask preparation, photolithography, deposition, etching and dicing. The process of preparation of the mask is explained in section 5.2.2 and the mask is used for depositing sensing film in the space between the SiO_2 HAR structures.

5.5.1 Deposition of sensing films and etching

The photolithography process explained in section 5.4.1 is used before coating polyisobutylene (PIB) sensing material for the detection of TCE vapor. To deposit the PIB film over the wafer, spin coating method is used. The solution is prepared by mixing PIB with cyclohexane solvent in the ratio of 1:30 and the mixing is done by using magnetic stirrer. The solution is then applied on the wafer and is spin coated at 5000 rpm for 60 s to have the desired thickness of 0.6 μm. The wafer is then dipped in acetone and ultra-sonication is done for 10 mins to remove the resist as well as the film over it leaving film between the HAR structures. The sample is then heated in N_2 ambient at 60^{o}C for 1 hrs to remove the cyclohexane solvent present in the PIB film. The sample is cleaned using IPA and DI water and the optical image is taken. The output of optical profilometer and the photos of fabricated

devices are shown in figure 5.10. Thickness of the PIB film is 0.67 µm as measured using profilometer.

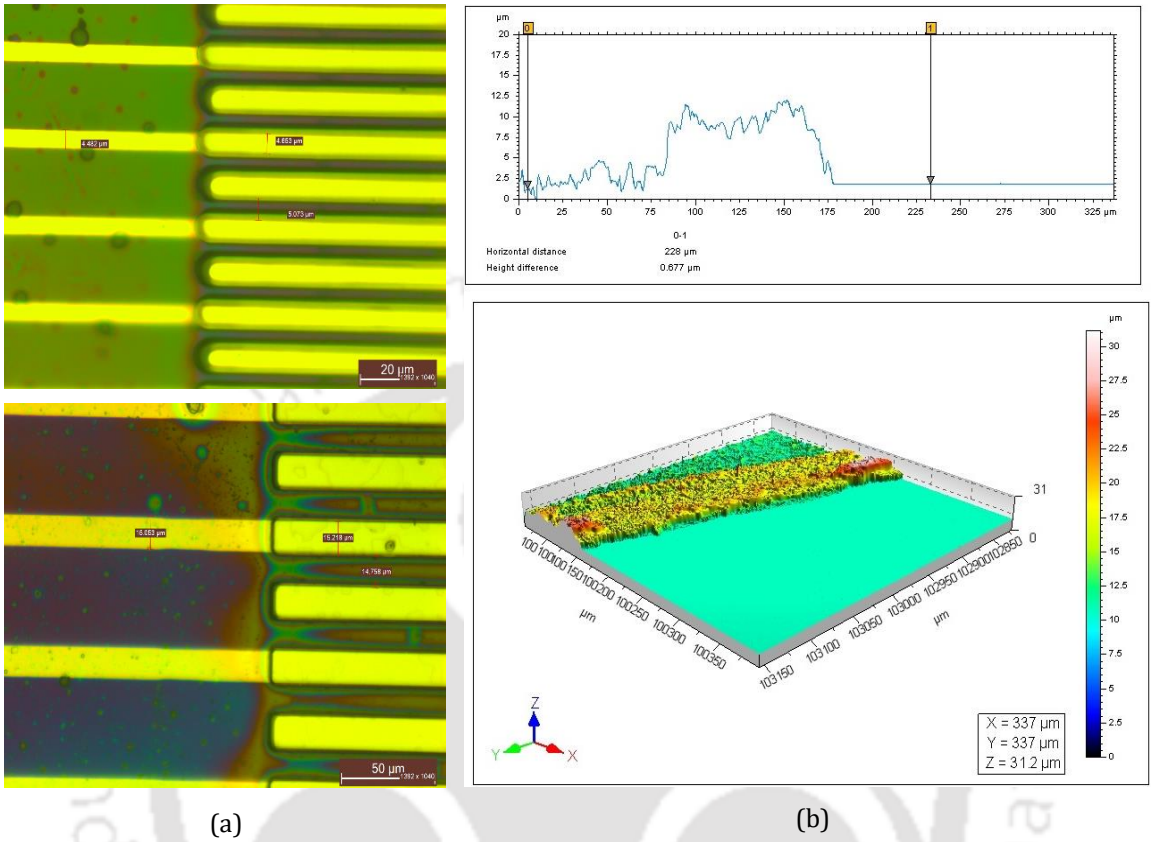

(a) (b)

Figure 5.10 (a) Optical images of fabricated devices having SiO_2 HAR structures with PIB sensing film. The device at the top has finger width of 5 µm and the device at the bottom has finger width of 15 µm. (b) PIB thickness measurement using optical profilometer.

5.5.2 Experimental setup for measuring TCE gas

An experimental setup as shown in figure 5.11 is developed to test the fabricated SAW devices with PIB sensing film for detecting TCE vapor. The device with matching circuit is fixed on the inner surface of the lid of the container. A hole with cap is made on the top of the lid to pour liquid TCE and a connector is fixed on the lid to connect the device to the network analyzer. The container is closed and is connected to the Agilent 8753ES network analyzer using a coaxial cable. The matching circuit for the fabricated device is designed as explained in section 5.4.4. The S_{11} parameter for the SAW device is measured using network analyzer to obtain the resonance frequency. The pure TCE of 2 ml is poured into the container through the hole without disturbing the setup and the cap is closed. TCE vaporizes at room

temperature and the PIB sensing film absorbs the TCE vapor that changes its properties and hence the resonance frequency of SAW device.

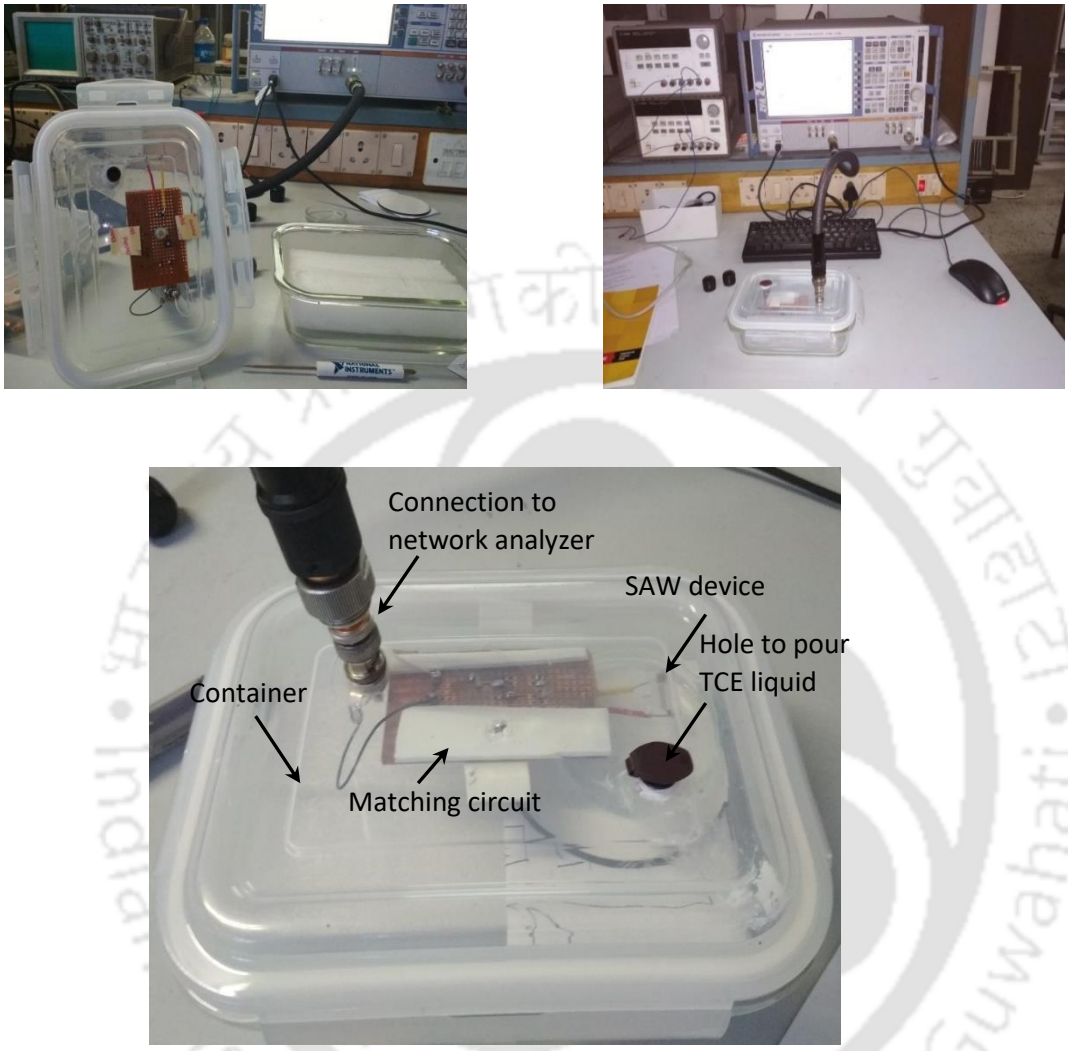

Figure 5.11 Experimental setup for detecting TCE vapor.

5.5.3 Experimental results

The response of SAW devices having finger width of 5 μm and 15 μm coated with 0.67 μm thick PIB film in the space between the SiO_2 HAR structures is tested at room temperature in absence of TCE vapor. The resonance frequencies of devices are observed at 129.74 MHz and 44.69 MHz respectively. Table 5.7 gives the resonance frequency of the devices in presence and absence of TCE vapor at different time intervals. The sensor response ($\Delta f = f_c - f_0$) is calculated by subtracting the resonance frequency (f_c) in presence of TCE vapor from resonance frequency before pouring TCE (f_0).

Table 5.7 Resonance frequency measured from network analyzer at different time intervals without TCE and with 2ml TCE poured into the container for device 1 of λ = 15 μm and device 2 of λ = 5 μm.

Device 1

Time (mins)	Frequency without TCE (MHz)	Frequency with TCE (MHz)
1	44.701	45.016
2	44.691	45.022
3	44.697	45.020
4	44.695	45.022
5	44.702	45.025
Average	223.486/5 = 44.697	225.105/5 = 45.021

Device 2

Time (mins)	Frequency without TCE (MHz)	Frequency with TCE (MHz)
1	129.76	130.08
2	129.74	130.085
3	129.76	130.098
4	129.72	130.085
5	129.73	130.085
Average	648.71/5 = 129.742	650.433/5 = 130.087

The experiment result shows increase in resonance frequency with absorption of TCE vapor and it is also observed in the simulations given in section 4.4.2.2 . A frequency shift of 324 kHz and 345 kHz is observed in device 1 and device 2.

5.6 Summary

This chapter presents the processes required for the fabrication of one-port SAW resonator with SiO_2 HAR structures and experimental results for sensing gases using the fabricated devices. The devices with IDT finger width of 5 µm and 15 µm are fabricated. Photolithography is performed on clean wafers using chromium masks followed by metal deposition and lift-off to realize the IDT pattern. The dimensions and the thickness of the IDTs are verified using optical microscope. SiO_2 layer of 3.5 µm thickness is deposited on the wafer using PECVD. A second stage photolithography is performed to retain the SiO_2 layer on top of the IDT fingers and etch out the remaining areas. The sensing film of Pd or PIB is coated in the space between the SiO_2 HAR structures. The devices are connected to a network analyzer via an appropriate L-section matching circuit for characterization. The frequency response of the devices is studied by plotting S_{11} parameter and the resonance frequency of the fabricated devices is obtained. The increase in resonance frequency is observed in presence of gases. The experimental results confirm that the proposed device used for sensing gases shows increase in resonance frequency in presence of gas and substantiate the simulation results.

6

Conclusion and future outlook

This thesis presents an investigation on one-port SAW resonator devices having structural changes introduced in conventional device configuration with focus on gas sensing applications. Two types of structural changes are proposed i) making trench in the space between each IDT finger pair, and ii) developing HAR structure on each IDT finger. Results of FE simulations of one-port SAW resonator with trenches show that the resonance frequency decreases as trench depth increases and at certain depth, the change in resonance frequency is maximum for given change in trench depth. FE simulation results of one-port SAW resonator with HAR structures show that when the structure height increases the resonance frequency of the device decreases and at certain structure height, the change in resonance frequency is maximum for given change in height of the structure. The large change in resonance frequency observed at certain trench depth and HAR structure height can be exploited for developing highly sensitive gas sensors by depositing sensing material in the trench or between HAR structures so that the swelling of sensing material due to absorption of gas changes effective trench depth or HAR structure height, and leads to large change in the device resonance frequency. Simulations on these devices for sensing gases have shown that the resonance frequency increases with absorption of gas, in contrast with conventional SAW devices which show decrease in frequency. The mechanism behind the unusual behavior exhibited by proposed devices is explained through more elaborate simulations that included individual effects of change in density and change in thickness of sensing material on absorption of gas, confirming that the change in thickness (swelling effect) is dominant and results in large change in resonance frequency as explained above.

The important contributions by the thesis are as follows.

- FE simulation of one-port SAW resonator with trench made in the space between each IDT finger pair is carried out using COMSOL Multiphyiscs. Eigenmode analysis is performed to study effect of trench depth on the resonance frequency. It is observed that

the resonance frequency decreases with increase in trench depth and the maximum change in resonance frequency occurs at trench depth of 0.14λ for YZ $LiNbO_3$ piezoelectric substrate.

- Simulation of a one-port SAW resonator with trenches coated with fluorinated bisphenol-containing polymer (BSP3) sensing film for sensing Dimethymethaphosponate (DMMP) gas is carried out. The effect of BSP3 film thickness on sensor response for a trench depth of 0.14λ is studied and it is observed that the thicker the sensing film the higher is the sensitivity. For a 76 nm thick BSP3 sensing film the proposed device has shown a sensitivity of about 35 kHz/mg/m^3, which is about 14 time greater than that observed using conventional SAW resonator. Another simulation for sensing hydrogen (H_2) gas using palladium as sensing film has shown a frequency shift of 4 MHz for 0.5% of H_2 gas, corresponding to a sensitivity of about 800 Hz/ppm.

- FE analysis of SAW one-port SAW resonator with thick IDT as HAR structure is simulated for IDT made of Ag, Au, Al and Ni metals. It is observed that the resonance frequency decreases with increase in IDT thickness and the thickness of IDT required for maximum change in resonance frequency is lower for materials of higher density. The proposed device using thick Ni IDT is simulated for sensing DMMP gas using fluoroalcholpolysiloxane (SXFA) film coated in the space between IDT fingers and it has shown a sensitivity of 5.64 kHz/mg/m^3 which is about 7 times greater than sensor based on conventional SAW one-port resonator.

- Simulation of one-port SAW resonator with SiO_2 HAR structure made over each IDT finger is carried out using COMSOL Multiphyiscs. It is observed that, the resonance frequency decreases with increase in height of SiO_2 HAR structure and the maximum change in resonance frequency occurs at height of 0.19λ of SiO_2 HAR structure for YZ $LiNbO_3$ piezoelectric substrate.
- The FE simulations of proposed SAW one-port resonator with 0.19λ thick SiO_2 HAR structure is carried out for sensing DMMP gas with SXFA sensing film coated in the space between SiO_2 HAR structures. The proposed device shows a sensitivity of about 6.15 kHz/mg/m^3 which is about 8.5 times greater than that using conventional device. Another device is simulated for sensing hydrogen (H_2) gas using palladium as sensing film has shown a frequency shift of 1.8 MHz for 0.5% of H_2 gas, corresponding to a sensitivity of about 360 Hz/ppm.

- Several one-port SAW resonators are fabricated on YZ $LiNbO_3$ wafer with SiO_2 HAR structure using UV-photolithography, metal lift-off and PECVD deposition techniques. Experiments are performed using fabricated devices for sensing H_2 gas and TCE vapor. The wafer is diced into two halves. The devices in one half are deposited with Pd film between SiO_2 HAR structures and used for sensing H_2 gas in a controlled environmental chamber. The device is connected to a network analyzer via an appropriate matching circuit to obtain the resonance frequency. The device shows an increase in resonance frequency in the presence of H_2 gas and a sensitivity of about 40 kHz/% equivalent to 4 Hz/ppm. The devices in the other half of the wafer are coated with PIB sensing film between SiO_2 HAR structures and used for sensing TCE vapor. These devices also show increase in resonance frequency in the presence of TCE vapor. Thus the experimental results confirm the increase in resonance frequency in presence of gas as observed in simulation results.

In summary, the present work introduces structural changes in basic one-port SAW resonator configuration leading to higher sensitivity in gas sensing applications. The work is complementary to the recent developments in gas sensors focused on improving sensitivity by using modified sensing materials like bilayer films, nanoporous films and nanoparticles-embedded polymers. The objective of the research work is not to develop a particular gas sensor but to contribute new structures of SAW devices based on which variety of sensors can be developed.

This research work can be extended in the following directions:

- Analytical expressions for sensing gases using proposed devices can be derived.
- The use of bi-layer nanofilms, nanoporous films or nanoparticles-embedded polymers as sensing film, and their effects on sensitivity and LOD for sensing gases can be studied.
- The viscoelastic effect in sensing film because of absorption of gas is insignificant and not included in the present work. It may be included for more accurate simulation results.
- For CMOS compatibility, the SAW resonator can be designed on a silicon wafer with piezoelectric thin film deposition and HAR structures grown.
- One-port SAW resonator operating at high frequency may be investigated for sensing applications as the trench depth and height of HAR structures are reasonably small at high resonance frequency.

- In addition to gas sensors, the proposed structural changes in one-port SAW resonator can be explored in designing highly sensitive sensors for humidity, temperature, biomolecules, etc.

Material Constants of Lithium Niobate

Material constants of Lithium niobate used in the thesis are taken from [94]. The constants for Y cut Z- $LiNbO_3$ is given in below.

C. 1 Material constants of Y-Z cut $LiNbO_3$

Density (ρ) = 4647 kg/m^3

$$\text{Stiffness, } \mathbf{C}^E = \begin{pmatrix} 24.24 & 7.52 & 7.52 & 0 & 0 & 0 \\ 7.52 & 20.3 & 5.73 & 0 & 8.5 & 0 \\ 7.52 & 5.73 & 20.3 & 0 & -8.5 & 0 \\ 0 & 0 & 0 & 7.52 & 0 & 8.5 \\ 0 & 8.5 & -8.5 & 0 & 5.95 & 0 \\ 0 & 0 & 0 & 8.5 & 0 & 5.95 \end{pmatrix} \times 10^{10}\ \text{N/m}^2$$

$$\text{Piezoelectric constant , } \mathbf{e} = \begin{pmatrix} 1.33 & 0.23 & 0.23 & 0 & 0 & 0 \\ 0 & 0 & 0.0 & -2.5 & 0 & 3.7 \\ 0 & -2.5 & 2.5 & 0 & 3.7 & 0 \end{pmatrix} \text{C/m}^2$$

$$\text{Permittivity , } \boldsymbol{\varepsilon} = \begin{pmatrix} 28.7 & 0 & 0 \\ 0 & 85.2 & 0 \\ 0 & 0 & 85.2 \end{pmatrix}$$

References

[1] D. P. Morgan, "History of SAW devices," in Proceedings of the 1998 IEEE International Frequency Control Symposium , 1998.

[2] C. C. W. Ruppel and T. A. Fjeldly, *Advances in Surface Acoustic Wave Technology, Systems and Applications*, World Scientific, 2000.

[3] B. Drafts, "Acoustic wave technology sensors," *IEEE Transactions on Microwave Theory and Techniques*, vol. 49, pp. 795-802, April 2001.

[4] R. M. White and F. W. Voltmer, "Direct piezoelectric coupling to surface elastic waves," *Applied Physics Letters*, vol. 7, pp. 314-316, 1965.

[5] D. S. Ballantine Jr, R. M. White, S. J. Martin, A. J. Ricco, E. T. Zellers, G. C. Frye and H. Wohltjen, *Acoustic wave sensors: theory, design and physico-chemical applications*, Elsevier, 1996.

[6] T. Shigematsu, M. K. Kurosawa and K. Asai, "Nanometer stepping drives of surface acoustic wave motor," *IEEE Transactions on Ultrasonics, Ferroelectrics, and Frequency control*, vol. 50, pp. 376-385, 2003.

[7] Y. Kanemitsu, Y. Harada, Y. Tanaka, N. Nakano, H. Kuroda and K. Yamanaka, "Dynamics of picosecond laser-generated acoustic waves in solids," *Japanese Journal of Applied Physics*, vol. 28, 1989.

[8] M. E. Siemens, Q. Li, M. M. Murnane, H. C. Kapteyn, R. Yang, E. H. Anderson and K. A. Nelson, "High-frequency surface acoustic wave propagation in nanostructures characterized by coherent extreme ultraviolet beams," *Applied Physics Letters*, vol. 94, 093103, 2009.

[9] B. Lüthi, *Physical acoustics in the solid state*, vol. 148, Springer Science & Business Media, 2007.

[10] B. A. Auld, *Acoustic fields and waves in solids*, John wiley & sons, 1973.

[11] D. Morgan, *Surface acoustic wave filters: With applications to electronic communications and signal processing*, Academic Press, 2010.

[12] M. Thompson and D. C. Stone, *Surface-Launched Acoustic Wave Sensors: Chemical Sensing and Thin Film Characterization*, Wiley, 1997.

[13] J. W. Gardner, V. K. Varadan and O. O. Awadelkarim, Microsensors, *MEMS, and Smart Devices*, Wiley, 2001.

[14] M. Madou, *Fundamentals of Microfabrication and Nanotechnology: From MEMS to Bio-MEMS and Bio-Nems : manufacturing techniques and applications*, CRC Press, 2011.

[15] D. Royer, D. P. Morgan and E. Dieulesaint, *Elastic Waves in Solids I: Free and Guided Propagation*, Springer Berlin Heidelberg, 1999.

[16] L. A. Francis, J.-M. Friedt, C. Zhou and P. Bertrand, "In situ evaluation of density, viscosity, and thickness of adsorbed soft layers by combined surface acoustic wave and surface plasmon resonance," *Analytical Chemistry*, vol. 78, pp. 4200-4209, 2006.

[17] L. Bo, C. Xiao, C. Hualin, M. A. Mohammad, T. Xiangguang, T. Luqi, Y. Yi and R. Tianling, "Surface acoustic wave devices for sensor applications," *Journal of Semiconductors*, vol. 37, 021001, 2016.

[18] C. Caliendo, E. Verona and V. I. Anisimkin, "Surface acoustic wave humidity sensors: a comparison between different types of sensitive membrane," *Smart materials and structures*, vol. 6, 1997.

[19] W. P. Jakubik, "Surface acoustic wave-based gas sensors," *Thin Solid Films*, vol. 520, pp. 986-993, 2011.

[20] A. Afzal, N.Iqbal, A.Mujahid and R. Schirhagl, "Advanced vapor recognition materials for selective and fast responsive surface acoustic wave sensors: A review," *Analytica Chimica Acta*, vol. 787, pp. 36-49, 2013.

[21] J. D. N. Cheeke and Z. Wang, "Acoustic wave gas sensors," *Sensors and Actuators B: Chemical*, vol.59, pp. 146-153, 1999.

[22] T. M. A. Gronewold, "Surface acoustic wave sensors in the bioanalytical field: Recent trends and challenges," *Analytica Chimica Acta*, vol. 603, pp. 119-128, 2007.

[23] K. Länge, B. E. Rapp and M. Rapp, "Surface acoustic wave biosensors: a review," *Analytical and Bioanalytical Chemistry*, vol. 391, pp. 1509-1519, 2008.

[24] C. G. Fox and J. F. Alder, "Surface acoustic wave sensors for atmospheric gas monitoring. A review," *Analyst*, vol. 114, no. 9, pp. 997-1004, 1989.

[25] L. M. Dorozhkin and I. A. Rozanov, "Acoustic wave chemical sensors for gases," *Journal of Analytical Chemistry*, vol. 56, pp. 399-416, May 2001.

[26] G. Fischerauer, F. Dickert, P. Forth and U. Knauer, "Chemical sensors based on SAW resonators working at up to 1 GHz," IEEE *Ultrasonics Symposium Proceedings*, 1996.

[27] A. Bryant, D. L. Lee and J. F. Vetelino, "A surface acoustic wave gas detector," *IEEE Ultrasonics Symposium*, 1981.

[28] A. D'Amico, A. Palma and E. Verona, "Palladium-surface acoustic wave interaction for hydrogen detection," *Applied Physics Letters*, vol. 41, pp. 300-301, 1982.

[29] A. Bryant, M. Poirier, G. Riley, D. L. Lee and J. F. Vetelino, "Gas detection using surface acoustic wave delay lines," *Sensors and Actuators*, vol. 4, pp. 105-111, 1983.

[30] S. J. Martin, K. S. Schweizer, S. S. Schwartz and R. L. Gunshor, "Vapor sensing by means of a ZnO-on- surface acoustic wave resonator," *IEEE Ultrasonics Symposium*, 1984.

[31] A. J. Ricco, S. J. Martin and T. E. Zipperian, "Surface acoustic wave gas sensor based on film conductivity changes," *Sensors and Actuators*, vol. 8, pp. 319-333, 1985.

[32] A. DÁmico, A. Petri, P. Verardi and E. Verona, "NH3 surface acoustic wave gas detector," IEEE *Ultrasonics Symposium*, 1987.

[33] J. F. Vetelino, R. K. Lade and R. S. Falconer, "Hydrogen sulfide surface acoustic wave gas detector," *IEEE Transactions on Ultrasonics, Ferroelectrics, and Frequency Control*, vol. 34, pp. 156-161, 1987.

[34] M. S. Nieuwenhuizen, A. J. Nederlof, M. J. Vellekoop and A. Venema, "Preliminary results with a silicon-based surface acoustic wave chemical sensor for NO_2," *Sensors and Actuators*, vol. 19, pp.385-392, 1989.

[35] R. S. Falconer, J. F. Vetelino, D. J. Smith and M. J. Osborn, "An activation process for increased sensitivity of a SAW gas microsensor," IEEE *Ultrasonics Symposium Proceedings*, 1990.

[36] J. W. Grate and M. Klusty, "Surface acoustic wave vapor sensors based on resonator devices," *Analytical Chemistry*, vol. 63, pp. 1719-1727, 1991.

[37] K. V. Pfeifer, J. L. Sprung and T. R. Galloway, "Polymer-coated surface acoustic wave monitoring of CCl_4 in a steam reforming reactor," *Sensors and Actuators B: Chemical*, vol. 22, pp. 37-45, 1994.

[38] Y. J. Lee, H. B. Kim, Y. R. Roh, H. M. Cho and S. Baik, "Development of a SAW gas sensor for monitoring SO_2 gas," *Sensors and Actuators A: Physical*, vol. 64, pp. 173-178, 1998.

[39] M. Penza, E. Milella and V. I. Anisimkin, "Gas sensing properties of Langmuir-Blodgett polypyrrole film investigated by surface acoustic waves," *IEEE transactions on ultrasonics, ferroelectrics, and frequency control*, vol. 45, pp. 1125-1132, and 1998.

[40] K. Korsah, C. L. Ma and B. Dress, "Harmonic frequency analysis of SAW resonator chemical sensors: Application to the detection of carbon dioxide and humidity," *Sensors and Actuators B: Chemical*, vol. 50, pp. 110-116, 1998.

[41] K. Beck, T. Kunzelmann, M. Von Schickfus and S. Hunklinger, "Contactless surface acoustic wave gas," *Sensors and actuators A: Physical*, vol. 76, pp. 103-106, 1999.

[42] S. Qin, Z. Wu, Z. Tang, Y. Song, F. Zeng and D. Zhao, "The sensitivity to SO_2 of the SAW gas sensor with triethanolamine modified with boric acid," *Sensors and Actuators B: Chemical*, vol. 66, pp.240-242, 2000.

[43] D. D. Stubbs, S.-H. Lee and W. D. Hunt, "Molecular recognition for electronic noses using surface acoustic wave immunoassay sensors," *IEEE Sensors Journal*, vol. 2, pp. 294-300, 2002.

[44] S. Bender, F. L. Dickert, W. Mokwa and P. Pachatz, "Investigations on temperature controlled monolithic integrated surface acoustic wave (SAW) gas sensors," *Sensors and Actuators B: Chemical*, vol. 93, pp. 164-168, 2003.

[45] C.-Y. Shen, C.-P. Huang and W.-T. Huang, "Gas-detecting properties of surface acoustic wave ammonia sensors," *Sensors and Actuators B: Chemical*, vol. 101, pp. 1-7, 2004.

[46] A. T. Nimal, M. Singh, U. Mittal and R. D. S. Yadava, "A comparative analysis of one-port Colpitt and two-port Pierce SAW oscillators for DMMP vapor sensing," *Sensors and Actuators B: Chemical*, vol.114, pp. 316-325, 2006.

[47] B.-S. Joo, J.-S. Huh and D.-D. Lee, "Fabrication of polymer SAW sensor array to classify chemical warfare agents," *Sensors and Actuators B: Chemical*, vol. 121, pp. 47-53, 2007.

[48] S. Sivaramakrishnan, R. Rajamani, C. S. Smith, K. A. McGee, K. R. Mann and N. Yamashita, "Carbon nanotube-coated surface acoustic wave sensor for carbon dioxide sensing," *Sensors and Actuators B: Chemical*, vol. 132, pp. 296-304, 2008.

[49] X. Du, Z. Ying, Y. Jiang, Z. Liu, T. Yang and G. Xie, "Synthesis and evaluation of a new polysiloxane as SAW sensor coatings for DMMP detection," *Sensors and Actuators B: Chemical*, vol. 134, pp. 409- 413, 2008.

[50] T. Alizadeh and S. Zeynali, "Electronic nose based on the polymer coated SAW sensors array for the warfare agent simulants classification," *Sensors and Actuators B: Chemical*, vol. 129, pp. 412-423, 2008.

[51] A. T. Nimal, U. Mittal, M. Singh, M. Khaneja, G. K. Kannan, J. C. Kapoor, V. Dubey, P. K. Gutch, G. Lal, K. D. Vyas and others, "Development of handheld SAW vapor sensors for explosives and CW agents," *Sensors and Actuators B: Chemical*, vol. 135, pp. 399-410, 2009.

[52] R. Arsat, M. Breedon, M. Shafiei, P. G. Spizziri, S. Gilje, R. B. Kaner, K. Kalantar-zadeh and W. Wlodarski, "Graphene-like nano-sheets for surface acoustic wave gas sensor applications," *Chemical Physics Letters*, vol. 467, pp. 344-347, 2009.

[53] C. Wen, C. Zhu, Y. Ju, H. Xu and Y. Qiu, "A novel NO_2 gas sensor using dual track SAW device," *Sensors and Actuators A: Physical*, vol. 159, pp. 168-173, 2010.

[54] S. K. Jha and R. D. S. Yadava, "Development of surface acoustic wave electronic nose using pattern recognition system," *Defence Science Journal*, vol. 60, 2010.

[55] C. Wen, C. Zhu, Y. Ju, L. Liu, W. Li, D. Yan, H. Xu and Y. Qiu, "A SF6 gas sensor using a dual track SAW device based on multi-wall carbon nanotubes," *Smart Materials and Structures*, vol. 20, 035006, 2011.

[56] C. Lim, W. Wang, S. Yang and K. Lee, "Development of SAW-based multi-gas sensor for simultaneous detection of CO_2 and NO_2," *Sensors and Actuators B: Chemical*, vol. 154, pp. 9-16, 2011.

[57] D. Matatagui, J. Mart\'i, M. J. Fernández, J. L. Fontecha, J. Gutiérrez, I. Gràcia, C. Cané and M. C. Horrillo, "Chemical warfare agents simulants detection with an optimized SAW sensor array," *Sensors and Actuators B: Chemical*, vol. 154, pp. 199-205, 2011.

[58] C. Tasaltin, M. A. Ebeoglu and Z. Z. Ozturk, "Acoustoelectric effect on the responses of SAW sensors coated with electrospun ZnO nanostructured thin film," *Sensors*, vol. 12, pp. 12006-12015, 2012.

[59] C. Wang, Y. Wang, S.-y. Zhang, L. Fan and X.-j. Shui, "Characteristics of SAW hydrogen sensors based on InO_x/128° YX-LiNbO3 structures at room temperature," *Sensors and Actuators B: Chemical*, vol. 173, pp. 710-715, 2012.

[60] V. B. Raj, H. Singh, A. T. Nimal, M. Tomar, M. U. Sharma and V. Gupta, "Effect of metal oxide sensing layers on the distinct detection of ammonia using surface acoustic wave (SAW) sensors," *Sensors and Actuators B: Chemical*, vol. 187, pp. 563-573, 2013.

[61] M. Asad and M. H. Sheikhi, "Surface acoustic wave based H_2S gas sensors incorporating sensitive layers of single wall carbon nanotubes decorated with Cu nanoparticles," *Sensors and Actuators B: Chemical*, vol. 198, pp. 134-141, 2014.

[62] Y.-L. Tang, Z.-J. Li, J.-Y. Ma, Y.-J. Guo, Y.-Q. Fu and X.-T. Zu, "Ammonia gas sensors based on ZnO/SiO_2 bi-layer nanofilms on ST-cut quartz surface acoustic wave devices," *Sensors and Actuators B: Chemical*, vol. 201, pp. 114-121, 2014.

[63] S. Thomas, M. Cole, A. De Luca, F. Torrisi, A. C. Ferrari, F. Udrea and J. W. Gardner, "Graphene-coated Rayleigh SAW resonators for NO_2 detection," *Procedia Eng*, vol. 87, pp. 999-1002, 2014.

[64] H. Singh, V. B. Raj, J. Kumar, U. Mittal, M. Mishra, A. T. Nimal, M. U. Sharma and V. Gupta, "Metal oxide SAW E-nose employing PCA and ANN for the identification of binary mixture of DMMP and methanol," *Sensors and Actuators B: Chemical*, vol. 200, pp. 147-156, 2014.

[65] C. Viespe, "Surface Acoustic Wave Sensors Based on Nanoporous Films for Hydrogen Detection," *Key Engineering Materials*, vol. 605, pp. 331–334, 2014.

[66] V. B. Raj, H. Singh, A. T. Nimal, M. Tomar, M. U. Sharma and V. Gupta, "Origin and role of elasticity in the enhanced DMMP detection by ZnO/SAW sensor," *Sensors and Actuators B: Chemical*, vol. 207, pp. 375-382, 2015.

[67] F.-Q. Xu, W. Wang, X.-F. Xue, H.-L. Hu, X.-L. Liu and Y. Pan, "Development of a wireless and passive SAW-based chemical sensor for organophosphorous compound detection," *Sensors*, vol. 15, pp. 30187-30198, 2015.

[68] W. Wang, H. Hu, G. Chen, X. Xie and S. He, "Optimization of a BSP3-coated surface acoustic wave chemical sensor," *IEEE Sensors Journal*, vol. 15, pp. 6730-6737, 2015.

[69] W. Wang, H. Hu, X. Liu, S. He, Y. Pan, C. Zhang and C. Dong, "Development of a room temperature SAW methane gas sensor incorporating a supramolecular cryptophane a coating," *Sensors*, vol. 16, 73, 2016.

[70] H. Singh, V. B. Raj, J. Kumar, F. Durani, M. Mishra, A. T. Nimal and M. U. Sharma, "SAW mono sensor for identification of harmful vapors using PCA and ANN," *Process Safety and Environmental Protection*, vol. 102, pp. 577-588, 2016.

[71] L. Yang, C. Yin, Z. Zhang, J. Zhou and H. Xu, "The investigation of hydrogen gas sensing properties of SAW gas sensor based on palladium surface modified SnO_2 thin film," *Materials science in semiconductor processing*, vol. 60, pp. 16-28, 2017.

[72] L. Rana, R. Gupta, M. Tomar and V. Gupta, "ZnO/ST-quartz SAW resonator: An efficient NO_2 gas sensor," *Sensors and Actuators B: Chemical*, vol. 252, pp. 840-845, 2017.

[73] C. Viespe and D. Miu, "Surface acoustic wave sensor with Pd/ZnO bilayer structure for room temperature hydrogen detection," *Sensors*, vol. 17, 1529, 2017.

[74] N. H. Ha, N. H. Nam, D. D. Dung, N. H. Phuong, P. D. Thach and H. S. Hong, "Hydrogen gas sensing using palladium-graphene nanocomposite material based on surface acoustic wave," *Journal of Nanomaterials*, vol. 2017, 2017.

[75] X. Le, X. Wang, J. Pang, Y. Liu, B. Fang, Z. Xu, C. Gao, Y. Xu and J. Xie, "A high performance humidity sensor based on surface acoustic wave and graphene oxide on AlN/Si layered structure," *Sensors and Actuators B: Chemical*, vol. 255, pp. 2454-2461, 2018.

[76] L. Rana, R. Gupta, R. Kshetrimayum, M. Tomar and V. Gupta, "Fabrication of surface acoustic wave based wireless NO_2 gas sensor," *Surface and Coatings Technology*, vol. 343, pp. 89-92, 2018.

[77] C. Viespe and D. Miu, "Characteristics of surface acoustic wave sensors with nanoparticles embedded in polymer sensitive layers for VOC detection," *Sensors*, vol. 18, p. 2401, 2018.

[78] D. Miu, R. Birjega and C. Viespe, "Surface acoustic wave hydrogen sensors based on nanostructured Pd/WO_3 bilayers," *Sensors*, vol. 18, 3636, 2018.

[79] A. A. Vives, *Piezoelectric Transducers and Applications*, Springer, 2004.

[80] C. Campbell, *Surface acoustic wave devices and their signal processing applications*, Elsevier, 2012.

[81] W. R. Smith, H. M. Gerard, J. H. Collins, T. M. Reeder and H. J. Shaw, "Analysis of interdigital surface wave transducers by use of an equivalent circuit model," *IEEE Transactions on Microwave Theory and Techniques*, vol. 17, pp. 856-864, 1969.

[82] V. Plessky and J. Koskela, "Coupling-of-modes analysis of SAW devices," *International Journal of High Speed Electronics and Systems*, vol. 10, pp. 867-947, 2000.

[83] G. Tobolka, "Mixed matrix representation of SAW transducers," *IEEE transactions on sonics and ultrasonics*, vol. 26, pp. 426-427, 1979.

[84] S. Datta and B. J. Hunsinger, "Element factor for periodic transducers," *IEEE Transactions on Sonics and Ultrasonics*, vol. 27, pp. 42-44, 1980.

[85] K.-J. Bathe, *Finite element procedures*, Klaus-Jurgen Bathe, 2006.

[86] C. Multiphysics, "COMSOL Multiphysics/Reference Manual Version 4.4," 2013.

[87] R. Lerch, "Simulation of piezoelectric devices by two-and three-dimensional finite elements," I*EEE transactions on ultrasonics, ferroelectrics, and frequency control*, vol. 37, pp. 233-247, 1990.

[88] S. J. Ippolito, K. Kalantar-Zadeh, D. A. Powell and W. Wlodarski, "A 3-dimensional finite element approach for simulating acoustic wave propagation in layered SAW devices," *IEEE Ultrasonics Symposium*, 2003.

[89] X. Wang and G. Xu, "Numerical study of the effects of film properties to the mass sensitivity of surface acoustic wave sensors," *Proceedings of the IEEE International Frequency Control Symposium and Exposition*, 2005.

[90] M. Z. Atashbar, B. J. Bazuin, M. Simpeh and S. Krishnamurthy, "3D FE simulation of H2 SAW gas sensor," *Sensors and Actuators B: Chemical*, vol. 111, pp. 213-218, 2005.

[91] E. I. M. M. Gowini and W. A. Moussa, "A finite element model of a MEMS-based surface acoustic wave hydrogen sensor," *Sensors*, vol. 10, pp. 1232-1250, 2010.

[92] S. Cular, S. K. R. S. Sankaranarayanan and V. R. Bhethanabotla, "Enhancing effects of microcavities on shear-horizontal surface acoustic wave sensors: A finite element simulation study," *Applied Physics Letters*, vol. 92, 244104, 2008.

[93] K. M. M. Kabir, G. I. Matthews, Y. M. Sabri, S. P. Russo, S. J. Ippolito and S. K. Bhargava, "Development and experimental verification of a finite element method for accurate analysis of a surface acoustic wave device," *Smart Materials and Structures*, vol. 25, 035040, 2016.

[94] A. W. Warner, M. Onoe and G. A. Coquin, "Determination of elastic and piezoelectric constants for crystals in class (3 m)," *The journal of the acoustical society of America*, vol. 42, pp. 1223-1231, 1967.

[95] K.-Y. Hashimoto, *Surface acoustic wave devices in telecommunications*, Springer, 2000.

[96] J. Koskela, V. P. Plessky and M. M. Salomaa, "SAW/LSAW COM parameter extraction from computer experiments with harmonic admittance of a periodic array of electrodes," *IEEE transactions on ultrasonics, ferroelectrics, and frequency control*, vol. 46, pp. 806-816, 1999.

[97] R. S. Falconer, "A versatile SAW-based sensor system for investigating gas-sensitive coatings," *Sensors and Actuators B: Chemical*, vol. 24, pp. 54-57, 1995.

[98] C. Caliendo, P. Verardi, E. Verona, A. DtextquotesingleAmico, C. D. Natale, G. Saggio, M. Serafini, R. Paolesse and S. E. Huq, "Advances in SAW-based gas sensors," *Smart Materials and Structures*, vol. 6, pp. 689-699, 1997.

[99] H. Wohltjen, "Mechanism of operation and design considerations for surface acoustic wave device vapor sensors," *Sensors and Actuators*, vol. 5, pp. 307-325, 1984.

[100] S. J. Martin, G. C. Frye and S. D. Senturia, "Dynamics and response of polymer-coated surface acoustic wave devices: effect of viscoelastic properties and film resonance," *Analytical Chemistry*, vol. 66, pp. 2201-2219, 1994.

[101] K. M. Lakin, "Perturbation theory for electromagnetic coupling to elastic surface waves on piezoelectric substrates," *Journal of Applied Physics*, vol. 42, pp. 899-906, 1971.

[102] S. Ahmadi, F. Hassani, C. Korman, M. Rahaman and M. Zaghloul, "Characterization of multi- and single- structure SAW sensor [gas sensor]," *Proceedings of IEEE in Sensors* , 2004.

[103] M. N. Hamidon, S. A. Mousavi, M. M. Isa, A. Ismail and M. A. Mahdi, "Finite element method on mass loading effect for gallium phosphate surface acoustic wave resonators," *in Proceedings of the World Congress Engineering*, 2009.

[104] M. B. Dühring, V. Laude and A. Khelif, "Energy storage and dispersion of surface acoustic waves trapped in a periodic array of mechanical resonators," *Journal of Applied Physics*, vol. 105, 093504, 2009.

[105] V. Laude, L. Robert, W. Daniau, A. Khelif and S. Ballandras, "Surface acoustic wave trapping in a periodic array of mechanical resonators," *Applied physics letters*, vol. 89, 083515, 2006.

[106] V. Laude, A. Khelif, T. Pastureaud and S. Ballandras, "Generally polarized acoustic waves trapped by high aspect ratio electrode gratings at the surface of a piezoelectric material," *Journal of Applied Physics*, vol. 90, pp. 2492-2497, 2001.

[107] W. Wang, S. He, S. Li, M. Liu and Y. Pan, "Advances in SXFA-coated SAW chemical sensors for organophosphorous compound detection," *Sensors*, vol. 11, pp. 1526-1541, 2011.

[108] H. Singh, V. Bhaskerraj, J. Kumar, U. Mittal, M. Mishra, F. Durani, A. T. Nimal and M. U. Sharma, "SAW E-nose using single sensor with temperature modulation," *in 9th International Conference on Industrial and Information Systems (ICIIS)*, 2014.

[109] C. G. Bostan, B. Serban, V. Avramescu and I. Georgescu, "Simulation of SAW gas sensors with polymer layers using the finite element method," *in International Semiconductor Conference (CAS)*, 2010.

[110] Y.-G. Zhao, M. Liu, D.-M. Li, J.-J. Li and J.-B. Niu, "FEM modeling of SAW organic vapor sensors," *Sensors and Actuators A: Physical*, vol. 154, pp. 30-34, 2009.

List of publications

Journals

- V. Lukose and H. B. Nemade, "Finite element simulation of one-port surface acoustic wave resonator with thick interdigital transducer for gas sensing," *Microsystem Technologies,* vol. 25, pp. 441-446, Feb 2019.

- V. Lukose, & H.Nemade, “Simulation of surface acoustic wave one-port resonator having trenches containing BSP3 film employed for sensing DMMP gas with high sensitivity,” *(under review)*.

Proceedings

- V. Lukose, & H.Nemade, “Simulation of one-port SAW resonator with trenches containing palladium for sensing hydrogen,” *Proceedings of 1st national conference on micro and nano fabrication (mnf 2013),* pp. 163-165, 2013.